CHALMERS
UNIVERSITY OF TECHNOLOGY

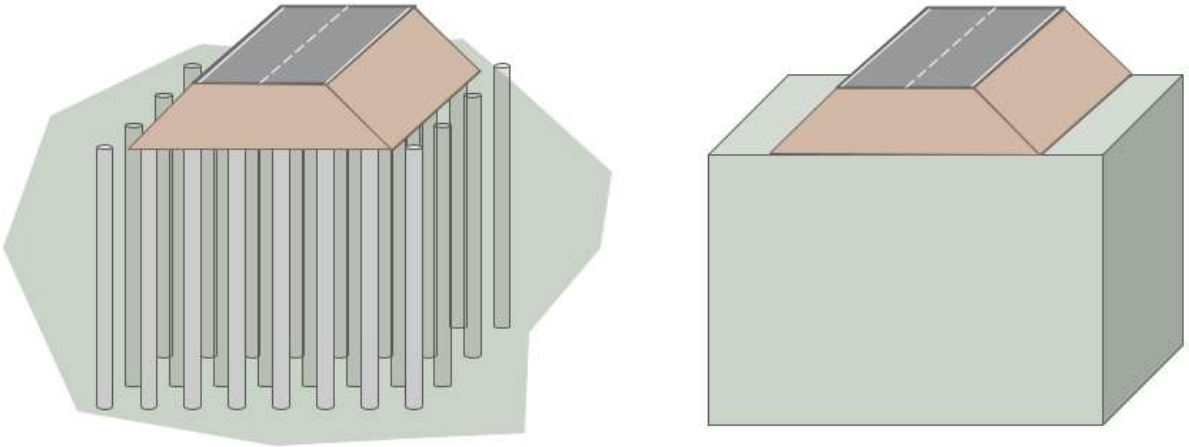

Settlement analysis and environmental assessment of deep mixing binders

A Plaxis 2D study with Volume Averaging Technique

Master's Thesis in Structural Engineering and Building Technology

VIKTORIA PRAHL BLACKBY
LEO WAHLGREN

DEPARTMENT OF ARCHITECTURE AND CIVIL ENGINEERING

CHALMERS UNIVERSITY OF TECHNOLOGY
Gothenburg, Sweden 2021
www.chalmers.se

Master's thesis ACEX30

Settlement analysis and environmental assessment of deep mixing binders

A Plaxis 2D study with Volume Averaging Technique

Master's Thesis in the Master's Programme Structural Engineering and Building Technology

VIKTORIA PRAHL BLACKBY
LEO WAHLGREN

CHALMERS
UNIVERSITY OF TECHNOLOGY

Department of Architecture and Civil Engineering
Division of Geology and Geotechnics
Geotechnics Research Group
Chalmers University of Technology
Gothenburg, Sweden 2021

Settlement analysis and environmental assessment of deep mixing binders
A Plaxis 2D study with Volume Averaging Technique

Master's Thesis in the Master's Programme Structural Engineering and Building Technology

VIKTORIA PRAHL BLACKBY
LEO WAHLGREN

Examensarbete ACEX30
Institutionen för arkitektur och samhällsbyggnadsteknik
Chalmers tekniska högskola, 2021

Department of Architecture and Civil Engineering
Division of Geology and Geotechnics
Geotechnics Research Group
Chalmers University of Technology
SE-412 96 Gothenburg
Sweden
Telephone: +46 (0)31 772 1000

Cover: An illustration of a discrete and a homogenized representation (Volume Averaging Technique) of deep mixed columns under a road embankment.

Typeset in LaTeX
Department of Architecture and Civil Engineering
Gothenburg, Sweden 2021

Settlement analysis and environmental assessment of deep mixing binders

Master's Thesis in the Master's Programme Structural Engineering and Building Technology

VIKTORIA PRAHL BLACKBY
LEO WAHLGREN

Department of Architecture and Civil Engineering
Division of Geology and Geotechnics
Geotechnics Research Group
Chalmers University of Technology

Abstract

Constructing road embankments on soft clay is combined with a high risk of excessive settlements and stability problems. As a ground improvement measure, deep mixing is often used by injecting cement as columns in the soil to increase the strength and stiffness. The cement production is a heavy source of green house gas emissions and implementing cementitious binder substitutes with lower environmental impact is a vital key for a sustainable construction future. This thesis aimed to investigate the deep mixing performance on vertical settlements and compare the environmental impact between SH cement, Multicem and a mixture of 80 % Slag Bremen and 20 % cement.

The vertical settlement assessment was carried out with the finite element software Plaxis 2D, incorporating Volume Averaging Technique. Volume Averaging Technique homogenises the material models S-CLAY1S and MNhard in order to capture the behaviour of enhanced clay, S-CLAY1S for clay and MNhard for mixed columns. The soil and column data were gathered from both empirical assumptions and a geotechnical study for an existing road project. A material optimisation process in terms of volume ratio was performed by investigating the smallest amount of binder columns necessary to reach the settlement demands for a road embankment. Based on the volume ratio, each binder's environmental impact was estimated with a simplified life cycle assessment.

The results from the optimisation study showed that the binder recipes exhibited a close range of required volume ratios, despite varying stiffnesses. From the life cycle assessment estimations, Slag Bremen mixture and Multicem yielded less $kg\ CO_2$-eq per meter road section than SH cement, 70 % and 50 % respectively. The most obvious finding to emerge from this study was that SH cement's high stiffness did not compensate for it's high emissions.

Keywords: Carbon dioxide equivalents, Deep mixing, Geotechnics, Life Cycle Assessment, Soft clay, MNhard, Plaxis 2D, S-CLAY1S, Soft soils, Volume Averaging Technique.

Acknowledgements

We would like to express our appreciation to our supervisors Ayman Abed, senior lecturer at Chalmers and Mats Larsson, senior consultant at Sweco Sweden AB for your valuable expertise and guidance into interesting aspects of the subject. The completion of our thesis would not have been possible without your support and helpful advises. We would also like to extend our gratitude to Jelke Dijkstra, professor at Chalmers and Magnus af Petersens at Sweco Sweden AB for your commitment, in believing in our project and the appreciated guidance. Special thanks to Emma Backteman and Märta Lidén at Sweco Sweden AB for your useful knowledge and contributions. Thanks should also go to Minna Karstunen, professor at Chalmers for introducing us into the subject and giving practical experience. Finally, we would like to extend our gratitude to friends and families for all patience and love.

Viktoria Prahl Blackby & Leo Wahlgren
Gothenburg, June 2021

Contents

Abbreviations

CRS	Constant Rate of Strain
FE	Finite Element
GWP	Global Warming Potential index
IL	Incremental Load
NC	Normal Consolidated
OC	Over Consolidated
OCR	Over Consolidation Ratio
POP	Pre-Overburden Pressure
UDSM	User Defined Soil Model
VAT	Volume Averaging Technique

Nomenclature

Roman letters

A_c	surface area of column
A_s	surface area of soil
a	absolute rate of destructuration
b	relative rate of destructuration
c'	effective cohesion
c_u	undrained shear strength
$\boldsymbol{D}^c$	stiffness matrix for column material
$\boldsymbol{D}^s$	stiffness matrix for soil material
$\boldsymbol{D}^{eq}$	equivalent material stiffness matrix
E	Young's modulus
E_{50}	stiffness modulus for primary loading
E_{50}^{ref}	reference stiffness modulus for primary loading
E_{ur}	unloading/reloading stiffness modulus
E_{ur}^{ref}	reference stiffness modulus for unloading/reloading
e	void ratio
e_0	initial void ratio
f	yield function
f_t	allowable tensile stress
G	shear modulus
G_{50}	shear modulus for primary loading
E_{50}^{ref}	reference shear modulus for primary loading
G_{ur}	shear modulus for unloading/reloading
G_{ur}^{ref}	reference shear modulus for unloading/reloading
K_0	lateral earth pressure coefficient at rest
$K_{0,NC}$	lateral earth pressure coefficient at rest for normally consolidated soil
M_c	critical state line compression
M_e	critical state line extension
m	power for stress dependent stiffness law
p'	mean effective stress
p'_m	size of yield surface
p'_{mi}	size of instrinsic yield surface
p'_{ref}	reference stress
q	deviatoric stress
q_a	quantity asymptote

q_f	maximum failure stress
R_f	ratio of failure stress to hyperbolic asymptote
S_t	sensitivity of soil
$\boldsymbol{S}_1^c$	strain distribution matrix between column and equivalent strain increment
$\boldsymbol{S}_1^s$	strain distribution matrix between soil and equivalent strain increment
$Sk.\text{-}B$	Skempton-B parameter for undrained loading
V_p	volume of pores
V_s	volume of solids
v	specific volume
w	water ratio
w_L	liquid limit
x	number of bonds
x_0	initial amount of bonding

Greek letters

$\boldsymbol{\alpha}$	degree of asnisotropy
$\boldsymbol{\alpha}_d$	deviatoric fabric tensor
α_o	initial degree of anisotropy
$\boldsymbol{\beta}$	relative effectiveness of rotation hardening
ε	strain
$\dot{\varepsilon}$	strain rate
$\boldsymbol{\varepsilon}$	strain vector
$\dot{\boldsymbol{\varepsilon}}$	strain rate vector
ε_d^p	plastic devaiatoric strain
ε_v^p	plastic volumetric strain
η	stress ratio
η_{K0}	stress ratio for one dimensional compression
κ	swelling index
λ	compression index
λ_i	instrinsic compression index
μ	absolute effectiveness of rotation hardening
ν'	effective Poisson's ratio
ρ_s	compact density
ρ_w	water density
σ	total stresses
$\boldsymbol{\sigma}$	stress vector
$\dot{\boldsymbol{\sigma}}$	stress rate vector
σ'	effective stress
σ_1'	principal effective vertical stress
σ_2'	principal effective vertical stress
σ_3'	principal effective horizontal stress/confining pressure
σ_c'	pre consolidation pressure
σ_0'	effective pressure at rest
$\boldsymbol{\sigma_d}$	deviatoric stress vector

τ	shear stress
ϕ'	effective friction angle
ϕ'_{cv}	effective critical state friction angle
ψ'	effective dilatancy angle
Ω_c	volume ratio of column
Ω_s	volume ratio of soil

List of Figures

List of Tables

1
Introduction

Construction on soft ground areas is a challenge due to the high risk of slope instability and excessive settlements. To enhance the often low strength of soft soils when constructing a road embankment, deep mixing with cement is a common ground improvement method used in Sweden (Larsson, 2006). Besides water, cement is the most used material on earth (Watts, 2019) due to its many advantages, such as high strength, flexibility and long durability. However, the cement production is a heavy source of carbon dioxide emissions and produces around 8 % of the global carbon dioxide emissions per year (Rodgers, 2018). Implementing materials which have a lower carbon footprint but nevertheless mimicking the material characteristics of cement is a vital key for a sustainable construction sector and future.

1.1 Problem description

The Swedish consulting firm, Sweco Sweden AB is on behalf of the Swedish Transport Administration investigating the geotechnical conditions and ground improvements of road 56 between Bie and Alberga, location in figure 1.1. The road needs to be enhanced and widened to ensure acceptable traffic safety. Widening the road will as a consequence implicate redirection of some road sections onto areas with soft soil deposits. Because of the high risk of settlement and stabilisation issues in soft soils, deep mixing is chosen as a strengthening enhancement before constructing the new road. Three different binder recipes have been proposed for deep mixing; quick hardening cement (SH cement), Multicem and a mixture of 80 % Slag Bremen and 20 % cement. Laboratory testing has been performed on clay specimens mixed with the binders after 28 days of hardening, where the specimens were uniaxially compressed to determine their performance. At equal concentration, the more environmentally friendly binders Multicem and Slag Bremen mixture exhibited a lower stiffness and strength compared to SH cement. The most optimal material choice would preferably be a binder which has a low environmental impact but yet achieves the geotechnical requirements.

This thesis focuses on performing a finite element settlement analysis of an embankment section of the new road, along with comparing the environmental impact of different binders. To perform the analysis a new research technique, Volume Averaging, is used as a user defined soil model in the software Plaxis 2D. Numerical modelling is a helpful tool in order to predict the complex behaviour of an embank-

ment with deep mixed columns in soft soil. Volume Averaging Technique facilitates a smooth design optimisation of the columns. With the life cycle assessment tool Carbon Cost, developed by Sweco Sweden AB, the carbon dioxide equivalents for the different binder mixtures are estimated.

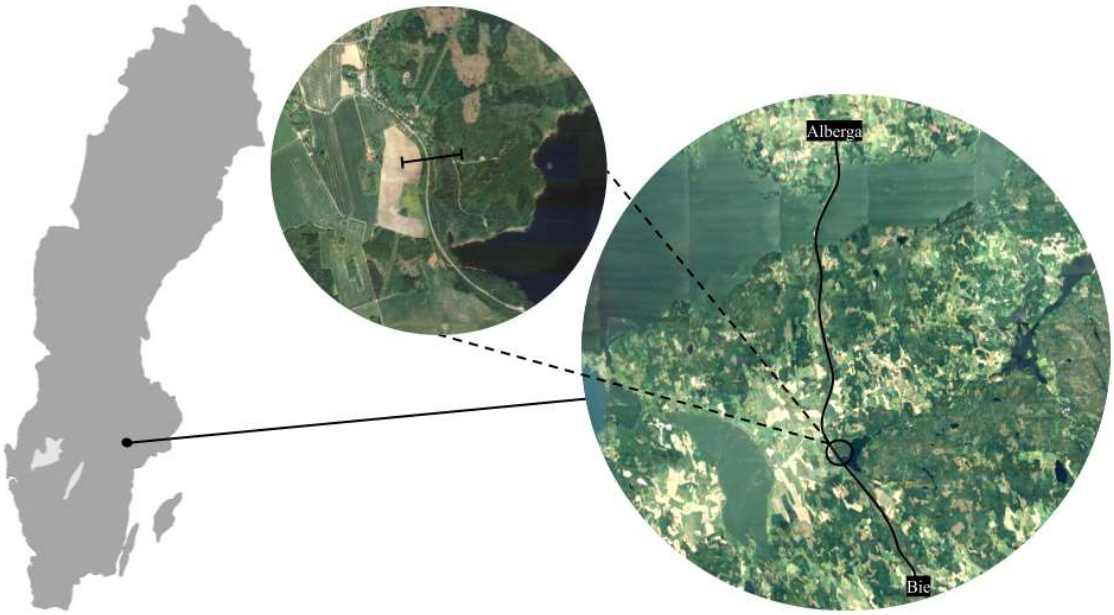

Figure 1.1: *Road 56 between Bie and Alberga and section of interest (maps from Google Earth).*

1.2 Aim and objectives

The aim is to investigate the deep mixing performance and the environmental impact of SH cement, Multicem and a mixture of 80 % Slag Bremen and 20 % cement in soft clay under a road embankment. Specified objective for the geotechnical performance is to reduce the amount of material but yet achieve the requirements of maximum 300 mm vertical deformations during 40 years of service life. Another objective is to compare the carbon dioxide equivalents per meter road section between the three binders.

1.3 Limitations

It is not possible to entirely replicate the reality in a numerical model and predictions of the long-term settlement behaviour in soft clay is very complex. Thus some general limitations have been identified:

- Only one section of the embankment and soil profile is investigated - other results and conclusions could be yielded at different road sections.

- Volume Averaging Technique does not incorporate creep behaviour of the soil, creep settlements will therefore not be captured in the analysis.
- Road demands regarding differential settlements and slope stability will not be taken into account, due to time limitations.
- Only three binder recipes are investigated. Several other mixtures and recipes could be included in this kind of analysis.
- No installation effect from the deep mixed columns is considered in the soil.
- No difference in hardening rate between the deep mixture binders are considered, which could be of importance for the construction method and construction duration.
- Due to limitations with Volume Averaging Technique, the optimisation of column patterns is narrowed down to only include uniform column arrangements.
- A complete life cycle assessment of each binder recipe is not included in this thesis. Instead the tool Carbon Cost is used to estimate the environmental impact.
- The thesis does not investigate cost aspects for the different mixing recipes.
- The heat development from curing of the columns is not considered in the analysis.

1.4 Method

Initially a literature study was performed to gain knowledge about; the geotechnical conditions on site, soil behaviour and numerical soil models, deep mixing and different binders as well as finite element modelling with Plaxis including Volume Averaging Technique. The literature study was followed by deriving all necessary parameters from empirical studies and soil tests performed on site specimens. After the soil profile was created in Plaxis the parameters were validated and revised in Plaxis' built in soil test tool. A volume ratio optimisation for all deep mixing binders was then performed by using Volume Averaging Technique. Volume ratio describes in percentage how much of the soil which is enhanced and was iterated until the deformation demands were achieved. Volume Averaging Technique was utilised to merge the constitutive soil model S-CLAY1S and column model MNhard into one homogeneous soil medium, which allowed for a change of volume ratios without constructing a new soil model for every case. As a final step the binders and their corresponding volume ratios were evaluated in a life cycle assessment tool, to compare $kg\ CO_2$-eq per meter embankment. Figure 1.2 highlights the main steps of the method.

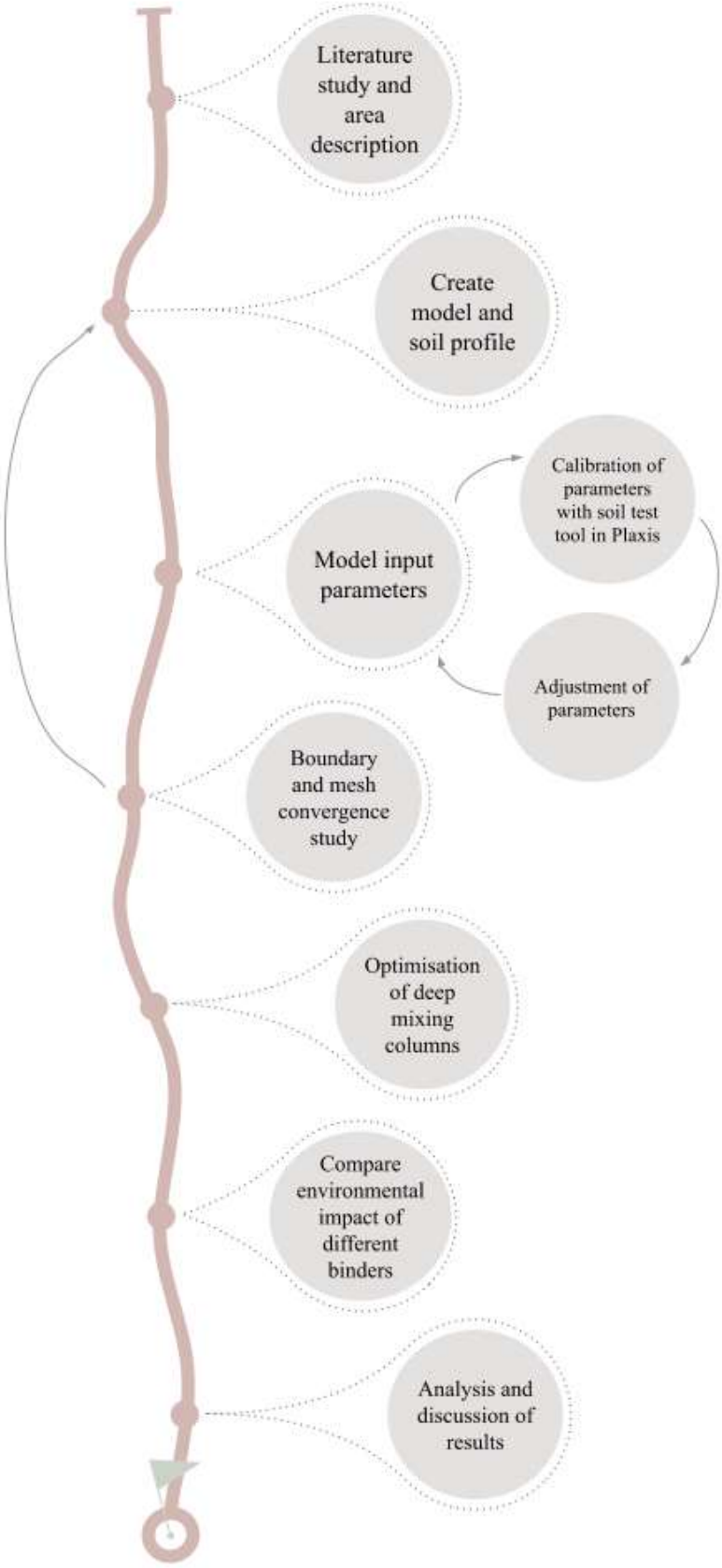

Figure 1.2: *Flow chart of the thesis composition.*

2

Behaviour of soft soil

Due to soft soil's characteristics of high water content, low density and low strength there is a high risk of settlements and stability problems. Therefore before constructing, the soil needs to be examined to know its often complex behaviour. Soft soil consists of microscopic soil particles, either in the form of minerals from deposited eroded rock, organic decay or a mixture of them both (Larsson, 2008).

2.1 Deformation properties of soft clay

Clay is composed of eroded rock particles with a diameter of less than 0.0002 mm (Larsson, 2008). Clay has inter molecular bindings which are not purely frictional, and therefore allows for large voids containing high amounts of bounded water and gas (Sällfors, 2013). The higher the water content, the softer the clay. Clay is highly anisotropic due to both the composition of the clay and the history of horizontal layering, which affects how the soil deforms in different directions (Wood, 1990). The high water content and the low strength in soft small grained soils result in large irreversible deformations. The deformation behaviour is dependent on the anisotropy, stress level in different directions, strain rate and stress history (Sällfors, 2013). A categorisation of the deformations is usually divided into two types of strains, volumetric or deviatoric, displayed in figure 2.1.

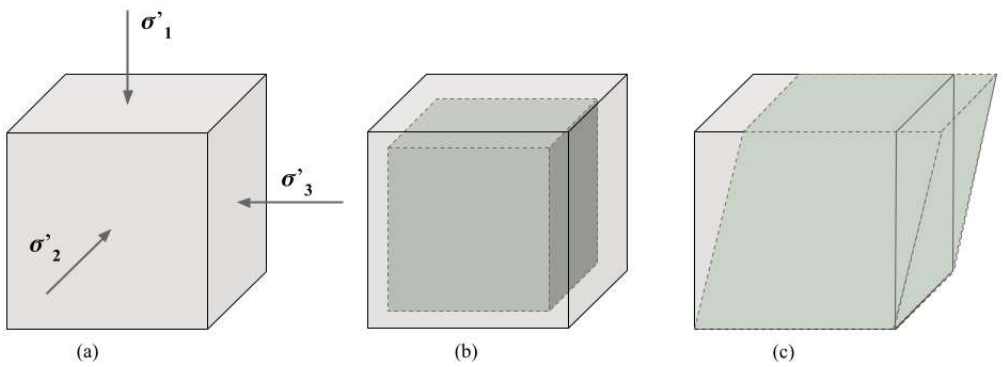

Figure 2.1: *(a) Principle effective compression stresses (b) volumetric strain (c) deviatoric shear strain.*

For a virgin soil deposit, the relationship between the horizontal and vertical stresses

can be described with the earth pressure coefficient at rest $K_{0,NC}$. For frictional soils the coefficient is often determined by Jacky's empirical formula (2.1). Clay's earth pressure coefficient is more accurately estimated with the liquid limit w_L according to equation (2.2) (Larsson et al., 2007). For an overconsolidated soil, the lateral earth pressure can be determined by equation (2.3) based on the overconsolidation ratio, OCR.

$$K_{0,NC} = 1 - \sin\phi \tag{2.1}$$

$$K_{0,NC} \approx 0.31 + 0.71 \times (w_L - 0.2) \tag{2.2}$$

$$K_0 = K_{0,NC} OCR^{\,0.5\ or\ 0.6} \tag{2.3}$$

The small particles in clay induce a soil structure with low permeability (Wood, 1990). Together with the often high water content, the deformation behaviour is linked with the flow of pore water, referred as consolidation (Olsson, 2010). When a soil is loaded and the stresses increase, an excess pore pressure is built up from the disturbance of pore water equilibrium, which causes the water to flow and dissipate into the neighbouring soil with lower pore pressures. Due to the low permeability, the consolidation process can progress over a long time period and can be regarded as different stages of consolidation (Augustesen et al., 2004). The primary consolidation is refereed to as the volume change induced by the dissipation of pore water. After some time when the pore water gradually has diminished, the secondary consolidation, also refereed as creep, takes place and is instead governed by a combination of pore water dissipation and the restructuring of the soil skeleton (Olsson, 2010).

The compression and hence the deformation behaviour can be determined through an oedometer test, either with constant rate of strain (CRS) or incremental loading (IL). Figure 2.2 displays an oedometer test with (a) the effective stress in logarithmic scale versus void ratio ($e = V_p/V_s$) and (b) the effective stress in linear scale versus strain ε. The soils ability to increase and decrease in volume is characterised by the compression index λ and the swelling index κ, which can be determined from the slope of the graph at the loading respectively the unloading-reloading phase. The instrinsic compression index λ_i represents the slope of the curve at great stresses, and is used in advanced models to predict the restructuring of internal bonds which causes a soil hardening.

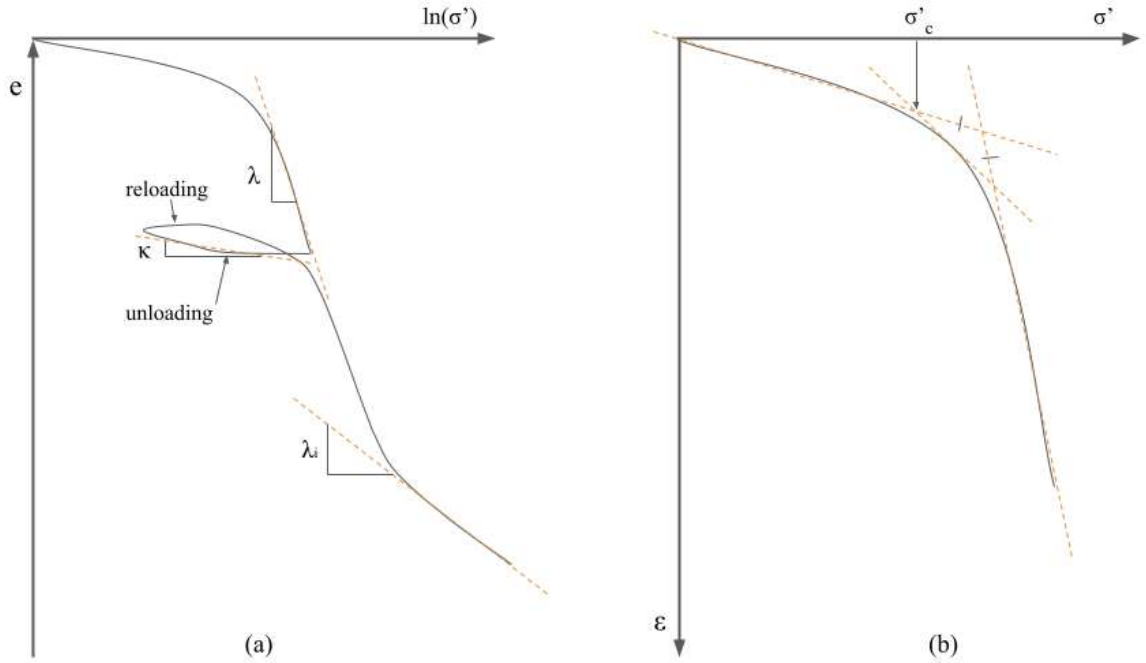

Figure 2.2: *Oedometer test (a) displaying compression, swelling and instrinsic compression indices and (b) displaying determination of pre-consolidation pressure according to Sällfors method (Sällfors, 2013).*

The stress history of soft soil is usually described in terms of the preconsolidation pressure σ_c' and can as well be determined through an oedometer test. The pre-consolidation pressure indicates the yielding point for a soil and is the transition from elastic to plastic behaviour (Olsson, 2010), see figure 2.2. The yielding point implies the previous maximum stresses the clay has experienced (Larsson, 1978). All stresses above this point induce a degradation of the bonds between particles and hence cause large deformations. With a pre-loading method it is possible to increase the preconsolidation pressure and hence increase the yielding point, which makes the soil less prone to deform when loaded, due to the already experienced large stresses.

From σ_c' the overconsolidation ratio (OCR) and Pre-Overburden Pressure (POP) can be evaluated, which are two different ways of describing the stress history. OCR and POP are determined from either the ratio or the difference between the preconsolidation pressure and pressure at rest, see equation (2.4). An OCR value around one implies a normal consolidated clay, whereas an OCR superior to 1.5 indicates an overconsolidated clay (Larsson, 2008). A dry crust clay is an example of an overconsolidated clay, which has subjected to high stresses caused by water and temperature fluctuations close to the ground surface.

$$OCR = \frac{\sigma_c^{'}}{\sigma_0^{'}}, \quad POP = \sigma_c^{'} - \sigma_0^{'} \tag{2.4}$$

The yielding point determined from an oedometer test is only valid for one-dimensional compression. An anisotropic multidimensional behaviour of soil is better described with a yield surface (Wood, 1990). Figure 2.3 displays a yield surface modelled in a triaxial stress space in terms of deviatoric stress, $q = \sigma'_1 - \sigma'_3$ and mean stress $p' = (\sigma'_1 + 2\sigma'_3)/3$. The yielding surface can be established through triaxial tests with varying stress paths or by mathematical models. The preconsolidation pressure corresponds to one point on the yield surface boundary, called yield locus (Wood, 1990). All stresses within the surface induce an elastic response while stresses on the surface boundary cause irrecoverable plastic deformations.

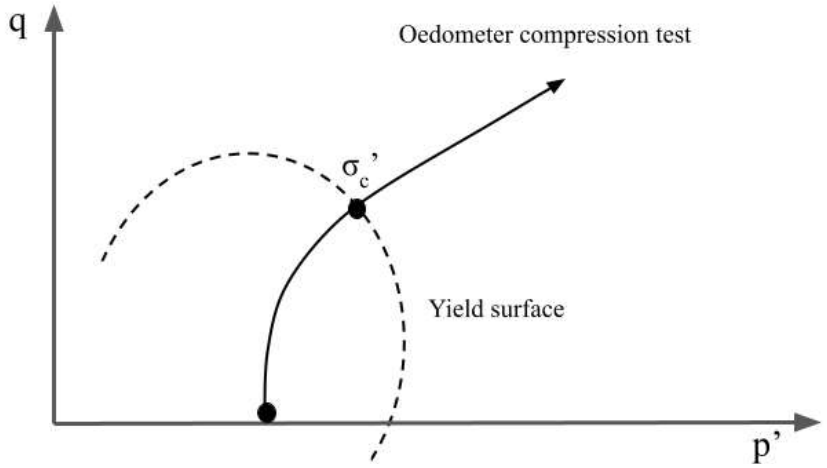

Figure 2.3: *Example of yield surface from triaxial test, with stress path from pure compression displayed with a solid line (figure modified from Wood, 1990).*

2.2 Failure mechanism and complex soil models

A yield surface is suitable for describing the serviceability soil behaviour of anisotropic deformations. However, the actual failure behaviour is often described by a failure criterion. The most basic and frequently used method is the Mohr-Coulomb failure criterion (Wood, 1990). If any stress condition induces a shear stress τ which intersects with the failure line, according to equation (2.5), the soil experiences a failure. The strength parameters are the effective cohesion c' and effective friction angle ϕ'.

$$\tau = |c' + \sigma'_1 \times tan(\phi')| \tag{2.5}$$

The stress path is described by a Mohr's stress circle with the principal compression main stresses σ'_1 ($\sigma'_{vertical}$) and σ'_3 ($\sigma'_{horizontal}$). One example of a failure stress state can be seen in figure 2.4, with constant horizontal stress and an increase of vertical stress, the Mohr circle expands in size until it touches the failure criterion (Sällfors, 2013).

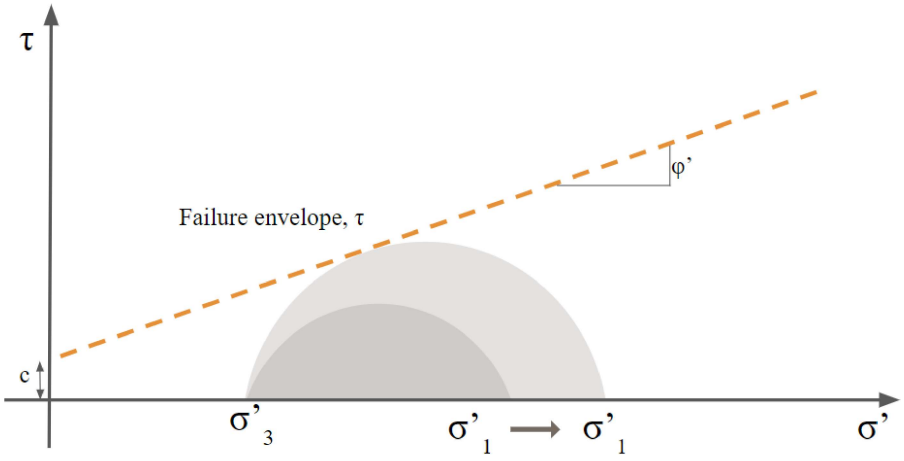

Figure 2.4: *Mohr-Coulomb compression shear failure: the area of the Mohr circle grows with the increasing difference between the principal stresses, until any point of the circle touches the failure envelope.*

Mohr-Coulomb failure can be transformed into the critical failure line M, used when modelling in a triaxial stress space (Wood, 1990). This assumes no cohesion at failure. For triaxial compression or extension the failure criteria is formulated according to equation (2.6).

$$M_c = \frac{6 \cdot \sin \phi'}{3 - \sin \phi'}, \quad M_e = \frac{6 \cdot \sin \phi'}{3 + \sin \phi'} \tag{2.6}$$

For saturated soils, such as clays with hydraulic conductivity, the short term failure criterion is better described with the undrained shear strength c_u (Wood, 1990). During undrained conditions, the shear strength is equal to the radius of the Mohr circle seen in figure 2.5. This is due to the fact that pore water takes up all the induced stresses from a momentarily increase of vertical stresses and the friction angle between the "unloaded" grains has no influence on the soil's strength.

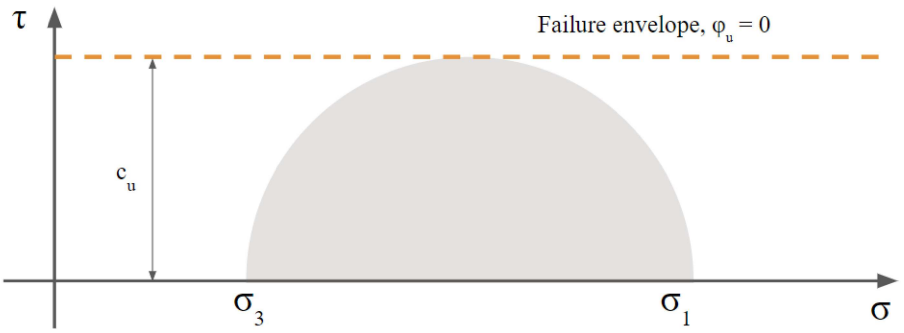

Figure 2.5: *Mohr-Coulomb failure criterion for undrained analysis, where* $\tau = c_u$.

The undrained shear strength, which is estimated through different laboratory and in-situ field tests, helps to understand the sensitivity of soils S_t. The sensitivity

is determined as the ratio between the undrained shear strength for natural and stirred soil (Larsson et al., 2007). Clays with high sensitivity are more likely to go to failure when disturbed due to the destructed bonds between particles.

Mohr-Coulomb failure module is a simplistic soil model since it does not consider anisotropy nor hardening behaviour of soil (Vogler, 2008). Mohr-Coulomb can be described as an elasto-perfectly plastic model and is suitable for stiffer soil materials such as friction soil or overconsolidated clay. More advanced soil models such as Modified Cam-Clay, S-CLAY1 and S-CLAY1S are developed with the concept of a combination of yield surface and failure mechanism to better accommodate for soft clay behaviour in finite element analysis. These models are further explained in chapter 4. See figure 2.6 for illustrations of elasto-perfectly plastic and elasto-plastic hardening material response.

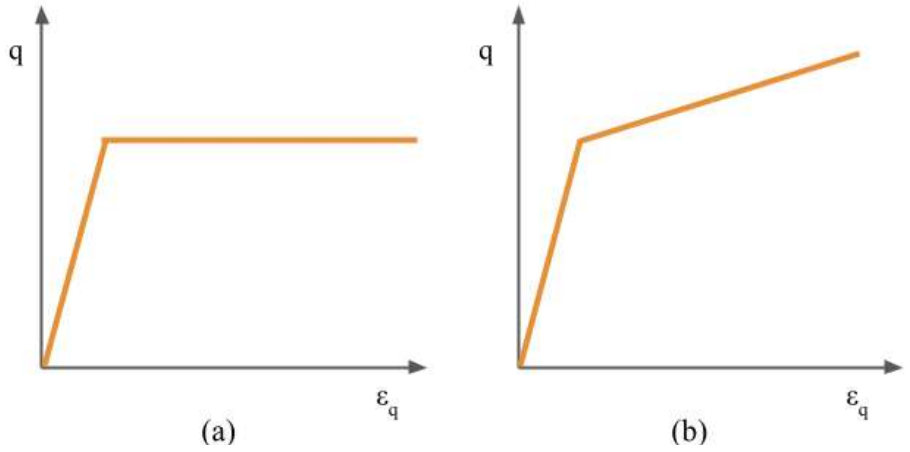

Figure 2.6: *Material response (a) elasto-perfectly plastic and (b) elasto-plastic hardening.*

3

Deep mixing in soft soils

Ground improvement measures are often necessary when constructing on soft soil. Different techniques can be utilised depending on the site specific conditions and soil properties (Chu et al., 2009). Deep mixing is a common soil strengthening method when constructing road and railway embankments due to the rapid construction time and the adaptability for various projects and sites (Larsson, 2006). A deep mixing binder, either in a dry or liquid state, is injected with the existing virgin soft soil to create a solid column with enhanced strength and decreased compressibility after hardening (Bruce, 2000). Dry binders are broadly used in Scandinavia (Larsson, 2006). The method is suitable for soft soils with a high natural moisture content above 30 %, in order to initiate the hardening reaction between the dry binder and the water in the soil (Russ, 2012). The binders which are further investigated in this thesis are quick hardening cement, Multicem and cement mixed with Slag Bremen.

3.1 SH cement

Cement is the most commonly used binder in the Nordic countries (Russ, 2012). It is produced by first burning limestone to calcium oxide powder (Soutsos and Domone, 2017), a process which produces heavy amounts of carbon dioxide emissions. Silicon dioxide is then added during the heating process to create cement. Quick hardening cement (hereinafter referred to as SH cement) has a slightly different chemical composition than ordinary cement, which increases the reaction rate (Soutsos and Domone, 2017).

3.2 Multicem

Multicem is a mixture of cement and cement kild dust, were the later is a by-product of the cement production (Lagerbeck, 2020). Even though the product has corresponding characteristics similar to cement, Multicem has in comparison a reduced amount of carbon dioxide emissions. Experiments on Multicem show a lower achieved strength and stiffness than specimens with Portland cement (Larsson, 2006). Therefore longer hardening time with more materials is to be expected.

3.3 Slag Bremen mixture

Slag is a by-product from steel production in Bremen, where it's taken from an iron melting furnace and is rapidly cooled and granulated to a fine powder (Soutsos and Domone, 2017). The slag powder can be used as a substitute for a portion of the cement to reduce the carbon dioxide emissions of a binder mixture. The chemical structure induces a slower reaction and has thereby a slower hardening rate compared to cement (Soutsos and Domone, 2017).

3.4 Installation procedure of deep mixed columns

The injection procedure is executed by a rotating hollow shaft, equipped with mixing blades, which screws its way down to a desired starting depth of the column. While the shaft is raised to the surface, the binder is injected and mixed with the soil to start the hardening process (Topolnicki, 2016). The injection procedure is illustrated in figure 3.1. Commonly used column diameters are 500, 600 or 800 mm and the required binder concentrations vary from 70 to 300 kg/m^3 depending on the type of soil and binder mixture (Larsson, 2006). Cement usually allows for a reduced binder concentration compared to other materials, like Slag Bremen mixture and Multicem.

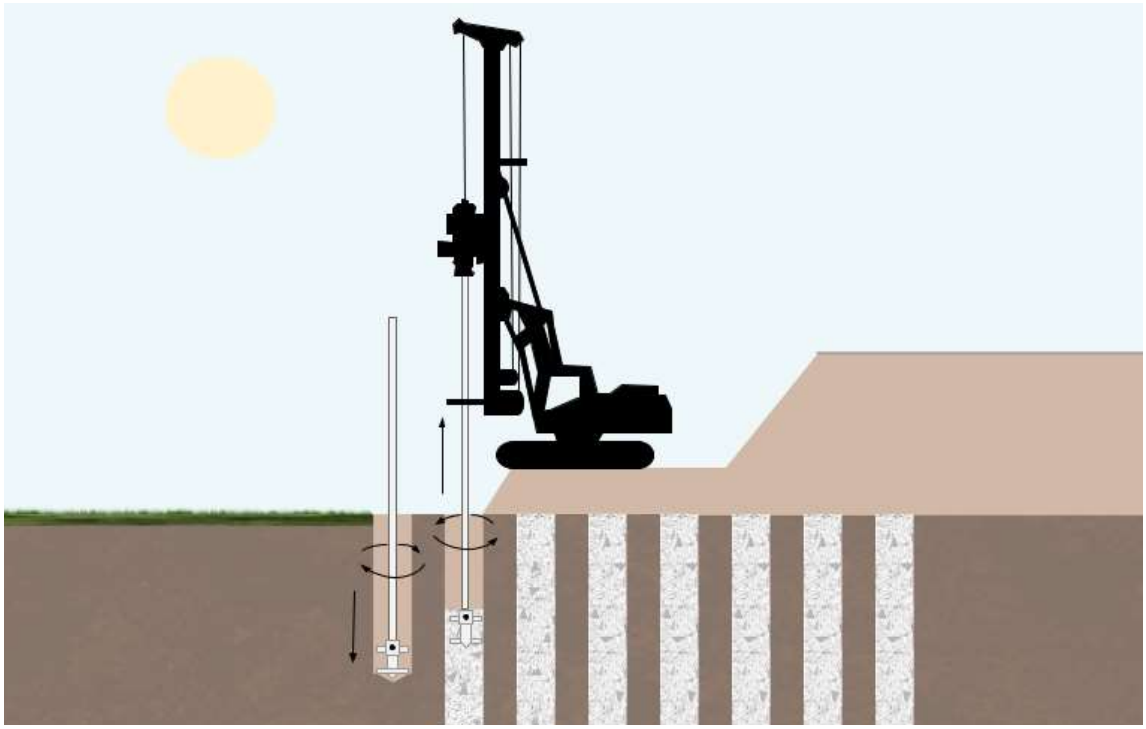

Figure 3.1: *Injection procedure of dry binders.*

The deep mixing method has some drawbacks. Even though laboratory experiments show promising strength results, the actual performance of the columns after in-situ

installation are difficult to ensure (Larsson, 2006). Soil's often in-homogeneous layering causes some uncertainties regarding the column performance, especially with possibilities of local weaknesses due to unsuccessful mixing. Deep mixing should therefore be combined with preloading of the soil, in order to increase the consolidation rate and reduce settlements. The columns can be injected as single columns or overlapping each other in a broad arrange of different patterns, depending on the site specific soil strengthening improvements, see figure 3.2. When deep mixing is used to decrease settlements and reduce the consolidation time, a triangular or grid pattern with a uniform c-c distance is often used (Larsson, 2006).

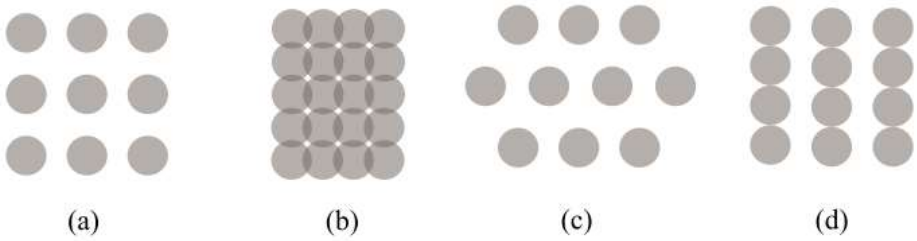

Figure 3.2: *Column arrangements; (a) grid pattern (b) block pattern (c) triangular pattern and (d) wall pattern.*

In zones where slope failure may occur for road embankments, the columns are often installed in block or wall patterns to increase stability (Larsson, 2006). Block stabilisation operates as one solid unit to increase the bending and shear strength. A block stabilisation may also prevent the influence of local weaknesses in columns from in-homogeneous mixing (Vogler, 2008). A minimum of 80 % of the soil surface is required to consist of columns to be regarded as a block stabilisation (Larsson, 2006).

3.5 Environmental impact of binders

With a life cycle assessment it is possible to compare the environmental impact between binders, by estimating the emitted carbon dioxide equivalents (CO_2-eq) during the life cycle of the material. The CO_2-eq is a comparison of emissions between different green house gases in terms of Global Warming Potential index. Global Warming Potential index describes the relative potency of a greenhouse gas, taking account of how long it remains active in the atmosphere (Cleveland and Morris, 2014). If a green house gas has two times the effect of global warming than carbon dioxide over a specific time span, the corresponding kg CO_2-eq are twice as large as the ones from carbon dioxide.

4

Constitutive material models

The deep mixing analysis is performed by using the finite element software Plaxis 2D. Numerical methods like finite elements are helpful when designing boundary value problems in both serviceability limit state and ultimate limit state (Vogler and Karstunen, 2008). Plaxis allows for calculating and simulating results of complex geotechnical geometries by adopting constitutive models. In this thesis the behaviour of clay is modelled with S-CLAY1S and deep mixed column material with MNhard model. Volume Averaging Technique simulates a two-dimensional model and adopts a smooth designing procedure.

4.1 Volume Averaging Technique (VAT)

Volume averaging is based on ideas of hierarchical systems of scale in nature and is a technique to smear out boundaries between different phases into one homogenised medium (Whitaker, 1999). Darcy's law is an example of this technique, which describes the flow of a fluid through a porous medium. Volume Averaging Technique (VAT) can be implemented in finite element models for deep mixed improved soil, where the two separate mediums are homogenised into one uniform soil layer (Becker and Karstunen, 2013), see figure 4.1.

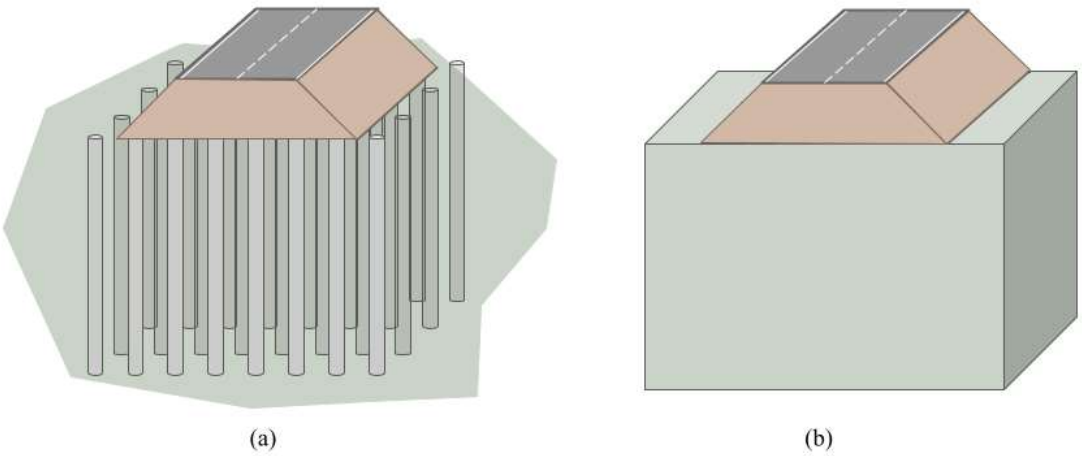

Figure 4.1: *(a) Discrete and (b) homogenised representation of the embankment problem (picture modified from Vogler, 2008).*

By modelling the columns in a uniform pattern and inducing a plain strain condition, the finite element problem can be reduced from a three-dimensional problem to two-dimensional and thus save computational time and costs (Vogler, 2008). An advantage with the VAT is the implementation of volume fractions of soil and columns in the global behaviour in the model. This facilitates an easy change of both geometrical and structural properties without remodelling the deep mixed columns. For the implementation of VAT, column patterns are restricted to an arrangement which supports plain strain conditions. This means that a uniform distribution of the columns are needed, for example rectangular, triangular and hexagonal patterns, see figure 4.2. Too few columns may violate the assumption of a homogenised medium and lead to inaccurate results (Vogler, 2008).

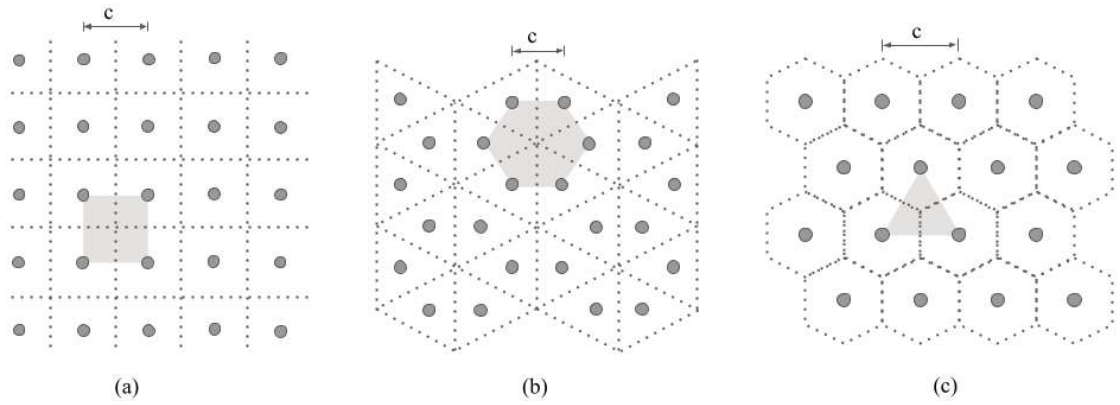

Figure 4.2: *Examples of uniform column patterns (a) rectangular (b) triangular and (c) hexagonal, modified from (picture modified from Vogler, 2008, p.143).*

Furthermore, all columns are assumed to be vertically installed. If modelling with an angle deviation, the columns need to have the same angle. VAT regards a perfect bonding which means equal vertical and shear displacement at the interface between the columns and the soil. Depending on the diameter and center to center distance of the deep mixed columns, the volume fractions can be calculated from the cross sectional areas of the columns and soil, figure 4.3, according to equation (4.1).

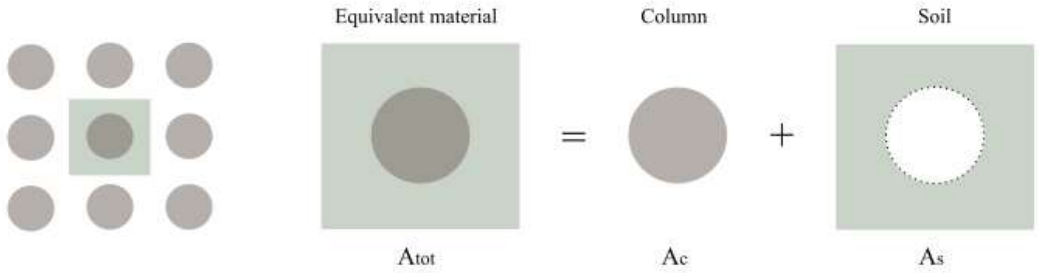

Figure 4.3: *Illustration of the homogenisation of the column and the soil material. (modified from Ayman Abed (personal communication)).*

$$\Omega_c = \frac{A_c}{A_{tot}} \quad , \quad \Omega_s = \frac{A_s}{A_{tot}} \tag{4.1}$$

With the volume fractions known, the equivalent total response of the homogenised material can be determined by the averaging rules for strain- $\dot{\boldsymbol{\varepsilon}}$ and stress rates $\dot{\boldsymbol{\sigma}}$, equation (4.2) and (4.3), respectively (Lee, 1993).

$$\dot{\boldsymbol{\varepsilon}}^{eq} = \Omega_s \, \dot{\boldsymbol{\varepsilon}}^{s} + \Omega_c \, \dot{\boldsymbol{\varepsilon}}^{c} \tag{4.2}$$

$$\dot{\boldsymbol{\sigma}}^{eq} = \Omega_s \, \dot{\boldsymbol{\sigma}}^{s} + \Omega_c \, \dot{\boldsymbol{\sigma}}^{c} \tag{4.3}$$

The individual material response is determined by total effective stress increments, equations (4.4) and (4.5). Where the material stiffness matrices for column $\boldsymbol{D}^c$ and soil $\boldsymbol{D}^s$ are the translation keys from strains to stresses, and are derived from their respective constitutive models.

$$(\dot{\boldsymbol{\sigma}}^{s})' = \boldsymbol{D}^{s} \, \dot{\boldsymbol{\varepsilon}}^{s} \tag{4.4}$$

$$(\dot{\boldsymbol{\sigma}}^{c})' = \boldsymbol{D}^{c} \, \dot{\boldsymbol{\varepsilon}}^{c} \tag{4.5}$$

The soft soil in this study is modelled by the elasto-plastic material model S-CLAY1S by Karstunen et al., 2005, which is suitable for predicting the plastic hardening behaviour of normal consolidated clay, since it accounts for anisotropy and change of interparticle bonding (Vogler, 2008). MNhard model is used for the deep mixed binder material, in order to capture the stress dependent stiffness of the columns. Each material's corresponding constitutive stiffens matrix are multiplied with the volume fractions, $\boldsymbol{S_1}^c$ and $\boldsymbol{S_1}^s$, and are assembled into one global equivalent stiffness matrix according to equation (4.6). The volume fraction is the relation between the soil and column strain increments.

$$\boldsymbol{D}^{eq} = \Omega_s \boldsymbol{D}^s \boldsymbol{S}_1^s + \Omega_c \boldsymbol{D}^c \boldsymbol{S}_1^c \tag{4.6}$$

VAT is implemented in Plaxis as an user defined soil model (UDSM) through a dynamic link library file (Vogler, 2008). The dynamic link library contains the two constitutional material models, S-CLAY1S and MNhard. Both material models exhibit non-liner behaviour with a stress dependent stiffness. In order for VAT to predict the stiffness matrices for each load corresponding stress, the load is applied in incremental steps. Stepsize is an optional parameter in VAT for strain application in sub-increments. According to Vogler (2008) stepsize is of minor importance for calculations in serviceability limit state. The finite element approximation is executed as an iteration procedure according to the scheme in figure 4.4.

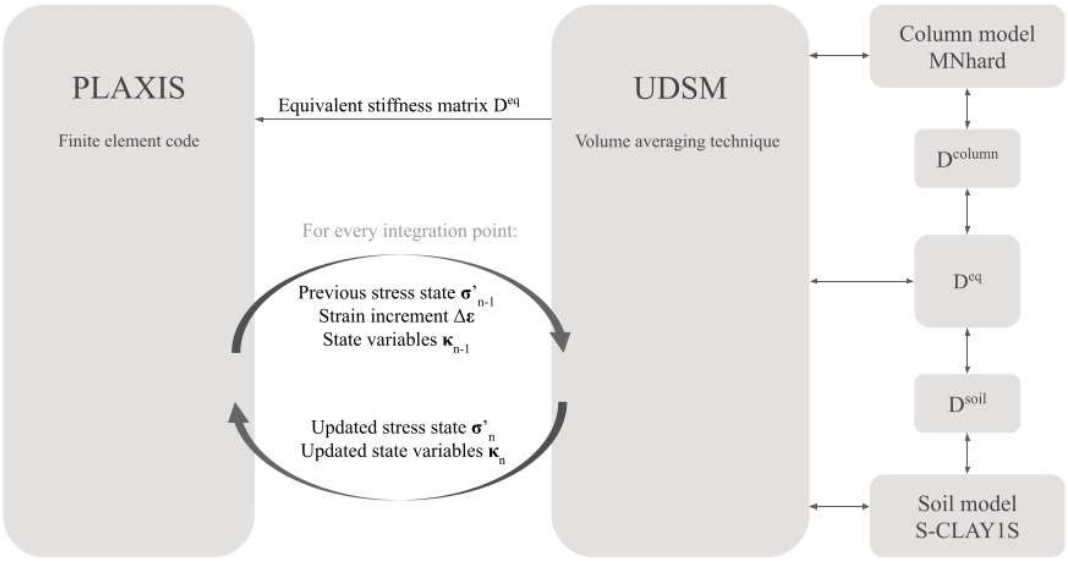

Figure 4.4: *Scheme of user defined soil model (UDSM) in Plaxis (modified from Vogler, 2008).*

4.2 S-CLAY1S

S-CLAY1S is a constitutive soil model used in finite element simulations to mimic the soil behaviour of normally consolidated clays in both serviceability deformation state and ultimate failure state (Vogler, 2008). The model is described by a yield surface, which is a sheared ellipsoid in the tree-dimensional stress space, derived from the function (4.7).

$$f = \frac{3}{2}\left[\{\boldsymbol{\sigma}_d - p' \cdot \boldsymbol{\alpha}_d\}^T\{\boldsymbol{\sigma}_d - p' \cdot \boldsymbol{\alpha_d}\}\right] - \left[M^2 - \frac{3}{2}\{\boldsymbol{\alpha}_d\}^T\{\boldsymbol{\alpha}_d\}\right]\left(p'_m - p'\right)p' = 0 \quad (4.7)$$

The S-CLAY1S model is an extension to Modified Cam-Clay and S-CLAY1. In addition to its precursor models, S-CLAY1S considers anisotropic behaviour of soil and degradation of interparticle bonding. The model incorporates three hardening laws. The first hardening law, equation (4.8), originates from Modified Cam-Clay and describes an isotropic elasto-plastic hardening behaviour of clay (Wheeler et al., 2003). The change of size of the yield surface p'_m depends on plastic volumetric strains. v is the specific volume and λ_i is the instrinsic compression index. An increase of the yield surface represents a soil hardening (Vogler, 2008).

$$\Delta p'_m = \frac{v \cdot p'_m}{\lambda - \kappa}\Delta\varepsilon_v^p \quad (4.8)$$

In figure 4.5 the yield surface is displayed with the critical failure line M, which depends on the effective friction angle. If the stress path intersects the yield locus

at the critical state line, plastic shear strains occurs which lead to failure (Vogler, 2008). The size of the yield surface, under constant volume, is assumed to depend on the volumetric strains. Therefore a larger effective friction angle and hence a steeper M-line only influence the shape of the surface.

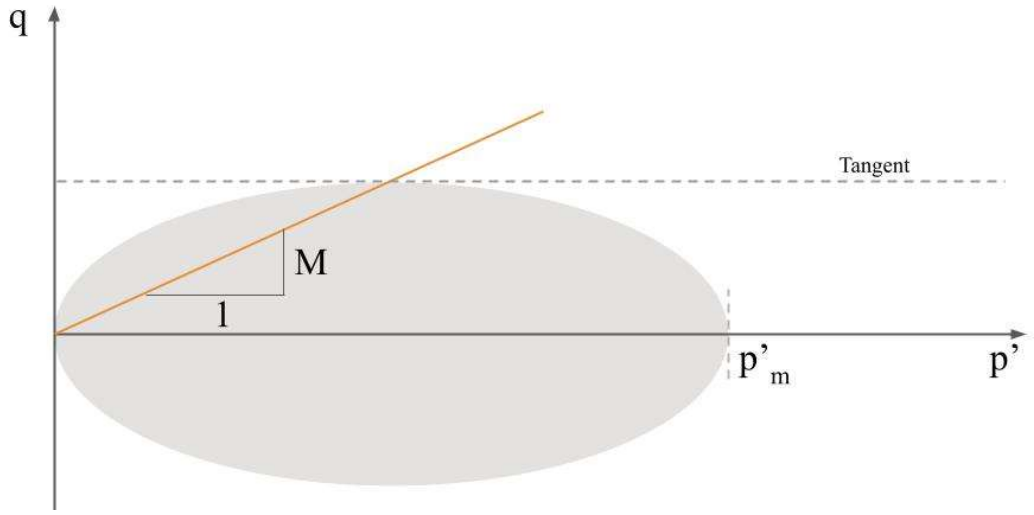

Figure 4.5: *Yield surface of Modified Cam-Clay model in the triaxial stress space.*

The second hardening law, equation (4.9) is introduced in the S-CLAY1 model by an inclination of the yield curve, describing the degree of plastic anisotropy $\boldsymbol{\alpha_d}$ (Karstunen et al. 2005), see figure 4.6.

$$\Delta\boldsymbol{\alpha}_d = \mu\left(\left[\frac{3\boldsymbol{\eta}}{4} - \boldsymbol{\alpha}_d\right]\langle\Delta\varepsilon_v^p\rangle + \beta\left[\frac{\boldsymbol{\eta}}{3} - \boldsymbol{\alpha}_d\right]\Delta\varepsilon_d^p\right) \tag{4.9}$$

The absolute effectiveness of rotation hardening μ is estimated from triaxial extension test but can also be calculated as an empirical value from equation (4.10) (Vogler, 2008).

$$\mu = \frac{(10\ldots20)}{\lambda} \tag{4.10}$$

The relative effectiveness of rotation hardening β can be calculated according to equation (4.11) and depends on the stress path η_{K0} and critical state variable M.

$$\beta = \frac{3(4M^2 - 4\eta_{K0}^2 - 3\eta_{K0})}{8(\eta_{K0}^2 - M^2 + 2\eta_{K0})} \tag{4.11}$$

The initial anisotropy is calculated from equation (4.12) and can be seen as a start value for a soil at rest.

$$\alpha_0 = \frac{\eta_{K0}^2 + 3\eta_{K0} - M^2}{3} \tag{4.12}$$

The stress ratio can be determined from formula (4.13), where ϕ'_{cv} is the friction angle at failure. For an embankment problem, ϕ'_{cv} is the same as the friction angle derived from laboratory testing.

$$\eta_{K0} = \frac{\sin \phi'_{cv}}{1 - \frac{2}{3} \sin \phi'_{cv}} \tag{4.13}$$

If the anisotropic parameters (α_0, μ and β) are set to zero the soil is assumed to be isotropic and the yield function is the same as for Modified Cam-Clay (Wheeler et al., 2003). The inclined yield surface has in addition to the Modified Cam-Clay two critical M-lines and the anisotropic behaviour induce different strengths, dependent on the magnitude of the effective compression stresses σ'_1 and σ'_3, see figure 4.6.

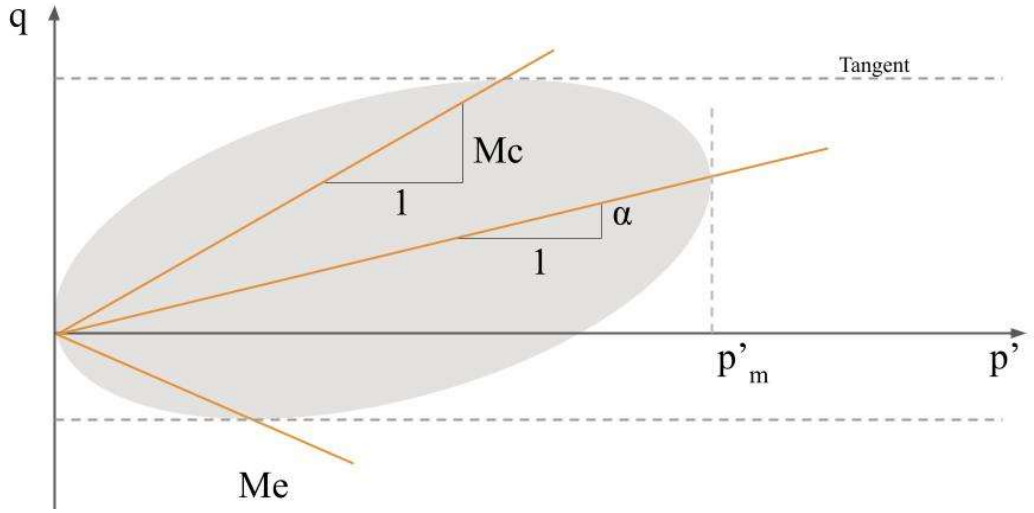

Figure 4.6: *Yield surface of the S-CLAY1 model in the triaxial stress space.*

The S-CLAY1S model considers degradation of interparticle bonding by introducing an instrinsic yield surface, representing a fully remoulded soil with reduced strength and stiffness (Vogler, 2008), see figure 4.7. The first hardening law is a modification of the one introduced in Modified Cam-Clay, now considering the size of the instrinsic surface, equation (4.14). The instrinsic yield surface corresponds to a fully plastified soil and is similar in both shape and inclination to the natural yield function (Karstunen et al., 2005).

$$\Delta p'_{mi} = \frac{v \cdot p'_{mi}}{\lambda_i - \kappa} \Delta \varepsilon_v^p \tag{4.14}$$

Equation (4.15) relates the natural yield surface, p'_m to the size of the yield surface of the instrinsic clay p'_{mi} depending on amount of bonding x.

$$p'_m = (1 + x)p'_{mi} \tag{4.15}$$

The third hardening law is formulated according to equation (4.16), and includes two new parameters a and b, representing the absolute and relative rate of degradation of bonding (Karstunen et al. 2005). According to Koskinen et al. (2002), Vogler (2008) and Wheeler et al. (2003) values for natural soft clays in northern Europe have been found around 8-11 and 0.2, for a and b respectively.

$$\Delta x = -ax\left(\left|\Delta\varepsilon_v^p\right| + b\left|\Delta\varepsilon_d^p\right|\right) \tag{4.16}$$

In total three new soil parameters a, b and x are added in the S-CLAY1S model compared to S-CLAY1. If x_0 is set to zero, no bonding exists and the natural yield surface will correlate with the instrinsic yield surface (Vogler, 2008).

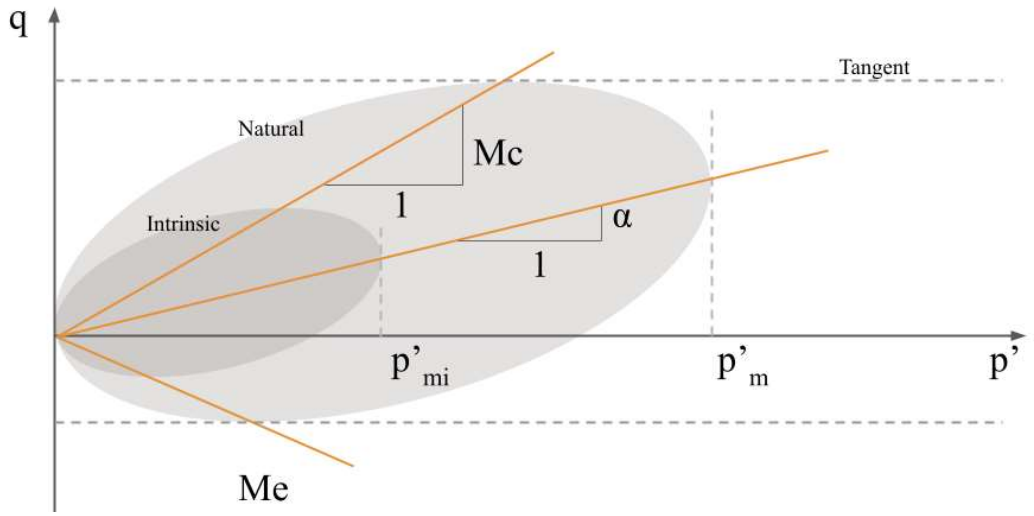

Figure 4.7: *Yield surface of the S-CLAY1S model in the triaxial stress space.*

The input parameters for the soil model, S-CLAY1S are summarised in table 4.1. Eight parameters describing the general behaviour of the soil, where either the OCR or POP value is chosen, and three parameters stating the initial soil conditions e_0, α_0 and x_0.

Table 4.1: *Input parameters for S-CLAY1S with required tests or equations.*

Type	Parameters	Description and unit	Required tests
Initial stress parameters	OCR	Overconsolidation ratio	Oedometer test (IL) alt. CRS test
	POP	Pre-Overburden Pressure [Pa]	Oedometer test (IL) alt. CRS test
	e_0	Initial void ratio	Index test
Conventional parameters	v'	Effective Poisson's ratio	Triaxial test
	λ_i	Instrinsic compression index	Oedometer test (IL) alt. CRS test
	κ	Swelling index	Oedometer test (IL) alt. CRS test
	M	Stress ratio at critical state in triaxial compression	Triaxial test alt. Equation (2.6)
Anisotropic parameters	α_0	Initial anisotropy	Triaxial test alt. Equation (4.12)
	μ	Absolute effectiveness of rotation hardening	Triaxial test alt. Equation (4.10)
	β	Relative effectiveness of rotation hardening	Triaxial test alt. Equation (4.11)
Destructuration parameters	x_0	Initial bonding	Estimated from sensitivity ($S_t - 1$)
	a	Absolute rate of destructuration	Back calculated from CRS and triaxial tests
	b	Relative rate of destructuration	Back calculated from CRS and triaxial tests

4.3 HNhard

MNhard model, developed by Benz, 2007, is implemented in VAT to capture the mechanical behaviour of deep mixed columns. The deep mixed column's vertical stiffness is highly dependent on the stress state in the horizontal direction, simulated in the model's nonlinear stress-strain performance (Vogler, 2008), see figure 4.8. MNhard includes a primary loading stiffness, an unloading and reloading stiffness and the Matsuoka-Nakai failure criteria. The Matsuoka-Nakai criteria predicts a smoother failure surface than the Mohr-Coulomb and is closer to the real failure behaviour of the column material, see figure 4.9. However, the failure criterion does not affect the results when designing in serviceability limit state (Becker and Karstunen, 2013).

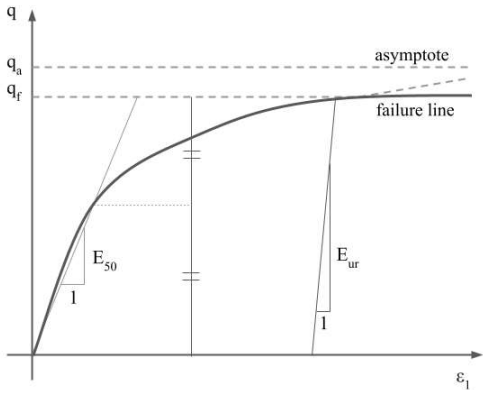

Figure 4.8: *Nonlinear stress-strain relationship in primary loading for a standard drained triaxial test (modified from Becker and Karstunen, 2013).*

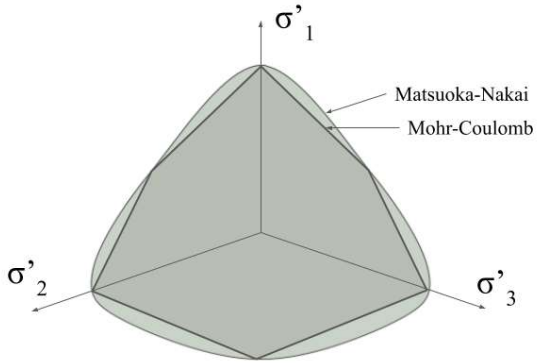

Figure 4.9: *Matsuoka-Nakai compared with the Mohr-Coulomb failure criterion in the octahedral plane (modified from Benz, 2007).*

The stress dependent Young's secant modulus for primary loading E_{50} can be calculated according to equation (4.17), where E_{50}^{ref} is the reference Young's modulus dependent on the reference confining stress p'_{ref} used in laboratory triaxial testing (Vogler, 2008). The stress dependent stiffness E_{50} is governed by the actual confining pressure σ'_3 in the soil. The stress dependency can be controlled by the power parameter m, which for dense sand and clay spans between 0.7-1.0. A low value of m means that the E_{50} becomes linear elastic, where the in-situ confining pressure gives small meaning for the stiffness. A value of one means that the stiffness is very sensitive to σ'_3. The purely elastic stress dependent Young's modulus for unloading and reloading E_{ur} can be estimated to 2.25 times larger than E_{50} (Vogler, 2008). For a road embankment, no unloading nor reloading will occur and the E_{ur} is of minor importance.

$$E_{50} = E_{50}^{ref}\left(\frac{c'\cos\phi' + \sigma'_3\sin\phi'}{c'\cos\phi' + p'_{ref}\sin\phi'}\right)^m \tag{4.17}$$

The asymptote of the maximum failure stress q_f is defined according to equation (4.18) where the relation to the quantity asymptote q_a equation (4.19), can be estimated by putting $R_f = 0.9$. The conservative value of 0.9 is suitable as a default value (Brinkgreve, 2002).

$$q_f = \frac{2\sin\phi'}{1-\sin\phi'}\left(c'\cot\phi' - \sigma'_3\right) \tag{4.18}$$

$$q_a = \frac{q_f}{R_f} \;\geq\; q_f \tag{4.19}$$

In the implementation of VAT, the shear modulus G is used instead of the compression modulus E as an input in parameter MNhard. The shear modulus is

determined based on the material isotropic relationship of Poisson's ratio according to equation (4.20).

$$G = \frac{E}{2(1+v')} \tag{4.20}$$

There are in total eleven input parameters for the constitutive model MNhard, table 4.2. The parameters are categorised into three strength parameters and seven stiffness parameters.

Table 4.2: *Input parameters in VAT for the constitutive column material, MNhard.*

Type	**Parameter**	**Description and unit**	**Parameter evaluation**
Strength parameters	c'	Effective cohesion $[Pa]$	Back calculated from laboratory test
	ψ'	Effective dilatancy angle [°]	Default value zero
	ϕ'	Effective friction angle [°]	Back calculated from laboratory test
Stiffness parameters	G_{ur}^{ref}	Reference shear modulus for unloading/reloading $[Pa]$	2.25 G_{50}^{ref}
	v'	Poisson's ratio [-]	Triaxial test
	m	Power of hyperbolic stress-strain law [-]	Back calculated from laboratory test
	p'_{ref}	Reference pressure for hyperbolic stress-strain law $[Pa]$	Equals the confining pressure σ'_3
	R_f	Ratio of failure stress to hyperbolic asymptote [-]	Default value 0.9
	f_t	Allowable tensile stress $[Pa]$	Default value zero
	G_{50}^{ref}	Reference modulus for primary loading $[Pa]$	Equation (4.17)
	Sk.B	Skempton-B parameter for undrained loading [-]	Default value one

5

Embankment study

The embankment study was based on soil data from a road project between Bie and Alberga. The soil at the site consists of a 1.5 meters thick layer of peat on top of 7.5 meters deep clay with varved layers of sand. Due to lack of laboratory tests on virgin peat, a dry crust was used instead to mimic a common geologic layering in Sweden. Beneath the clay there is a five meters layer of friction soil down to bed rock. The embankment is 20 meters wide at the top and 6 meters high, with a slope gradient of 1:2. As an initial building phase, the clay was enhanced with deep mixed columns. Thereafter the embankment was constructed in five stages, where each layer was left to preload the soil for a few days before constructing the next layer. The vertical settlements were then studied for a consolidation period of 40 years.

5.1 Geometry, mesh and boundary conditions

Due to symmetry, only half of the embankment was modelled, see figure 5.1. To ensure no boundary impact the model was extended 28 meters from the embankment toe and included two meters of the friction layer. For further details of boundary conditions and model boundary sensitivity, see appendix A. A plane strain finite model was used with 15-node triangular elements. Soil layers were assumed and modelled as horisontal layers. The 7.5 meters deep sandy clay was simplified to be a homogeneous clay, discretised into two layers. VAT was implemented beneath the embankment, where the two soil models S-CLAY1S and MNhard were homogenised to represent the deep mixed strengthened clay. S-CLAY1S was selected for the virgin unmixed clay and Mohr-Coulomb model was used for the embankment fill, the friction soil and the dry crust. From the geotechnical study, the ground water table was evaluated at 1.5 meters below ground surface.

A mesh convergence study regarding deformations dependency was performed, to ensure an optimal mesh discretisation which yielded low computational time while ensuring accurate results. In appendix B the final mesh and results from the convergence study of deformations are presented. For the analysis a fine mesh was chosen with refinements in the bottom layer of the embankment as well as in the soil layers in the deep mixing zone.

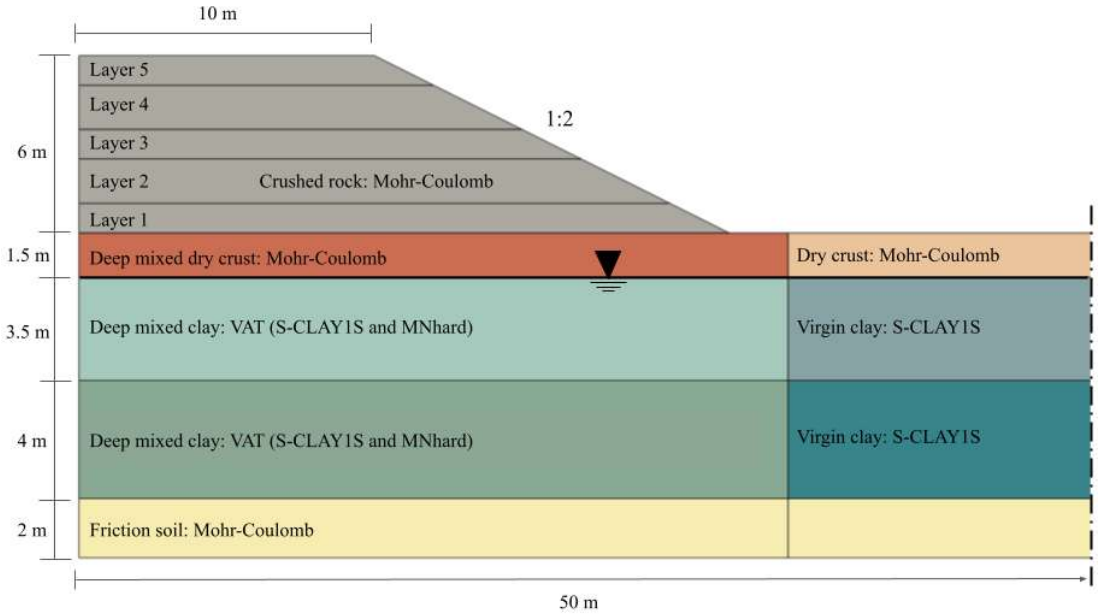

Figure 5.1: *Geometry of the model displaying embankment and soil layers.*

5.2 Derived clay parameters for S-CLAY1S

Since the soil behaviour varies with depth, a dicretisation into two soil layers was chosen for the analysis. In order to represent the deformation behaviour for the two layers, oedometer tests at 4 and 8 meters, respectively, were evaluated. From laboratory and field tests the basic soil constants were gathered and summarised in appendix C. From oedometer tests with constant rate of strain, the preconsolidation in terms of OCR/POP and the permeability were analysed and determined. The permeability was assumed to have the same value in the vertical and horizontal direction. The compression and swelling indices were initially estimated from the CRS-curves, according to figure 2.2. Because neither unloading nor reloading were implemented in the oedometer tests, κ was assumed to be equal to the slope of the elastic behaviour.

The slope of critical state line M, the anisotropic constants β and α_0 are all dependent on the friction angle. The effective friction angle could not be determined since no triaxial test were performed, and M, β and α_0 had to be back calculated and evaluated from an undrained triaxial test in Plaxis' soil test tool. The back calculation derived the constants which yielded the same undrained shear strength in the test tool as the one estimated from the geotechnical study at 4 and 8 meters depth. Figure 5.2 displays the compression stress path hitting the yield locus for different friction angles at 4 meters depth. The undrained shear strength corresponds to the maximum shear stress $((\sigma'_1 - \sigma'_3)/2)$ (Larsson et al., 2007). An equal calibration for the clay at 8 meters below ground surface together with derived parameters for the chosen friction angles can be seen in appendix D.

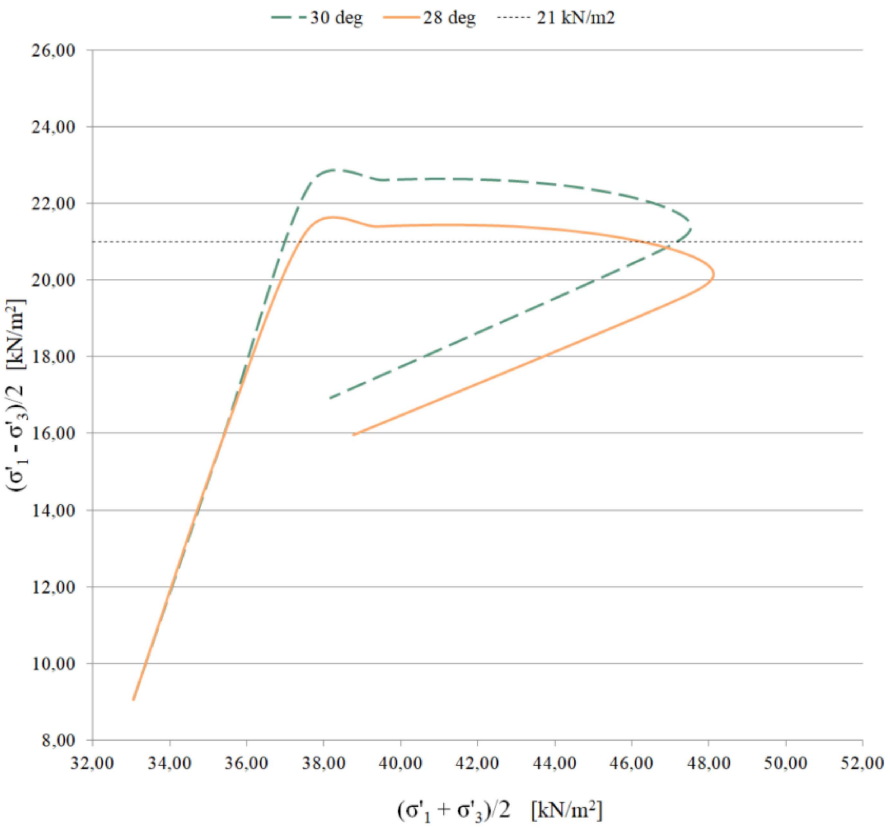

Figure 5.2: *Evaluation of friction angle for clay at 4 meters depth, an c_u of around 21 kN/m^2 at this depth is evaluated from the geotechnical study.*

The constants λ_i and κ have a major impact on the deformations and were therefore refined in the soil test tool in Plaxis. The refinements were executed by back calculating the constants, in order to derive a soil response which corresponded to the CRS-curves from the laboratory tests. The POP-value is governing the transition from elastic to elasto-plastic behaviour and was therefore set to the same value as the preconsolidation pressure at the corresponding sample depth. The destruction parameters a and b influence, along with λ_i, the remoulded clay's stiffness and were adjusted in the aforementioned range described in chapter 4.2 to correlate to the soil response at high stresses. Poisson's ratio ν' was set to 0.15 according to Larsson et al., 2007.

The sensitivity S_t from the laboratory tests were unreasonably large, probably caused by the influence of sand in the clay which gave unreasonable shear strengths after remoulding. Initial bonding x_0, dependent on the sensitivity, was therefore readjusted to match the soil response. Figure 5.3 displays the CRS-curve together with the refined curve from Plaxis soil test tool at 4 meters depth. In appendix D, the calibrated results of soil constants κ and λ at a depth of 8 meters are illustrated. Since the deformation behaviour is highly dependent on the Pre-Overburden Pressure, the POP values were slightly modified and a sensitivity analysis was performed and summarised in appendix E. All constants used in the soil model S-CLAY1S for the two clay layers are summarised in table 5.1.

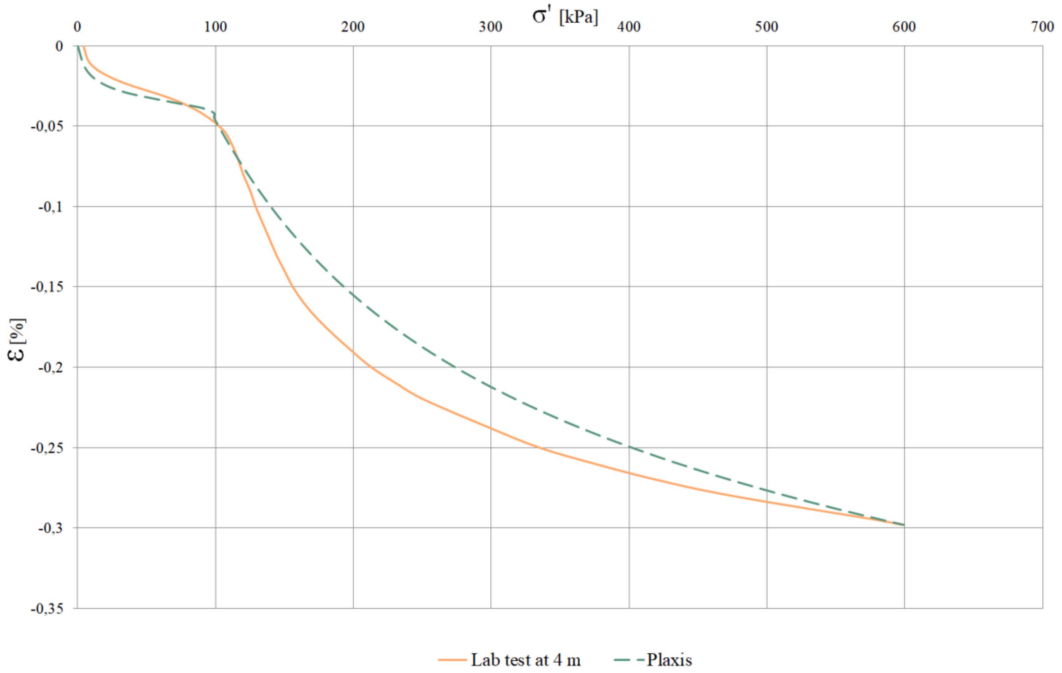

Figure 5.3: *Evaluation of parameters λ_i, κ and x_0 with Plaxis' soil test tool and compared with CRS test at 4 meters below ground surface.*

Table 5.1: *Input parameters in Plaxis for soil model S-CLAY1S. Either the POP or the OCR value can be used in the S-CLAY1S model.*

Type	Parameter	Description	Unit	Clay layer 1	Clay layer 2
General parameters	Drainage type	-	-	Undrained (A)	Undrained (A)
	γ_{unsat}	Effective unit weight	$[kN/m^3]$	17	18
	γ_{sat}	Buoyant unit weight	$[kN/m^3]$	17	18
	κ	Swelling index	-	0.016	0.014
	v'	Poisson's ratio	-	0.15	0.15
	λ_i	Instrinsic compression index	-	0.16	0.141
	M	Stress ratio at critical state	-	1.113	1.199
	μ	Absolute effectiveness of rotation hardening	-	21	38
	β	Relative effectiveness of rotation hardening	-	0.654	0.758
	a	Absolute rate of destructuration	-	10	10
	b	Relative rate of destructuration		0.2	0.2
	(OCR)	Overconsolidation ratio	-	1.54	1.22)
	POP	Pre-Overburden Pressure (compression negative value)	[Pa]	-37	-40
	e_0	Initial void ratio	-	1.4	1.12
	α_0	Initial anisotropy	-	0.426	0.457
	x_0	Initial bonding	-	6	4
	$Stepsize$	Optional parameter, implementation of strain in sub-increments	-	0	0
Flow parameters	k_x	Horizontal permeability	$[m/day]$	3.85E-4	8.56E-5
	k_y	Vertical permeability	$[m/day]$	3.85E-4	8.56E-5
Initial stress parameters	$k_{0,x}$	Lateral earth pressure	-	0.52	0.45
	$k_{0,z}$	Lateral earth pressure	-	0.52	0.45

5.3 Derived column parameters for MNhard

The clay and the dry crust under the embankment were improved with deep mixing columns in square patterns. Three binders in various concentrations were investigated.

- SH cement
- Multicem
- Slag Bremen mixture

Experiments have been performed on clay specimens mixed with the binders in concentrations of 100 and 150 kg/m^3. After 28 days of hardening, the deep mixture specimens were uniaxially compressed to determine the reference stiffness modulus E_{50}^{ref}. With Plaxis' soil test tool, the reference stiffness was used to replicate the compression curve from the laboratory results. Figure 5.4 displays Plaxis' compression curve of Slag Bremen mixture compared with the experimental data. A collection of the laboratory results and comparisons for each binder can be seen in appendix F.

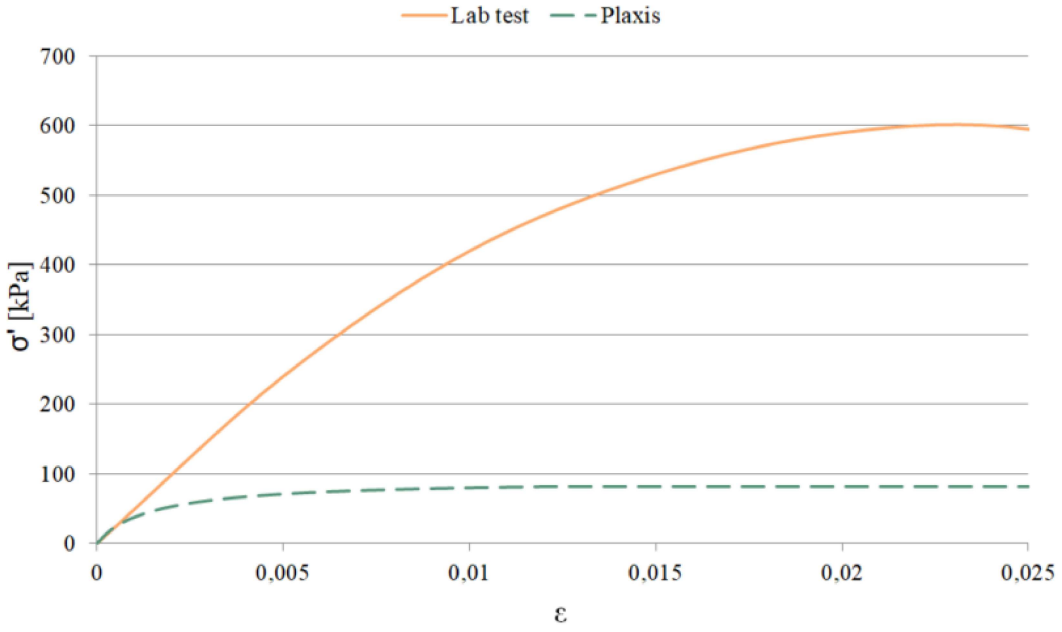

Figure 5.4: *Comparison of lab results from uniaxial compression test and soil test tool in Plaxis for binder material Slag Bremen mixture with 150 kg/m^3.*

The compression tests were uniaxial and therefore the reference confining stress was assumed to be zero, whereas the MNhard model is optimal for a triaxial stiffness response with a confining pressure above zero. The ultimate strength achieved in the laboratory test could not be obtained in the soil test tool and hence the curves couldn't be properly compared. The strength parameters; friction angle, dilatancy angle and cohesion were initially determined according to empiric values from Karstunen et al., 2005. Because the peak strength could not be obtained, these

values showed little importance to the stiffness in the soil test tool and were therefore the same for all binder recipes. However, as the analysis only focused on vertical deformations, the stiffness in terms of E_{50}/G_{50} was the important behaviour to evaluate. The stress dependency m was refined in the Plaxis' soil test tool in order to match the curves. A summary of all input parameters for MNhard model for respectively binder are presented in table 5.2.

Table 5.2: *Model input parameters for MNhard in VAT; three binders with different concentrations 100/150 kg/m^3.*

Type	Parameter	Description	Unit	SH cement	Slag Bremen mixture	Multicem
Strength parameters	c'	Effective cohesion	[Pa]	16	16	16
	ψ'	Effective dilatancy angle	[°]	0	0	0
	ϕ'	Effective friction angle	[°]	35	35	35
Stiffness parameters	G_{ur}^{ref} (100/150)	Reference shear modulus for unloading/reloading	[Pa]	39700/76000	12300/32900	32000/40200
	v'	Poisson's ratio	-	0.2	0.2	0.2
	m	Power of hyperbolic stress-strain law	-	0.7	0.7	0.7
	p'_{ref}	Reference pressure	[Pa]	0	0	0
	R_f	Ratio of failure stress	-	0.9	0.9	0.9
	f_{tens}	Allowable tensile stress	[Pa]	0	0	0
	G_{50}^{ref} (100/150)	Reference modulus for primary loading	[Pa]	17700/33800	5450/14600	14200/17900
	Sk.B	Skempton-B parameter for undrained loading	-	1	1	1

5.4 Empirical parameters for embankment fill, friction soil and dry crust for Mohr-Coulomb

The crushed stone fill in the embankment and the gravely moraine materials are drained friction soils and could hence be modelled with Mohr-Coulomb soil model. The soil constants were determined from empiric studies concluded by SGI (Larsson, 2008). Lateral earth pressure coefficient K_0 for both crushed rock and sand was calculated with respect to friction angle with Jaky's formula. For friction soils, an assumption of zero dilatancy is the most conservative case.

The dry crust was as well represented with Mohr-Coulomb model, as it can be seen as an overconsolidated soil with higher stiffness due to its exposure to large stresses induced from water and heat fluctuations. All parameters were determined as empirical values from Larsson, 2008, except for the permeability which was chosen to be equal with the permeability for the upper clay layer. The Young's modulus was increased for the enhanced dry crust under the embankment, through a rough estimation according to equation (5.1). Parameter E_{DC} represents the Young's modulus for the virgin dry clay and was empirically determined to be 10000 kN/m^2. E_{50}^{ref} depended on the binder which was currently analysed. All input parameters for crushed stone fill, friction soil and dry crust are summarised in table 5.3.

$$E_{Dc.enhanced} = E_{50}^{ref} \cdot \Omega_c + E_{DC} \cdot (1 - \Omega_c) \tag{5.1}$$

Table 5.3: *Parameters for embankment fill, friction soil and dry crust in Mohr-Coulomb model.*

Type	Parameter	Description	Unit	Crushed rock	Friction soil	Dry crust
General parameters	Drainage type	-	-	Drained	Drained	Drained
	γ_{unsat}	Effective unit weight	$[kN/m^3]$	18	12	17
	γ_{sat}	Buoyant unit weight	$[kN/m^3]$	21	19	17
Stiffness parameters	E'	Young's modulus	$[kN/m^2]$	50E3	30E3	10E3 or Eq. 5.1
	v'	Effective Poisson's ratio	-	0.35	0.3	0.15
Strength parameters	c'_{ref}	Cohesion	$[kN/m^2]$	2	2	20
	ϕ'	Effective friction angle	[°]	45	37	30
	ψ'	Effective dilatancy angle	[°]	0	0	0
Flow parameters	k_x	Horizontal permeability	$[m/day]$	1	1	0.385E-3
	k_y	Vertical permeability	$[m/day]$	1	1	0.385E-3
Initial stress parameters	$k_{0,x}$	Lateral earth pressure	-	0.29	0.3982	0.5
	$k_{0,z}$	Lateral earth pressure	-	0.29	0.3982	0.5

5.5 Construction phases

A sensitivity analysis was performed on final deformations with varying duration of embankment construction; 90, 180 and 240 days, in order to investigate how the construction time influenced the deformations after 40 years, see figure 5.5. The sum of deformations during and after construction were the same between the three cases, however a longer construction time accumulated a bigger portion of the deformations before the opening of the road. A construction time of 90 days were chosen, the most conservative case but yet a feasible time frame for the construction of a road embankment.

The deformation analysis consisted of a number of calculation steps in order to capture the soil behaviour during construction and road service life. The first step initialised the pore pressure and state parameters of the virgin soil with the K_0 value. The user defined soil model including VAT was then imported from the dynamic link library file. This was followed by the simulation of the deep mixing enhancement by replacing the untreated virgin clay with a VAT layer. Simultaneously, the dry crust under the embankment was strengthened by increasing the Young's modulus according to formula (5.1).

The embankment was constructed by adding one layer of the fill material at a time. Each layer was constructed for one day and afterwards the soil was permitted to consolidate for a number of days in order to simulate a preloading measure. After the first and second layer the soil consolidated for 15 days. After the third and fourth layer the consolidation period was 30 days. All building phases accumulated a total construction time of around 90 days. As a final analysis step, the fifth and

final layer was added, displacements were reset to zero and a consolidation analysis was performed for a time period of 40 years. This last step simulated the change in deformations from the opening of the road until 40 years of service life. A thorough summary of the construction phases can be seen in appendix G.

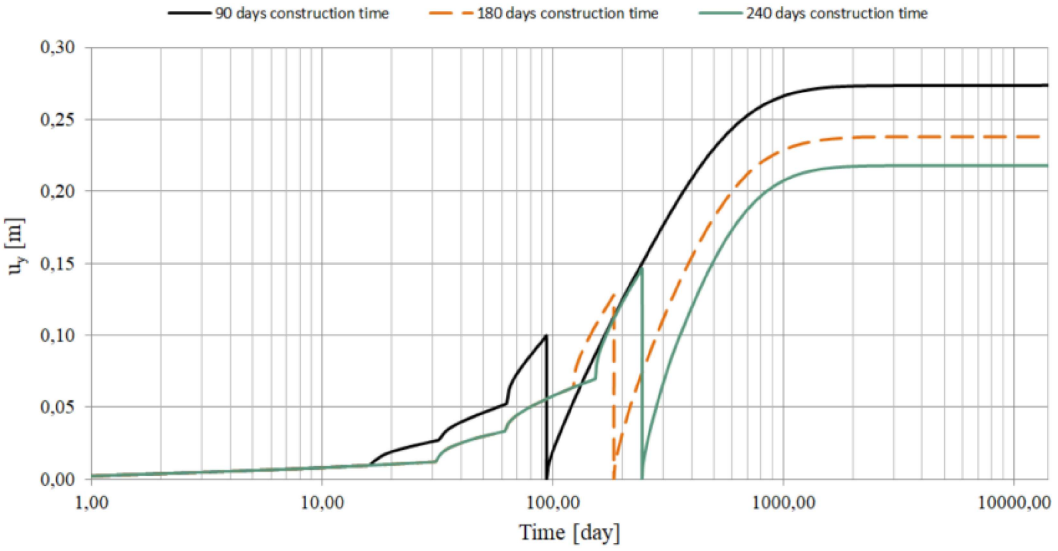

Figure 5.5: *Comparison of final deformations dependent on different construction phases of 90, 180 and 240 days respectively. Binder mixture Slag Bremen 150 kg/m^3 with a volume ratio of 22 %. Control point; at the center line under the embankment.*

5.6 Iteration process of volume ratio

In order to evaluate the binders and their respective soil enhancement performances, settlement analyses were performed for the different column stiffnesses. For each binder a design optimisation was achieved by iterating the volume ratio of the columns until the deformation requirements were fulfilled. To obtain a reasonable volume ratio with respect to feasibility, Ω_c was updated in integer steps until the settlement in the embankment top reached a value smaller than 300 mm after 40 years. With optimised volume ratio the center to center distance of the columns were calculated according to equation (5.2), valid for squared column patterns. The relation between volume ratio and center to center distance for the three most commonly used column diameters of 500, 600 and 800 mm is displayed in appendix H. Through the assumption of a uniformly deep mixing distribution, the center to center distance were converted to number of columns needed in the soil enhancement zone.

$$\Omega_c = \pi \frac{d^2}{4 \cdot c^2} \tag{5.2}$$

5.7 Assessment of environmental impact

As a final step in the analysis; $kg\ CO_2$-eq per meter road section were estimated in the life cycle assessment tool Carbon Cost by Sweco Sweden AB, based on the Swedish Transport Administration's climate model (Trafikverket, 2020). In the analysis the following life cycle stages were included: raw material supply, product transport, manufacturing and the construction on site, such as diesel combustion from the installation machines of the deep mixed enhancements. Included stages are highlighted in figure 5.6. The emissions from construction on site were estimated to 1.39 $kg\ CO_2$-eq per meter deep mixed column (Trafikverket, 2020). However, transportation of the material to the construction site was not included in the tool. Input parameters for the assessment were column diameter and average length, number of columns and binder concentration. The functional unit used to compare the different column binders was $kg\ CO_2$-eq per meter road embankment.

Product			Construction		Use stage							End of Life				Benefits and loads beyond the system boundary
A1	A2	A3	A4	A5	B1	B2	B3	B4	B5	B6	B7	C1	C2	C3	C4	D
Raw material supply	Transport	Manufacturing	Transport	Construction	Use	Maintenance	Repair	Replacement	Refurbishment	Operational energy use	Operational water use	Demolition	Transport	Waste processing	Disposal	Re-use, recovery and recycling potential

Figure 5.6: *Overview of a complete life cycle assessment. Included stages in the analysis are highlighted in grey.*

Table 5.4 displays the accumulated emissions from raw material supply, transportation and manufacturing. The values were gathered from the producers environmental product declarations in appendix I.

Table 5.4: *Carbon dioxide equivalents for each binder.*

Binder	**Carbon dioxide equivalents** [$kg\ CO_2$-eq/kg material]
SH-cement	775
Multicem	396
Slag Bremen mixture*	225

*A mixture which contains 80 % Slag Bremen and 20 % cement.

5.8 Control points

Results of vertical settlements and pore pressures were derived from control points according to figure 5.7. Point (A) is located at the symmetry line at the embankment top, in this point post-construction vertical deformations were extracted to analyse settlement requirements. In point (B), located at the symmetry line precisely under the embankment, the vertical deformations during the whole construction process were investigated. Point (C) is located in the zone where the greatest excess pore pressures exists, and graphs of pore water fluctuations were extracted from this point.

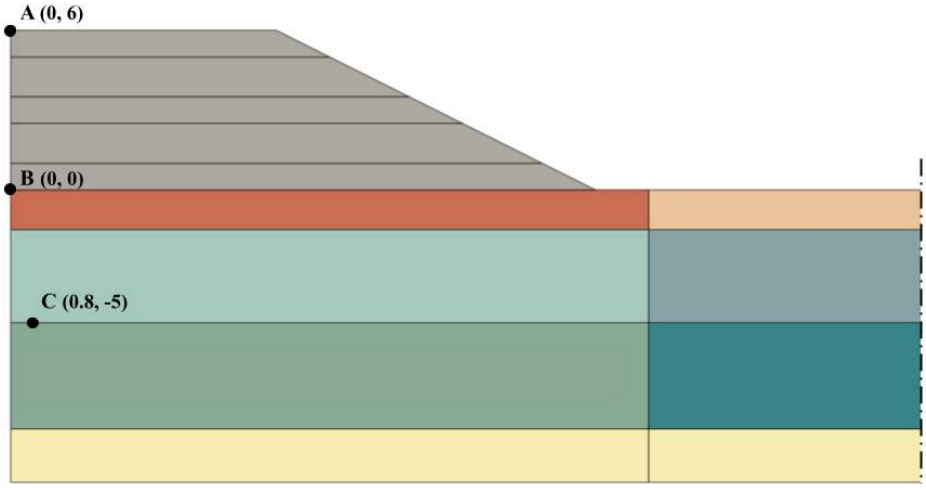

Figure 5.7: *Control points for deformations in (A) and (B) at center line. Control point for excess pore pressure in (C).*

6
Results

The material optimisation and the environmental emissions were based on a construction time of around 90 days and a consolidation analysis of 40 years for the three investigated binders with varying concentrations of 100 and 150 kg/m^3. Analyses of SH cement with a concentration of 150 kg/m^3 resulted in numerical failure and was therefore excluded in the study. All extracted results are valid for half the embankment.

6.1 Volume ratio optimisation

From the volume ratio optimisation; nearly identical deformations were obtained for all binders with a final vertical settlement of 270 mm in control point A (figure 6.1). The deformations converged around 1500 days which corresponds to 4 years. Slag Bremen mixture with 100 kg/m^3 exhibited the greatest difference in stiffness compared to the other binders and the deformation curve slightly differed from the others in appearance.

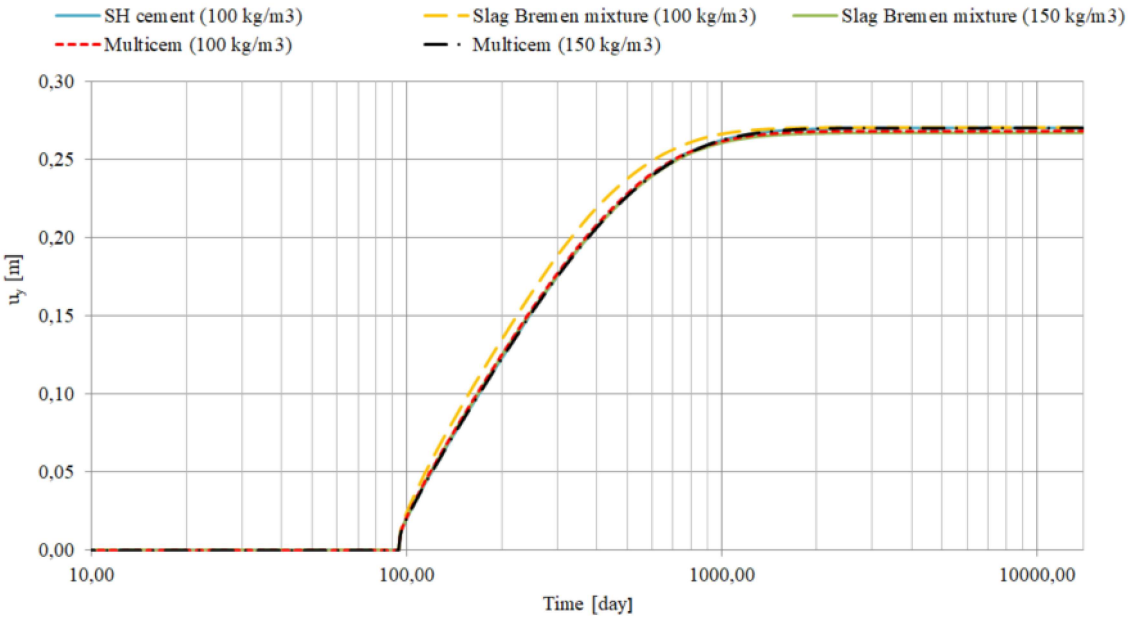

Figure 6.1: *Change in vertical deformations after construction until 40 years of service life. Control point (A) top of the embankment.*

The optimisation process resulted in a variation of volume ratios between 22 % and 28 %, see table 6.1. Binders with higher stiffness allowed for a lower volume ratio. A difference in stiffness of 3000 kPa resulted in only one percentage point variation in volume ratio. The low stiffness of Slag Bremen mixture with a concentration of 100 kg/m^3 yielded a prominent volume ratio of 28 %.

Table 6.1: *Volume ratios required to achieve the settlements demands, concluded for the binders and their corresponding stiffnesses.*

Type of binder	**Amount of admixture** $[kg/m^3]$	$\mathbf{G_{50}^{ref}}[kPa]$	**Volume ratio** [%]
SH cement	100	17700	22
	150	-	-
Slag Bremen mixture	100	5450	28
	150	14600	23
Multicem	100	14200	23
	150	17900	22

Vertical deformations between the top and the bottom of the embankment had a difference of 10 mm. Final deformations under the embankment converged at 260 mm, see figure 6.2. The deformations during construction were the largest for the Slag Bremen mixture with 100 kg/m^3 compared to the other binders. During the road service life, equally large deformations were yielded for all binders, with their corresponding required volume ratios according to table 6.1. The consolidation period between construction phases allowed for a tendency of deformation convergence. A deformed mesh after 40 years consolidation can be seen in appendix J.

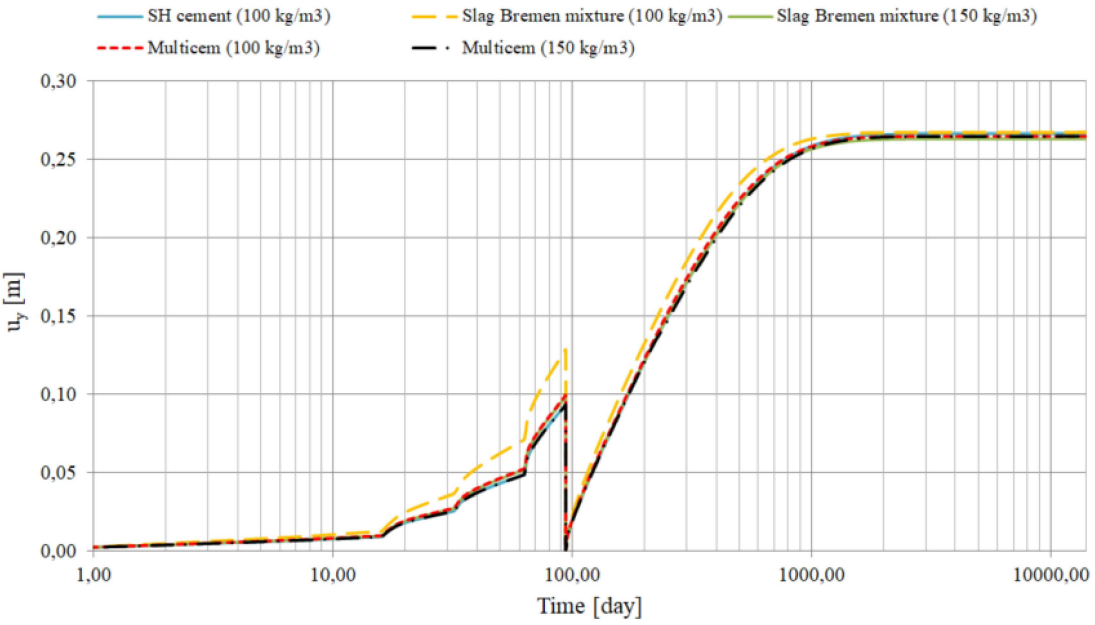

Figure 6.2: *Vertical deformations for all binder mixtures with their required volume ratios. Control point (B), bottom of the embankment. Deformations are reset after 94 days.*

The pore pressure behaviour coincided with the convergence of deformations at each construction stage. After the construction of a layer, the pore pressures initially increased and then started to diminish during the consolidation period between construction phases (figure 6.3). The curves of pore pressures and settlements exhibited close similarities in shape from the opening of the road, around 90 days, until 40 years of service life.

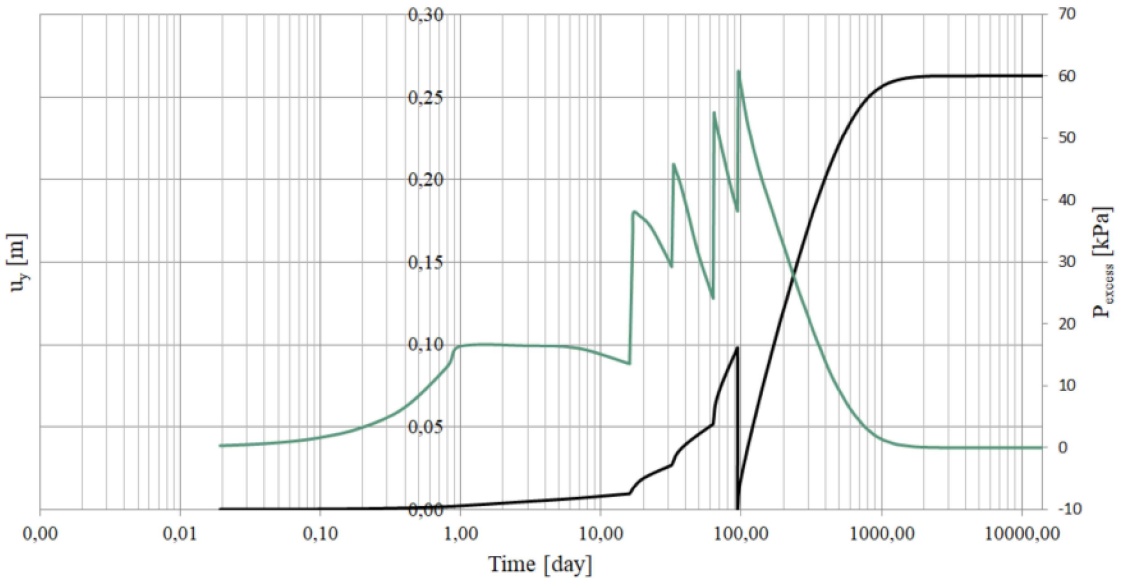

Figure 6.3: *Excess pore pressure compared to the deformations from the Bremen 150 kg/m^3-analysis. Excess pore pressure are extracted at control point (C), between the two clay layers and deformation analysis from control point (B).*

6.2 Environmental impact for different binders

In appendix H the converted center to center distances and number of columns are summarised with respect to the diameters of 500, 600 and 800 mm. One percentage point variation in volume ratio yielded insignificant difference in column arrangements. Slag Bremen mixture with 100 kg/m^3, regardless of the diameter, resulted in the lowest carbon dioxide equivalents per meter, which is 70 % less than for SH cement, see figure 6.4. SH cement generated by far the largest emissions of green house gases in all diameter classes, as an example approximately twice the $kg\ CO_2$-eq per meter compared to Multicem with 150 kg/m^3. Mutual trends are that the diameters have low impact on the emissions and that binders with concentrations of 150 kg/m^3 yielded greater $kg\ CO_2$-eq than corresponding binders with concentrations of 100 kg/m^3.

Figure 6.4: *Carbon dioxide equivalents per meter embankment for the different binders with respect to binder concentration [kg/m^3] and column diameters [mm].*

7
Discussion

An initial assumption was that the difference in stiffness would result in a greater divergence of the volume ratios between the binders. Nevertheless, all binders achieved the deformation requirement of maximum 300 mm after 40 years in a close range of low volume ratios. The results show that the difference in stiffness has small impact on volume ratio when the consolidation period of the soil is considered during the construction phase of the embankment. For instance, the Slag Bremen mixture with 100 kg/m^3 experiences the highest deformations during construction, but nevertheless shows very similar deformations after 40 years compare to the other binder mixtures.

Even though the Slag Bremen mixture with 100 kg/m^3 has the largest volume ratio, it produces the lowest $kg\ CO_2$-eq per meter road. SH cement has by far the largest environmental emissions, 70 % more than Slag Bremen mixture and nearly twice as much emissions than Multicem. The high stiffness of SH cement is not favourable enough to compensate for the high carbon dioxide emissions from raw material extraction and production. Some further outcomes are that a higher concentration of binder leads to greater emissions with a negligible increase in performance. When comparing the effect of column diameter on $kg\ CO_2$-eq, the emissions exhibit insignificant differences. The center to center distance are theoretical values. If they were to be adjusted to integer values feasible for construction, other green house gas emissions would be yielded.

Certain factors challenge the validity of the results in a general aspect; the specific soil conditions on site is decisive for the outcome of the results and the model is only representing one embankment section and cannot be representative for the whole road. The most suitable mixing recipe in this study is therefore not guaranteed to be valid for another project. Further controls in terms of differential settlements and stability are required in order to validate Slag Bremen mixture as the binder material with the lowest $kg\ CO_2$-eq.

7.1 Critical reviewing of the material, assumptions and choices

The duration of the embankment construction is noticed to have a major role for the deformation behaviour. The sensitivity analysis shows that even though the sum of all deformations reaches an equal value, a longer construction period accumulates

greater deformations during the embankment construction. This in turn, leads to less deformations during the 40 years consolidation period and hence required lower volume ratios.

The main obstacle for the use of advanced constitutive models is the amount of required parameters. In order to implement models as S-CLAY1S laboratory data of both one- and multi- dimensional stress conditions are required. A lack of these tests leads to deficient geo-mechanical information and empirical values had to be used instead. Without any triaxial tests available for clay, several strength parameters were cumbersome to predict for S-CLAY1S. However, the strength constants are not as important in a deformation analysis like this, but have yet a substantial role in the shape and behaviour of the yield surface. In addition to CRS-tests, incremental loading would be preferable for more trustworthy values for the compression behaviour in soil, as small changes of the conventional and the initial stress parameters were noticed to lead to large differences in results. An example of this is the Pre-Overburden Pressure, where small changes of the POP value gave several cm in differences of the final deformations. Apart from this, the organic soil layer of peat had to be excluded due to the lack of performed oedometer and triaxial tests. Furthermore, the S-CLAY1S model is representing the behaviour of a homogeneous clay. Whereas the clay at site has varving layers of sand, which is dubious to implement with lack of laboratory data. This could have been the cause of unreasonable initial high x_0-values. Based on the discussion regarding all the uncertainties, further calibration with the help of more laboratory test would be preferable. This is not a liability for the models. It is instead a recommendation to gather extra thorough soil data from site, to be able to implement these accurate and helpful soil models in the FE-analysis.

In order to decrease the number of derived clay parameters for S-CLAY1S and hence save time, the clay was discretised into only two homogeneous layers. The majority of the soil parameters vary with depth, such as Pre-overburden Pressure, compression and swelling index and permeability. A choice of two clay layers results in a model which most probably is representative of the real soil behaviour. Additional soil layers may not yield more accurate results.

The failed resemblance between the laboratory and Plaxis' curves for the MNhard model were a major discussion during the thesis work. The compression tests on the enhanced soil specimens were executed without any horizontal pressure. Whereas MNhard predicts the stress sensitive stiffness as a function of the confining pressure from the neighboring soil. The peak strength achieved in the laboratory test could not be obtained in the soil test tool and hence the full stress-strain curve could not be captured in the MNhard model. However, the stiffness response in MNhard was deemed sufficient when analysing the columns in serviceability limit states. In addition, the failed resemblance could have resulted in an overestimation of the stiffnesses, which may have been the cause of the numerical failure of SH cement with 150 kg/m^3. The exclusion of SH cement 150 kg/m^3 is believed to not affect the final results in any way, as 150 kg/m^3 had more environmental impact than 100 kg/m^3.

The comparison of the binder performance is based on data describing the strength and stiffness growth of the binder recipes after 28 days. However, both Multicem and the Slag Bremen mixture are expected to require longer hardening times before the maximum strength and stiffness are obtained.

7.2 Future studies

From the results and discussions some future studies are recommended to further compare the different binder types, and to receive deeper knowledge about deep mixing performance for long term consolidation analysis.

A broader comparison could be executed with both several other deep mixing recipes and stabilisation methods. It would also be interesting to perform several studies of other projects to obtain a more general picture of how more environmentally friendly binder recipes compare with ordinary cement. Unconventional and new techniques are often more expensive and labour intensive. Therefore it would be relevant to compare emissions with costs, both for construction and maintenance, in order to put the comparison in a more practical construction context.

The final deformations and hence the volume ratios were found to be sensitive to how long the consolidation period were allowed to prolong between each embankment stage. A future study of how much the construction time affects the long term consolidation behaviour and final deformations would be very interesting. How fast can the embankment be built with the less amount of binder materials possible? How would varying construction times affect the $kg\ CO_2$-eq? Could the embankment be constructed in such a way that the deep mixing enhancement becomes redundant? In a study like this, the hardening rates from the different binders would be interesting to include. What limitations in terms of construction time would the hardening rates result in?

Due to limitations in the current formulation of VAT, this thesis' main focus were on vertical deformations. In addition, creep behaviour is not considered and all long-term deformations may not have been captured. Further studies which include stability resistance of slope failure together with creep settlements are needed in order to fully validate the performance of the binder recipes. What effect would this have on the required volume ratios? For example, would block stabilisation, i.e volume ratios of 80 %, be necessary to ensure sufficient stability?

This study does not focus on a whole life cycle assessment. For example, transportation of material to the specific site is not included which is a crucial factor for the total emissions induced from road constructions. What outcome would this have for the more environmentally binders, where higher concentrations and hence more material is often needed in the deep mixing columns?

8

Conclusion

Since the cement production is a heavy source of green house gas emissions a vital key for a sustainable construction sector is to implement new material solutions which have lower carbon footprint, but still mimicking the material characteristics of cement. This thesis aimed to investigate the vertical settlement performance of three deep mixing binders with the finite element software Plaxis 2D, incorporating Volume Averaging Technique. Further, a simplified life cycle assessment allowed to compare the $kg\ CO_2$-eq per meter road embankment between the three analysed binders; SH cement, Multicem and a mixture of 80 % Slag Bremen and 20 % Portland cement.

Volume Averaging Technique as a numerical technique is a powerful tool for the deep mixing optimisation process and permits a thorough comparison of the geotechnical performance between the different binders. However, the reliability of the method is only ensured if the required laboratory tests are available. This is a strong illustration of the importance of executing all the necessary site investigations depending on which calculation procedure is the most optimal for the specific project.

Within the scope of the thesis and with the aforementioned limitations in mind, the conclusions of the results are; when implementing the consolidation period during the construction of the embankment, the difference in stiffness has a small impact on the volume ratios. Even though the Slag Bremen mixture has the highest volume ratio, it yields the lowest $kg\ CO_2$-eq per meter embankment of the three investigated alternatives - with 70 % less than SH cement. Furthermore, Multicem exhibits a similar stiffness to SH cement, however the generated $kg\ CO_2$-eq per meter road section from Multicem are 50 % less compared to the more conventional binder - an indication of the benefits associated with performing life cycle assessments for material choices.

References

Augustesen, A., Liingaard, M., & Lade, P. V. (2004). Evaluation of Time-Dependent Behavior of Soils. *International Journal of Geomechanics*, *4*(3), 137–156. https://doi.org/10.1061/(asce)1532-3641(2004)4:3(137)

Becker, P., & Karstunen, M. (2013). *Volume averaging technique in numerical modelling of floating deep mixed columns in soft soils.*

Benz, T. (2007). *Small-Strain Stiffness of Soils and its Numerical Consequences.*

Brinkgreve, R. (2002). Plaxis finite element code for soil and rock analyses.

Bruce, D. A. (2000). *An Introduction to the Deep Soil Mixing Methods as used in Geotechnical Applications* (technical report). Office of infrastructure Research and Development. McLean.

Chu, J., Varaksin, S., Klotz, U., & Mengé, P. (2009). *Construction processes* (Volume 4). https://doi.org/10.3233/978-1-60750-031-5-3006

Cleveland, C. J., & Morris, C. (Editors). (2014). *Dictionary of energy* (2nd edition). Elsevier.

Karstunen, M., Yildiz, A., & Krenn, H. (2005). Effect of Anisotropy and Destructuration on Behavior of Haarajoki Test Embankment. *International Journal of Geomechanics*, *5*(2), 87–97. https://doi.org/10.1061/(asce)1532-3641(2009)9:4(153)

Lagerbeck, T. (2020). Multicem. Retrieved May 4, 2021, from https://www.cementa.se/sv/multicem

Larsson, R. (1978). *Basic behaviour of Scandinavian soft clays* (technical report Number 4). https://doi.org/10.1016/0148-9062(78)91256-1

Larsson, R. (2006). *Djupstabilisering med bindemedels- stabiliserade pelare och massstabilisering* (technical report).

Larsson, R. (2008). *Jords egenskaper* (technical report Number 5).

Larsson, R., Sällfors, G., Bengtsson, P.-E., Alén, C., Bergdahl, U., & Eriksson, L. (2007). *Skjuvhållfasthet - utvärdering i kohesionsjord* (technical report). Swedish Geotechnical Insitute. Linköping.

Lee, J.-S. (1993). *Finite element analysis of structured media* (Doctoral dissertation). Swansea University.

Olsson, M. (2010). *Calculating long-term settlement in soft clays* – (technical report). Gothenburg.

Rodgers, L. (2018). Climate Change: The massive C02 emitter you may not know about. https://www.bbc.com/news/science-environment-46455844

Russ, J. C. (2012). *Ground improvement* (A. Bell & K. Kirsch, Editors; Third Edit). Taylor & Francis Group.

Sällfors, G. (2013). *GEOTEKNIK* (5TH). Cremona Förlag.

Soutsos, M., & Domone, P. (2017). *Construction Materials : Their nature and behaviour* (5th edition). Taylor & Francis Group. https://ebookcentral.proquest.com

Topolnicki, M. (2016). General overview and advances in Deep Soil Mixing. *XXIV Geotechnical Conference of Torine*, (February 2016), 1–30.

Trafikverket. (2020). Klimatkalkyl – infrastrukturens klimatpåverkan och energianvändning i ett livscykelperspektiv. https://www.trafikverket.se/tjanster/system-och-verktyg/Prognos--och-analysverktyg/Klimatkalkyl/

Vogler, U. (2008). *Numerical Modelling of Deep Mixing with Volume Averaging Technique* (Doctoral dissertation).

Vogler, U., & Karstunen, M. (2008). Application of volume averaging technique in numerical modelling of deep mixing. *Geotechnics of soft soils: Focus on ground improvements* (2009th edition, Pages 189–195). Taylor & Francis Group.

Watts, J. (2019). Concrete: the most destructive material on Earth. https://www.theguardian.com/cities/2019/feb/25/concrete-the-most-destructive-material-on-earth

Wheeler, S. J., Näätänen, A., Karstunen, M., & Lojander, M. (2003). An anisotropic elastoplastic model for soft clays. *Canadian Geotechnical Journal*, *40*(2), 403–418. https://doi.org/10.1139/t02-119

Whitaker, S. (1999). *Theory and Applications of Transport in Porous Media* (technical report Number 1).

Wood, D. M. (1990). *Soil behaviour and critical state soil mechanics*. Cambridge University Press. https://doi.org/10.1201/9781351255400-1

A

Boundary conditions

This appendix contains the boundary conditions for the model together with a sensitivity analysis of boundaries. Because of the permeable and stiff gravely moraine the bottom boundary for groundwater flow is open and is restricted from horizontal and vertical movements, see figure A.1. Groundwater boundary at the symmetry line is closed and the right vertical boundary and the top boundary is open. Vertical boundaries are restricted from horizontal movements and the top boundary is free to move in any direction.

Figure A.2 illustrates the vertical deformations at symmetry line of the model. Horizontal displacements at the top of the ground surface are presented in figure A.3. The analysis is performed on Slag Bremen mixture with a concentration of 150 kg/m^3. The two figures display that the models exhibits no deformations at the right and bottom border, the model is determined to have a sufficient size for capturing all the results.

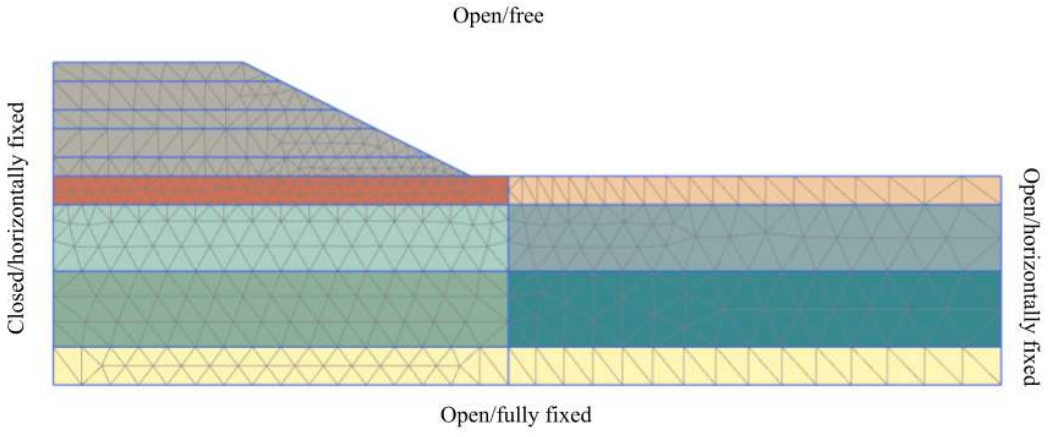

Figure A.1: *Boundary conditions; deformations and groundwater flow*

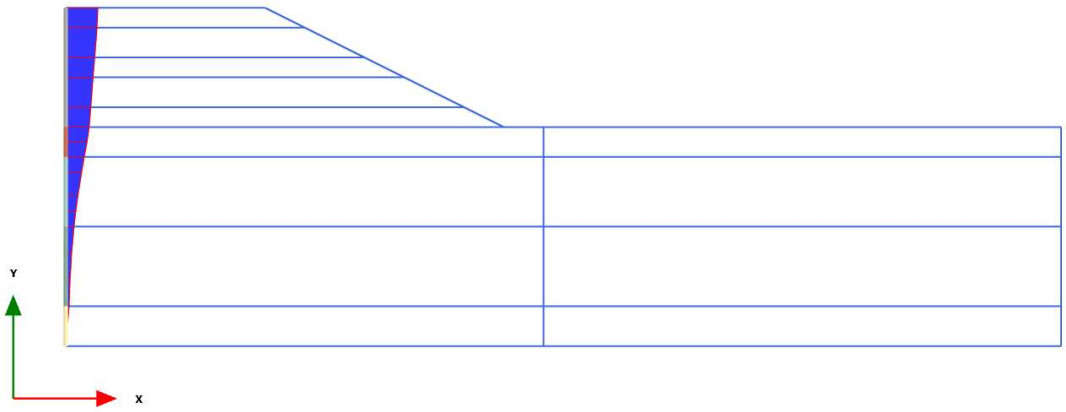

Figure A.2: *Deformation with depth at symmetry line of the model. Slag Bremen mixture with 150 kg/m^3.*

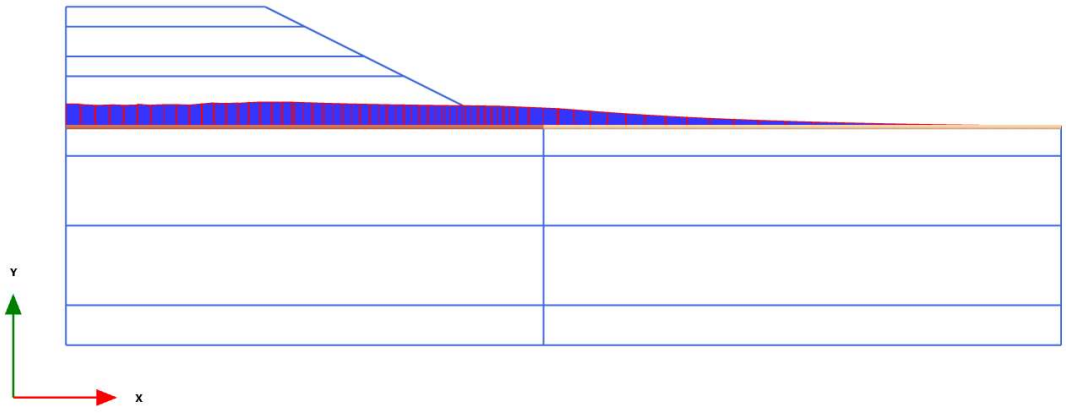

Figure A.3: *Horizontal deformations of Slag Bremen mixture with 150 kg/m^3, directly under the ground surface.*

B

Mesh sensitivity

In this appendix, a mesh sensitivity analysis is concluded. A convergence study is performed on the vertical deformations extracted from point at the center line, under the embankment (figure B.1). A mesh sensitivity is performed with coarse, medium, fine and very fine mesh quality with local refinements under the embankment. The deformations converges for a fine mesh size with refinements according to figure B.2. The model with final mesh size used for the analysis is presented in figure B.3.

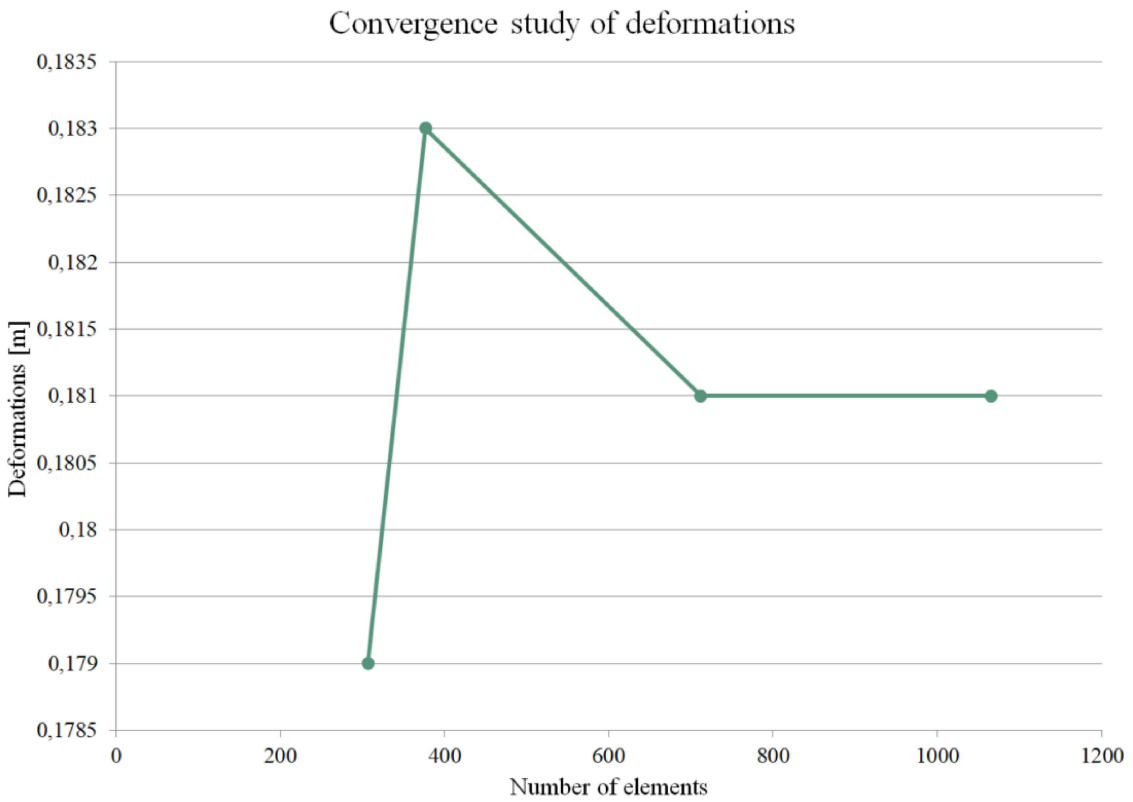

Figure B.1: *Convergence study of deformations with number of element on x-axis and deformations in [m] on y-axis. Graph representing deformations for coarse, medium, fine and very fine mesh size.*

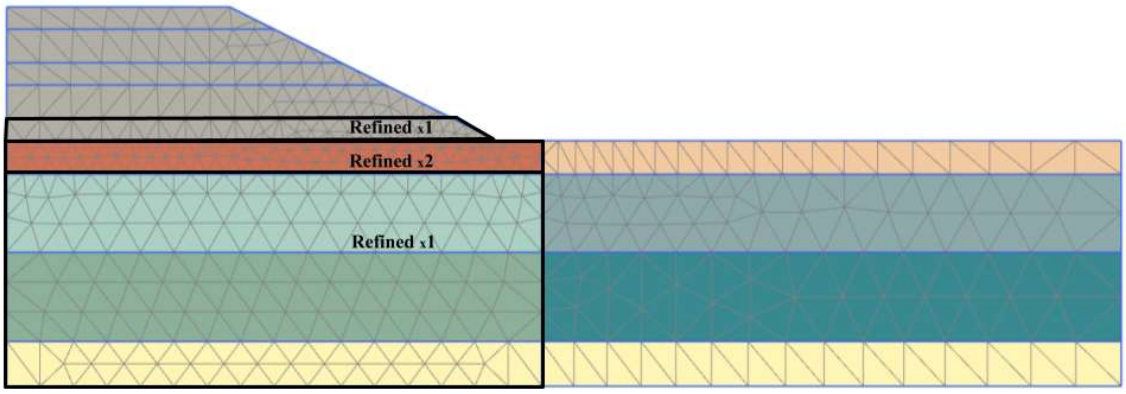

Figure B.2: *Fine mesh with refinements under in the first layer of the embankment and in the soil under the embankment.*

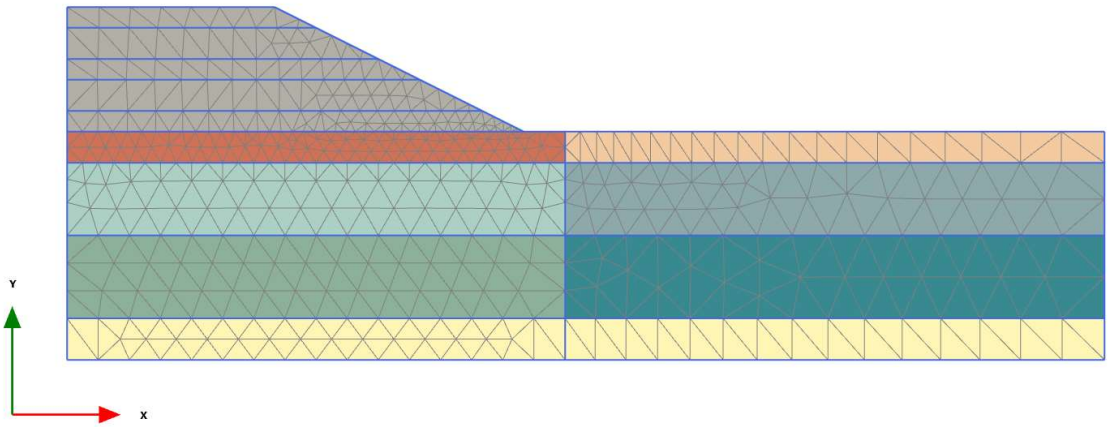

Figure B.3: *Fine mesh size used in the analysis.*

C

Compilation of soil parameters from geotechnical study

In this appendix the basic soil constants derived from the geotechnical investigations are summarised and compiled in tables C.1, C.2 and C.3. The appendix also includes CRS-tests for 4 meters and 8 meters depth in figures C.1 and C.2 and estimated compression parameters are summarised in table C.4.

Table C.1: *Conventional clay parameters from the initial geotechnical study.*

Depth $[m]$	**Unit weight** $[t/m^3]$	**Undrained shear strength** $[kPa]$	**Sensitivity**	**Liquid limit** [%]	**Water ratio** [%]
3	1.69	11	183	32	51
4	1.74	21	80	39	50
5	1.82	24	32	35	38
6	1.76	25	49	35	44
7	1.81	-	-	39	42
8	1.85	30	30	33	36

Initial void ratio is derived from the measured water content according to formula (C.1) from Larsson, 2008

$$e_0 = \frac{w \cdot \rho_s}{\rho_w} \tag{C.1}$$

ρ_s is estimated to be 2.7-2.8 $[t/m^3]$ for swedish clays according to Larsson, 2008.

Table C.3: *Evaluated clay parameters from CRS tests.*

Depth $[m]$	σ'_c $[kPa]$	M_0 $[kPa]$	M_L $[kPa]$	**Permeability** $[m/s]$
3	55	2750	244	1.0E-08
4	92	4600	423	5.7E-10
5	112	5600	839	2.8E-9
6	101	5050	719	1.5E-9
7	-	-	-	-
8	166	8300	983	4.8E-10

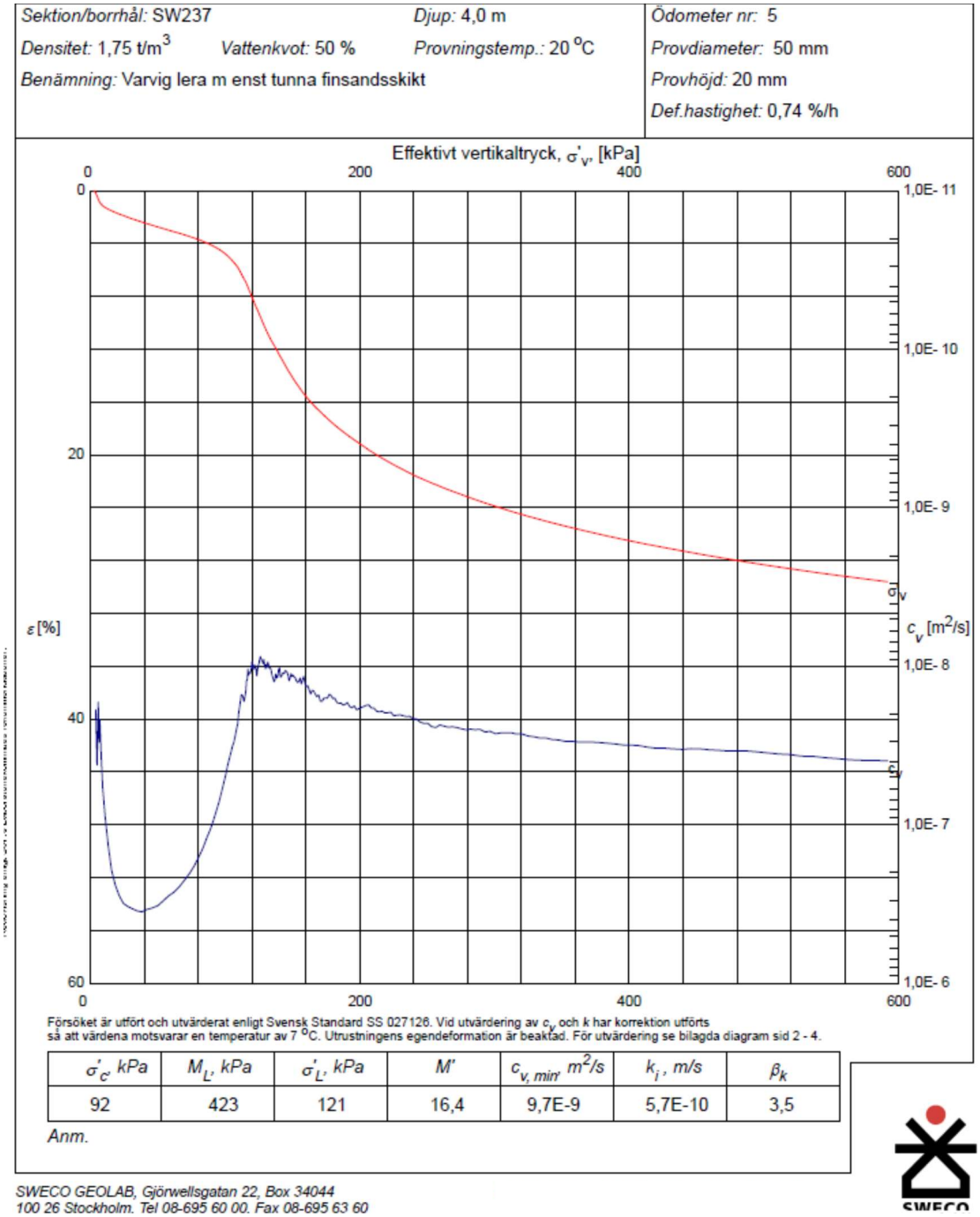

Figure C.1: *Oedometer test at 4 meters depth.*

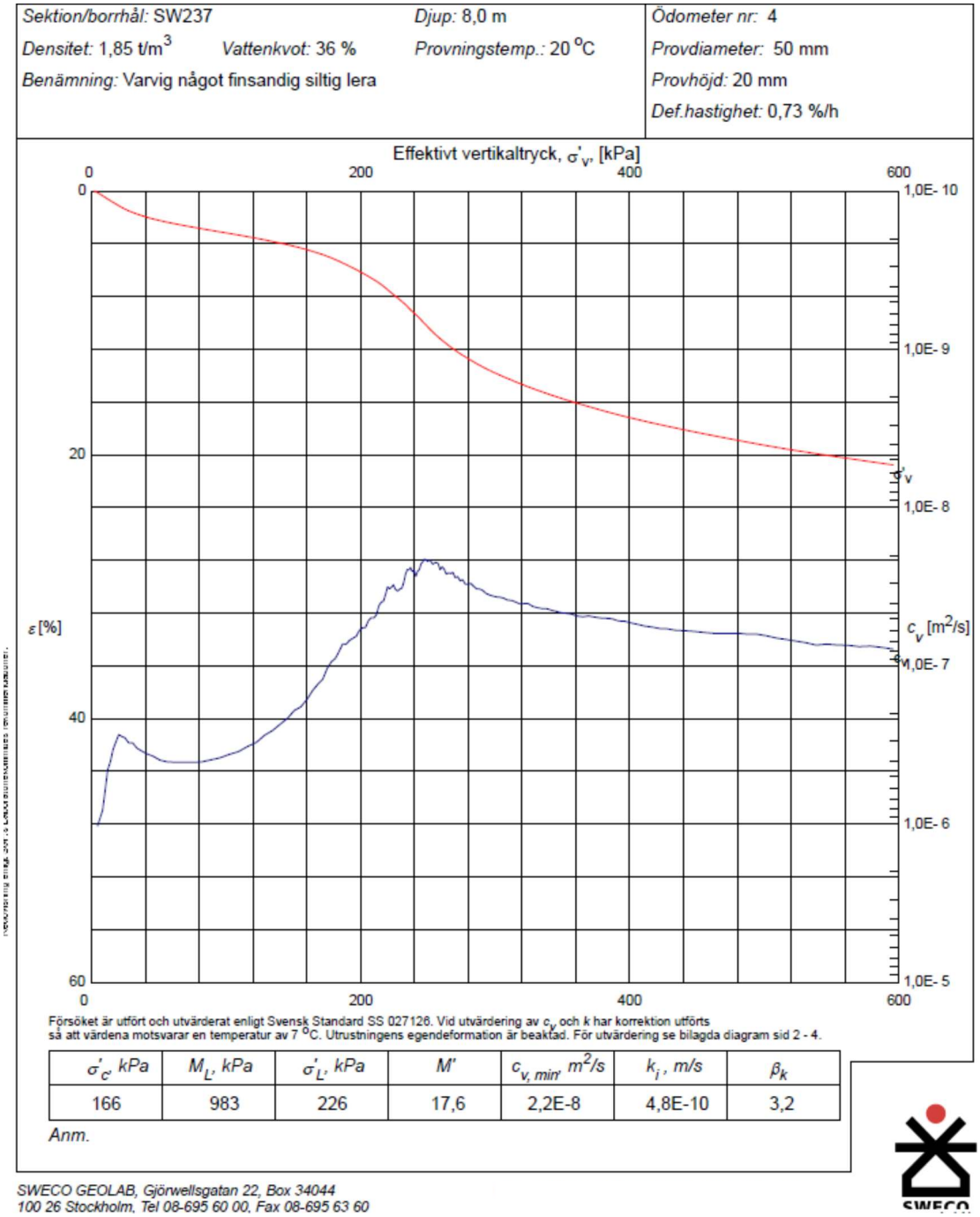

Figure C.2: *Oedometer test at 8 meters depth.*

Table C.2: *Clay parameters estimated by authors.*

Depth $[m]$	e_0	σ'_v $[kPa]$	**OCR**	**POP** $[kPa]$	σ'_h $[kPa]$	K_0 $[kPa]$
3	1.43	38	1.44	17	18	0.48
4	1.4	55	1.66	37	32	0.57
5	1.05	73	1.53	39	38	0.52
6	1.21	90	1.12	11	40	0.44
7	1.16	108	-	-	-	-
8	1.12	126	1.31	40	48	0.45

With equation (C.2) the compression and swelling constants can be estimated from the CRS-curves.

$$\lambda, \kappa, \lambda_i = \frac{de_2 - de_1}{\sigma'_{v2} - \sigma'_{v1}} \tag{C.2}$$

Where the void ratio e can be estimated from the initial void ratio and strain increment at the corresponding stress, equation (C.3).

$$de = e_0 - \dot{(}1 + e_0) \cdot \dot{\varepsilon} \tag{C.3}$$

Table C.4: *Compression parameters estimated from CRS-tests at 4 meters and 8 meters depth.*

Depth $[m]$	λ	κ	λ_i
4	0.72	0.036	0.16
8	0.38	0.024	0.143

D

Refinements of soil constants κ, λ_i and ϕ'

This appendix summarises the refinement analysis performed for the soil constants κ, λ_i and ϕ'. The Evaluation of friction angle with undrained shear strength is displayed in figure D.1. Back calculated values for M, α_0 and β to match the undrained shear strength are concluded in table D.1. Evaluation and comparison of compression and swelling indices with Plaxis' built in soil test tool and CRS-test at 8 meter depth can be seen in figure D.2

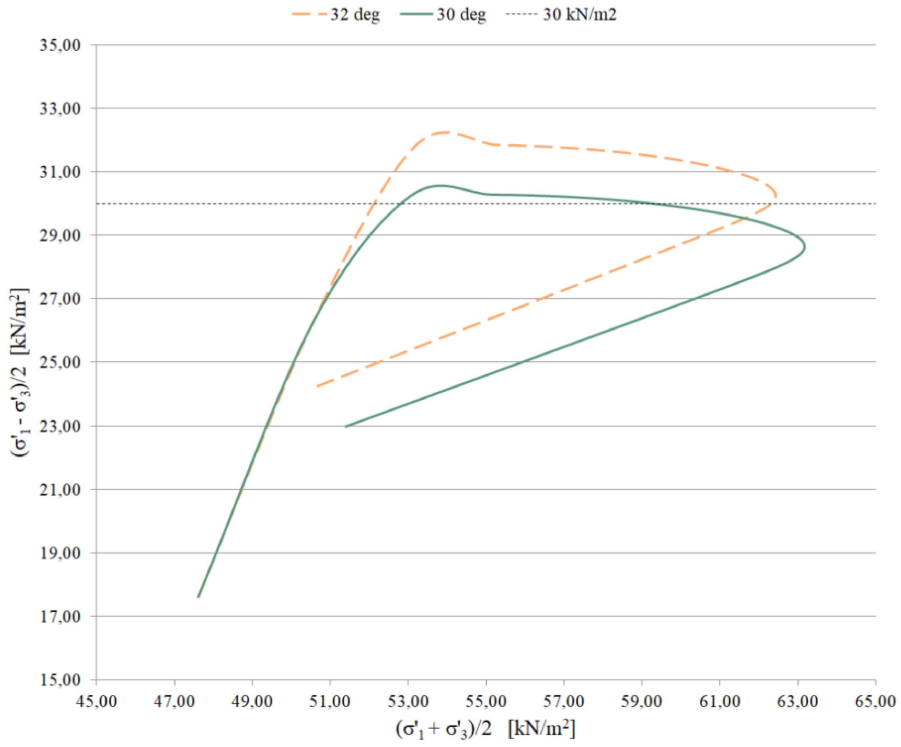

Figure D.1: *Evaluation of friction angle for the clay at 8 meters depth, an c_u of around 30 kN/m^2 at this depth is evaluated from the geotechnical study.*

Table D.1: *Soil constants M, α_0 and β derived from friction angle at depth of 4 and 8 meters, respectively.*

Depth [m]	ϕ' [°]	M	α_0	β
4	28	1.113	0.426	0.654
8	30	1.119	0.457	0.758

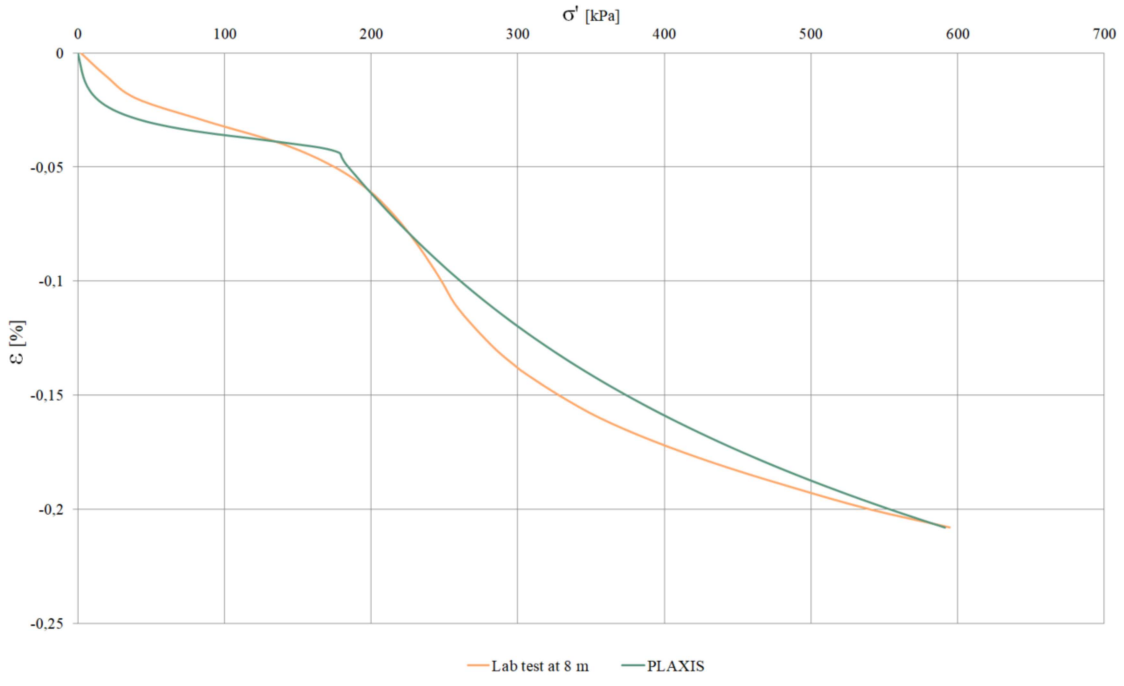

Figure D.2: *Evaluation of parameters λ_i and κ with Plaxis' built in soil test tool and compared with CRS test at 8 meters below ground surface.*

E

POP Sensitivity

In this appendix, a sensitivity analysis regarding the POP-values impact on deformations are presented in figure E.1, with vertical deformations in meter on y-axis and time in day on x-axis. A change in POP-vales induced great deviations in final deformations after 40 years. POP-values of 37 and 40, were chosen respectively for the two clay layers.

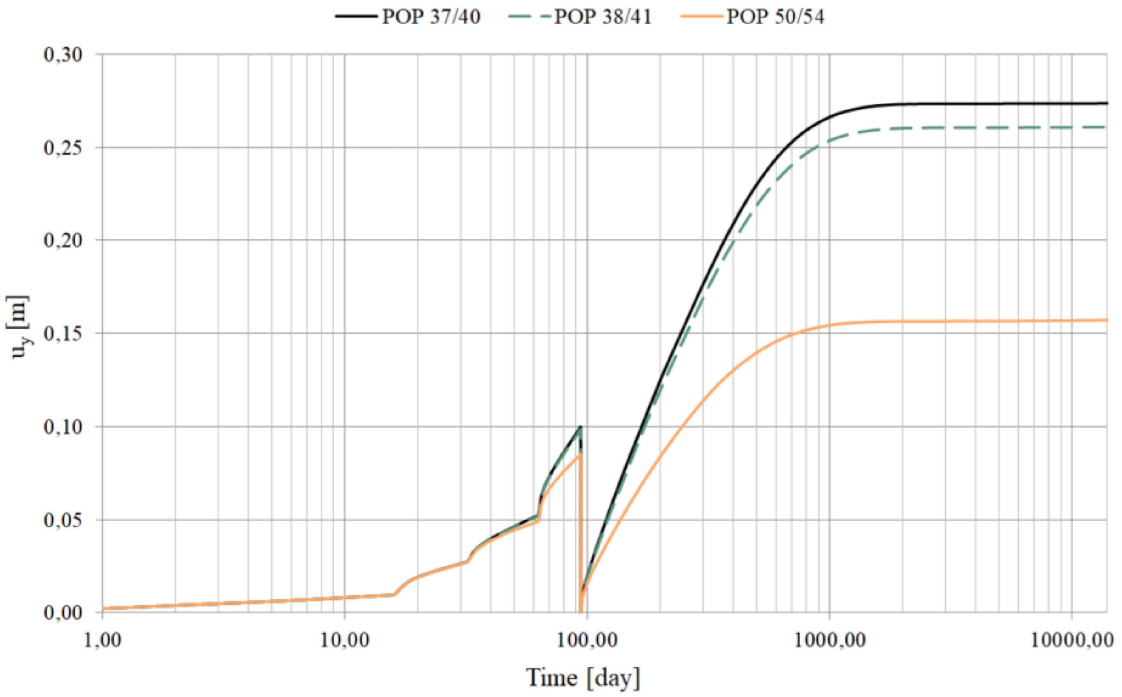

Figure E.1: *Sensitivity analysis of POP value for model with binder material Slag Bremen mixture with* $150kg/m^3$.

F

Evaluation of MNhard parameters

A summary of the deep mixed compression curves and parameter evaluations for MNhard is displayed in this appendix. Uniaxial tests performed on enhanced soil specimens with SH cement, Slag Bremen mixture and Multicem from the geotechnical study are presented in figures F.1, F.2, F.3, F.4, F.5 and F.6. Evaluation and comparison of MNhard parameters with uniaxial tests in Plaxis' built in soil test tool are summarised in figures F.7, F.8, F.9, F.10 and F.11.

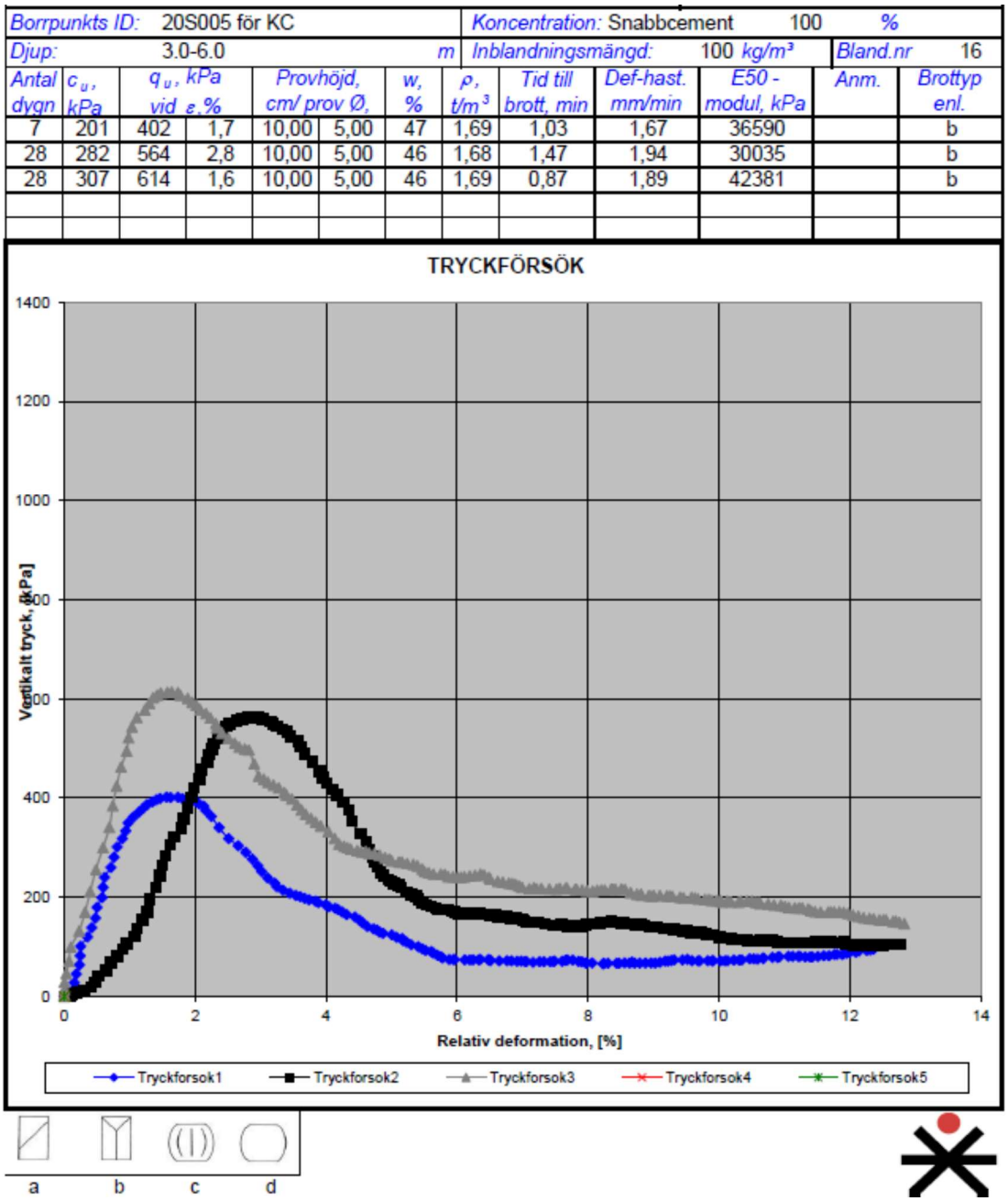

Figure F.1: *Uniaxial test on SH cement 100 kg/m^3.*

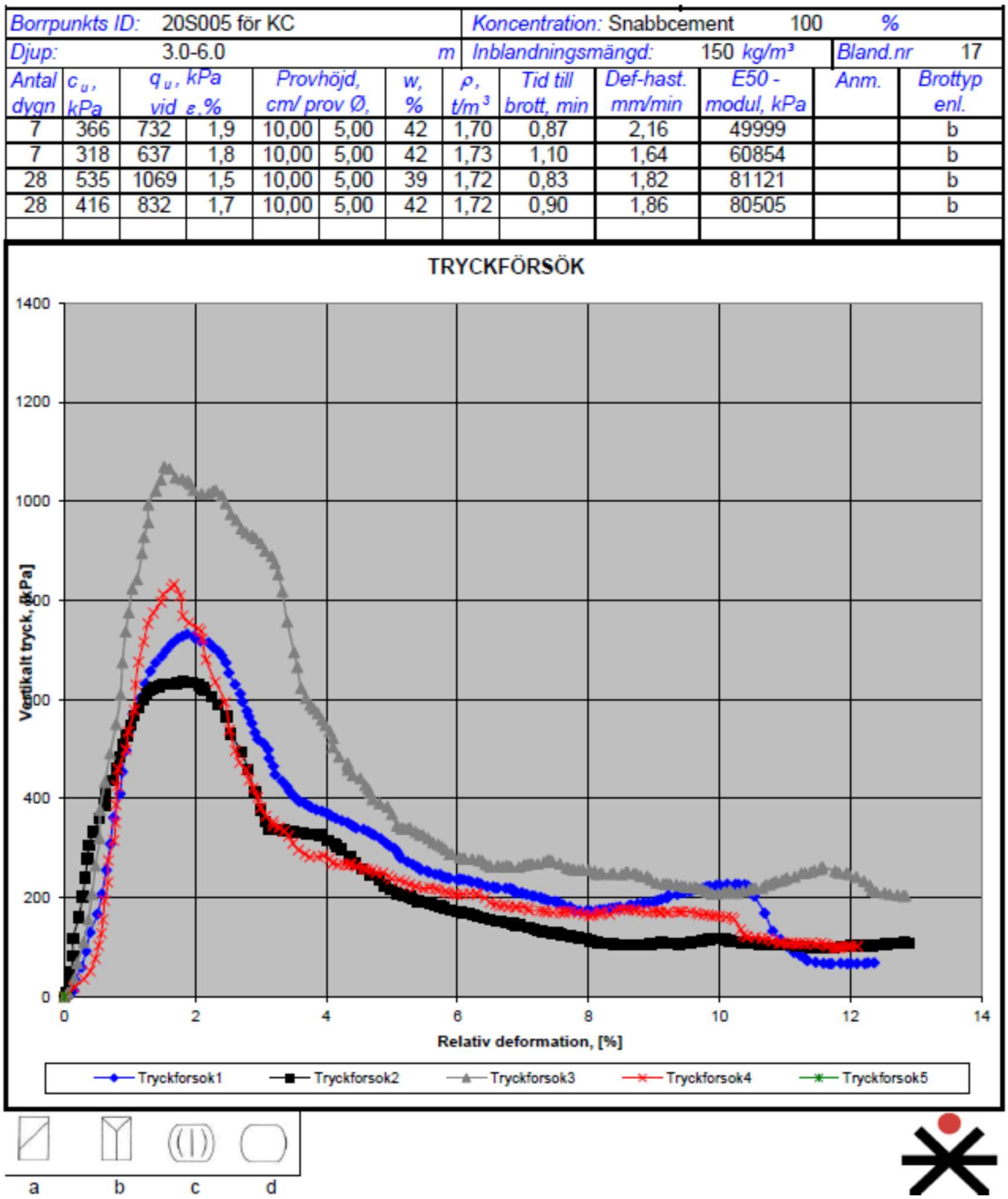

Borrpunkts ID:	20S005 för KC					Koncentration:	Snabbcement	100	%		
Djup:	3.0-6.0				m	Inblandningsmängd:	150 kg/m³		Bland.nr	17	
Antal dygn	c_u, kPa	q_u, kPa vid ε,%		Provhöjd, cm/ prov Ø,		w, %	ρ, t/m³	Tid till brott, min	Def-hast. mm/min	E50 - modul, kPa	Anm.	Brottyp enl.
7	366	732	1,9	10,00	5,00	42	1,70	0,87	2,16	49999		b
7	318	637	1,8	10,00	5,00	42	1,73	1,10	1,64	60854		b
28	535	1069	1,5	10,00	5,00	39	1,72	0,83	1,82	81121		b
28	416	832	1,7	10,00	5,00	42	1,72	0,90	1,86	80505		b

Figure F.2: *Uniaxial test on SH cement with 150 kg/m^3.*

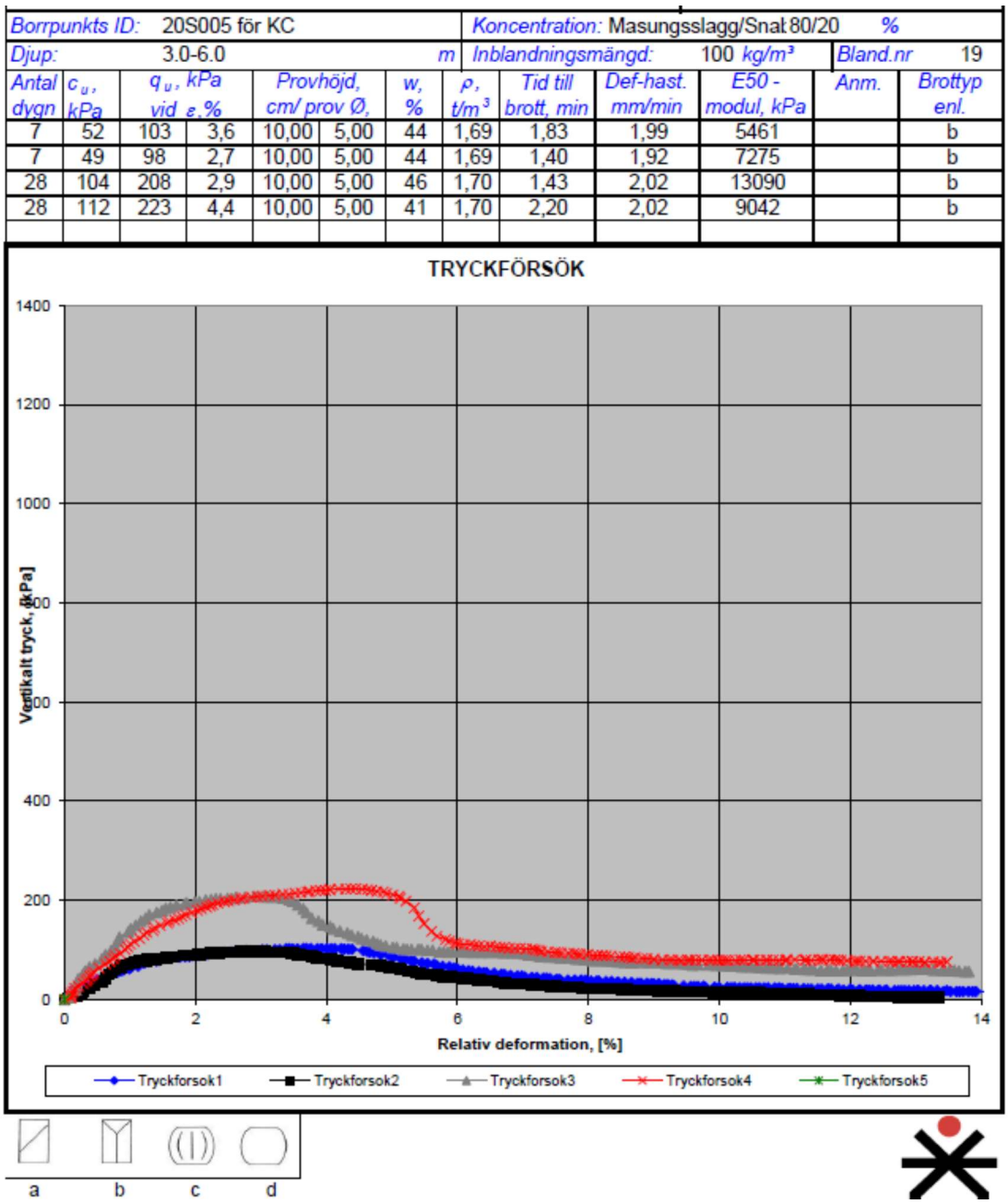

Figure F.3: *Uniaxial test on Slag Bremen mixture with 100 kg/m^3.*

Borrpunkts ID:	20S005 för KC						Koncentration:	Masungsslagg/Snal	80/20	%		
Djup:	3.0-6.0					m	Inblandningsmängd:	150 kg/m³		Bland.nr	20	
Antal dygn	c_u, kPa	q_u, kPa vid ε,%		Provhöjd, cm/ prov Ø,		w, %	ρ, t/m³	Tid till brott, min	Def-hast. mm/min	E50 - modul, kPa	Anm.	Brottyp enl.
7	111	221	1,8	10,00	5,00	46	1,71	1,00	1,77	19936		b
7	121	242	2,2	10,00	5,00	44	1,70	1,07	2,02	21633		b
28	307	613	2,4	10,00	5,00	41	1,68	1,30	1,86	40356		b
28	300	601	2,5	10,00	5,00	41	1,68	1,20	2,11	35092		b

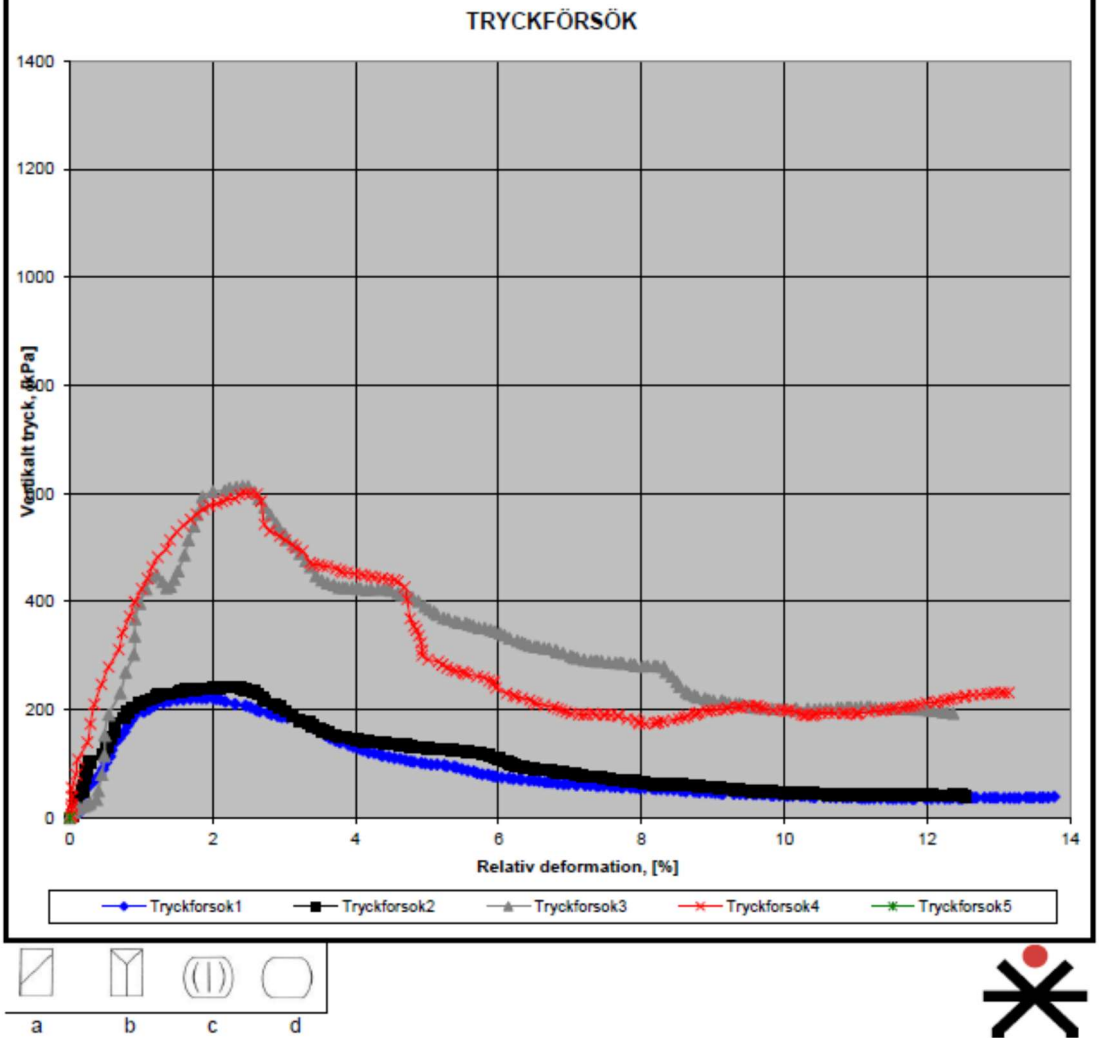

Figure F.4: *Uniaxial test on Slag Bremen mixture with 150 kg/m^3.*

Borrpunkts ID:	20S005 för KC						Koncentration:	Multicem	100	%		
Djup:	3.0-6.0					m	Inblandningsmängd:	100 kg/m³			Bland.nr	22
Antal dygn	c_u, kPa	q_u, kPa vid	ε,%	Provhöjd, cm/ prov Ø,		w, %	ρ, t/m³	Tid till brott, min	Def-hast. mm/min	E50 - modul, kPa	Anm.	Brottyp enl.
7	98	196	2,4	10,00	5,00	45	1,72	1,20	1,98	16820		b
7	84	168	2,7	10,00	5,00	46	1,72	1,37	1,94	23099		b
28	155	310	1,7	10,00	5,00	45	1,72	0,90	1,93	34102		b
28	167	334	1,5	10,00	5,00	45	1,73	0,87	1,74	39370		b

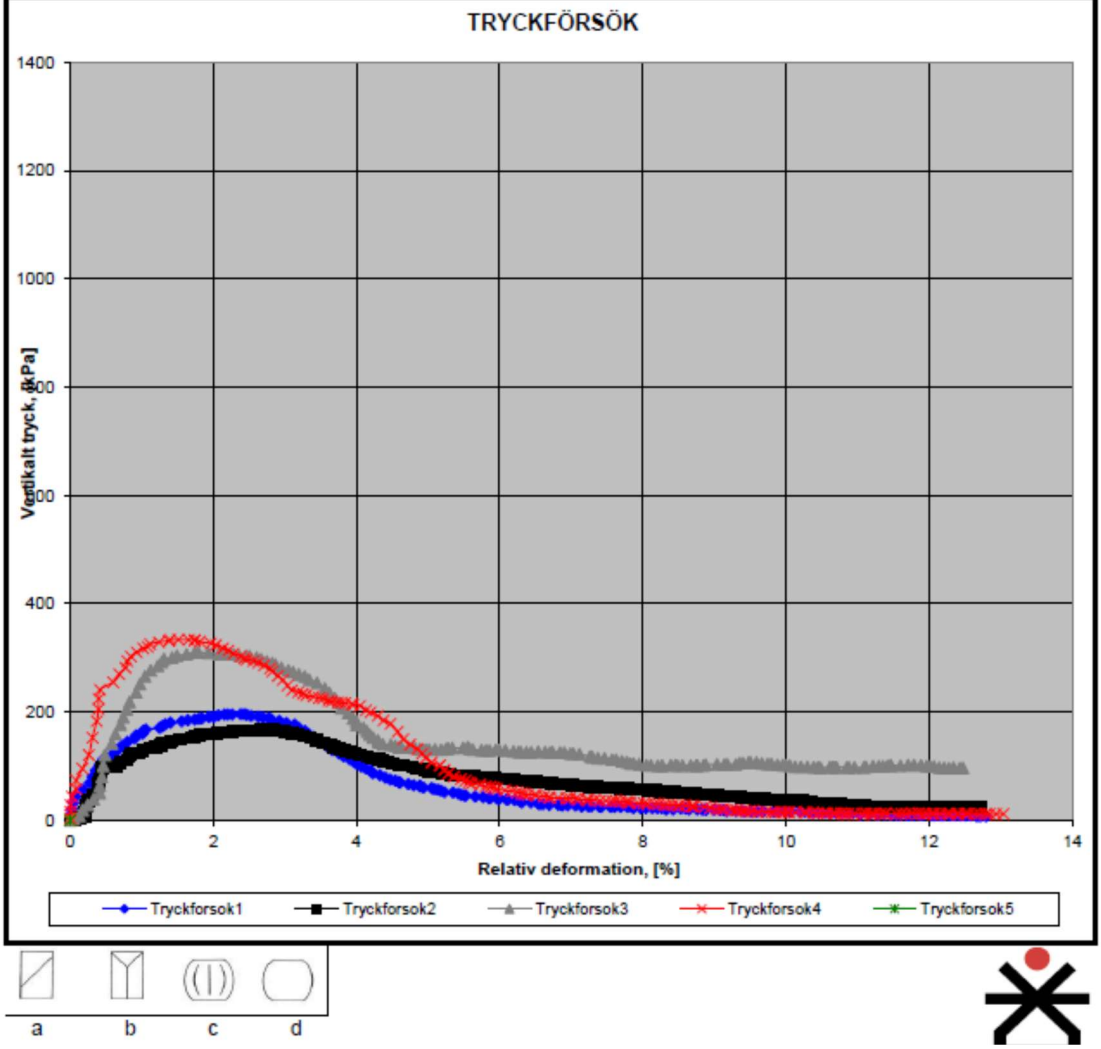

Figure F.5: *Uniaxial test on Multicem with 100 kg/m³.*

Borrpunkts ID:	20S005 för KC						Koncentration: Multicem			100 %		
Djup:	3.0-6.0					m	Inblandningsmängd:	150 kg/m³			Bland.nr	23
Antal dygn	c_u, kPa	q_u, kPa vid ε,%		Provhöjd, cm/ prov Ø,		w, %	ρ, t/m³	Tid till brott, min	Def-hast. mm/min	E50 - modul, kPa	Anm.	Brottyp enl.
7	128	255	2,0	10,00	5,00	44	1,71	1,10	1,82	24199		b
7	129	258	2,7	10,00	5,00	45	1,71	1,30	2,05	14907		b
28	217	434	1,3	10,00	5,00	44	1,72	0,73	1,76	52740		b
28	258	517	1,9	10,00	5,00	43	1,72	1,03	1,88	42881		b

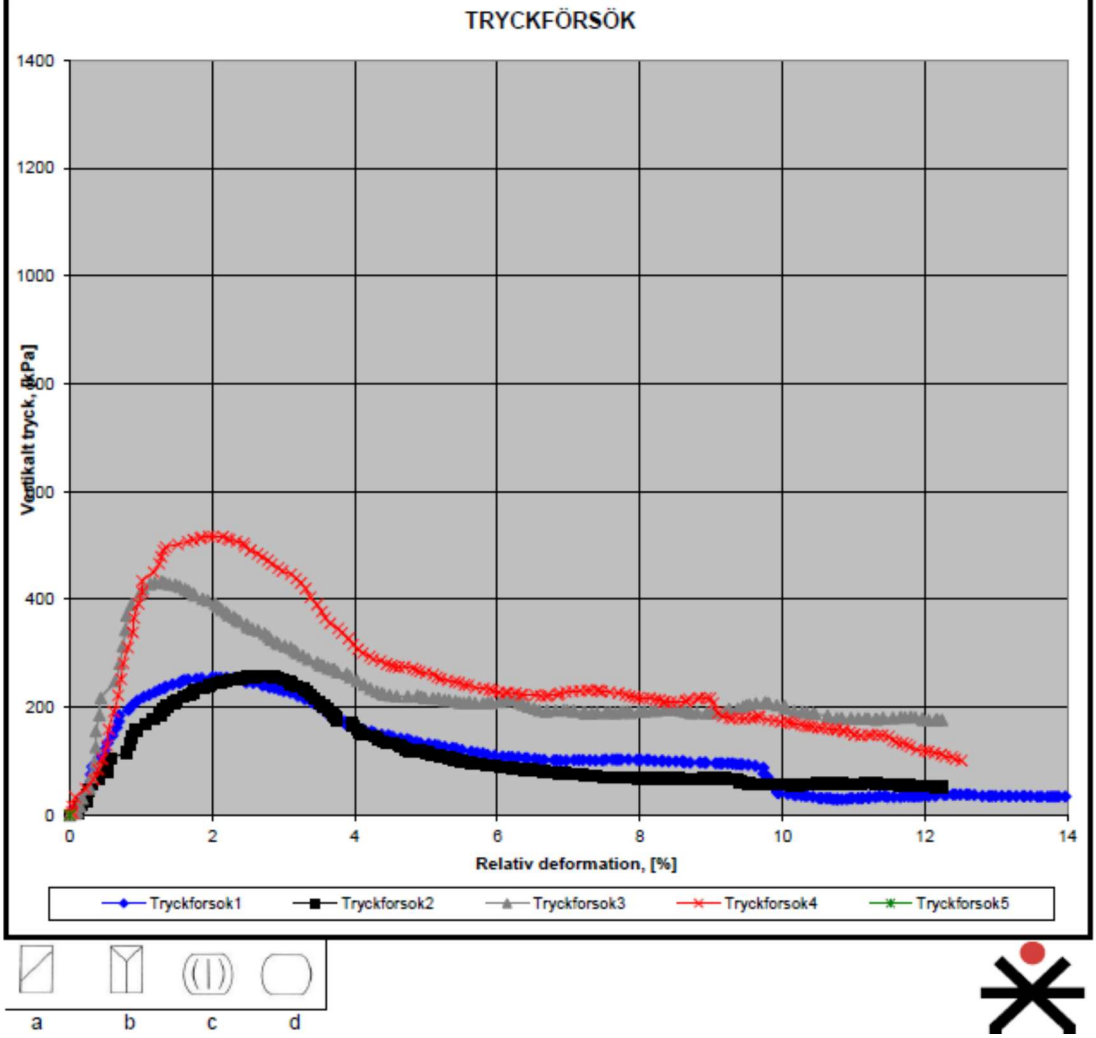

Figure F.6: *Uniaxial test on Multicem with 150 kg/m^3.*

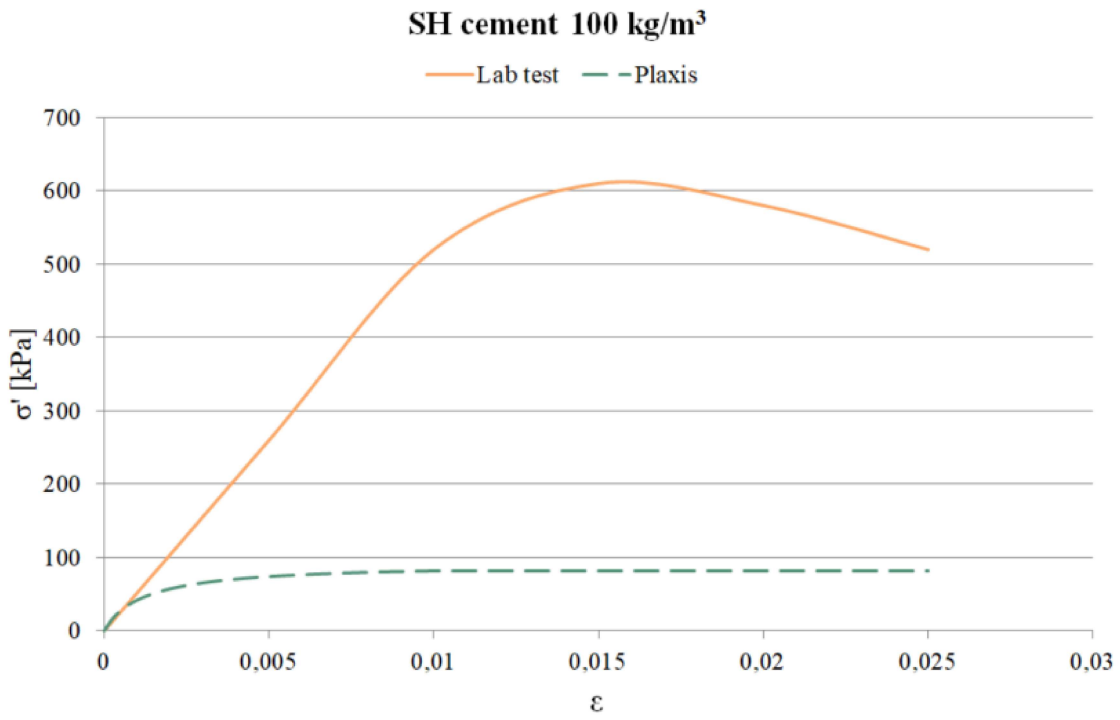

Figure F.7: *Evaluation and comparison of SH cement with 100 kg/m³.*

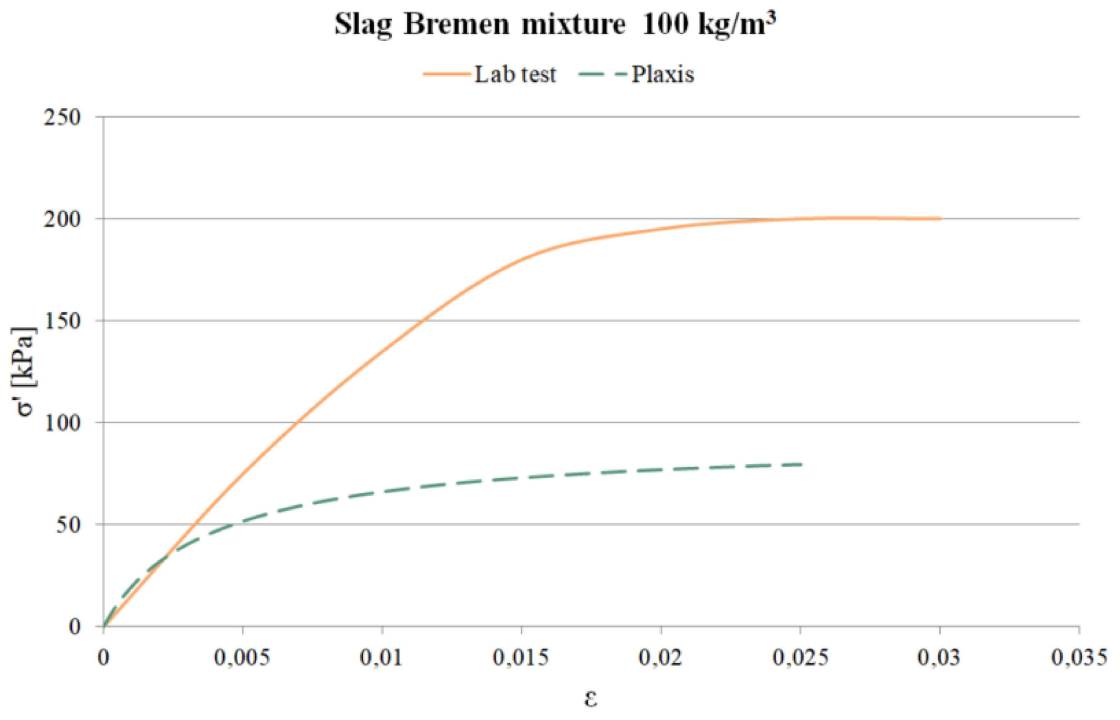

Figure F.8: *Evaluation and comparison of Slag Bremen mixture with 100 kg/m³.*

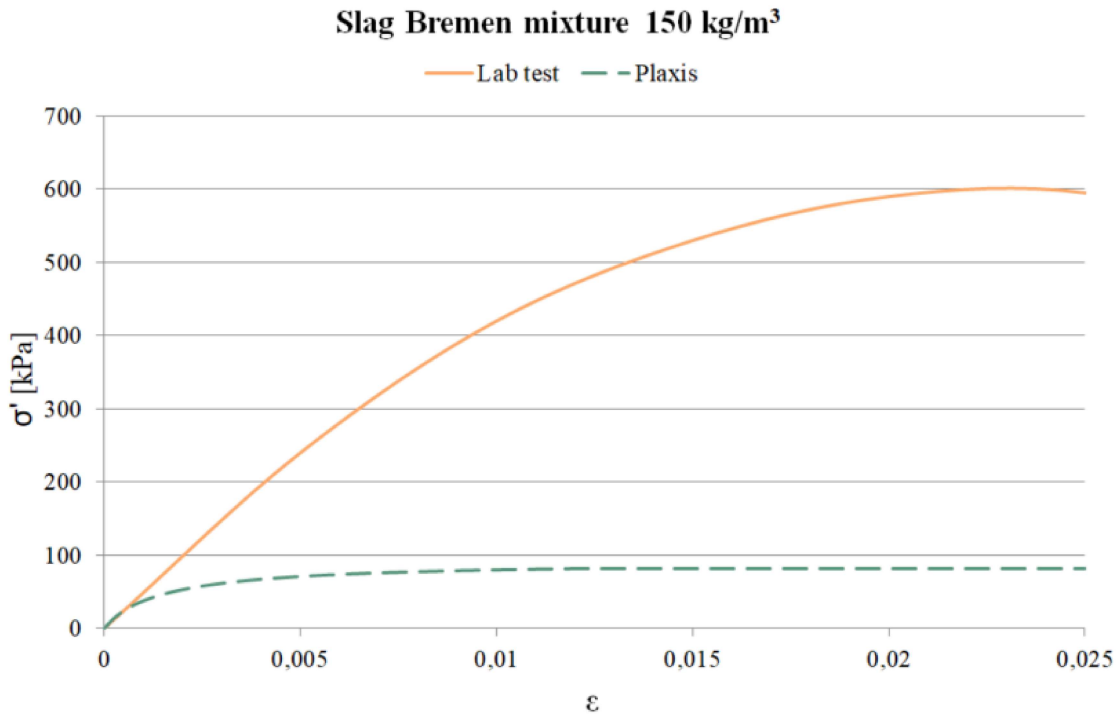

Figure F.9: *Evaluation and comparison of Slag Bremen mixture with 150 kg/m³*

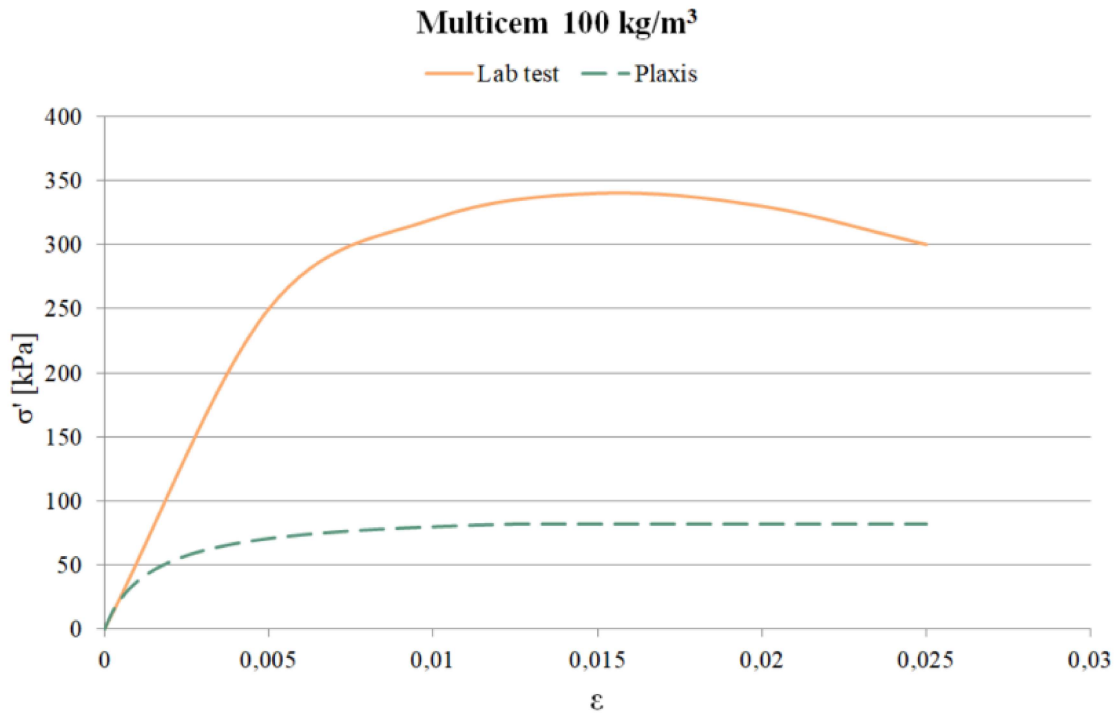

Figure F.10: *Evaluation and comparison of Multicem with 100 kg/m³*

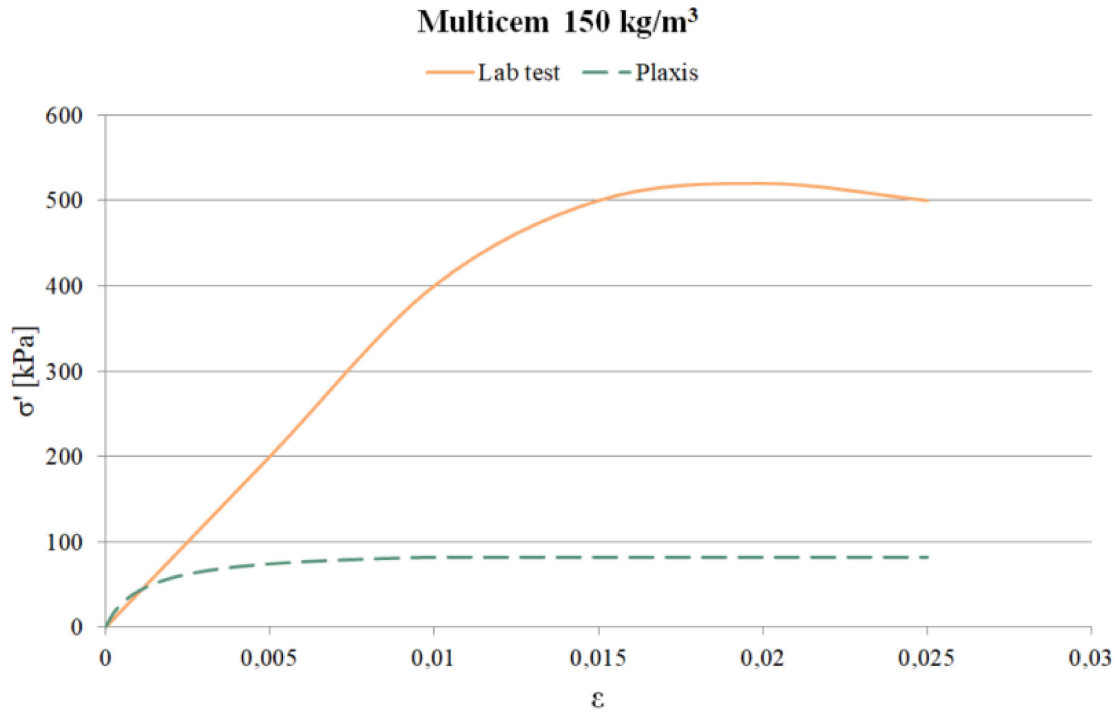

Figure F.11: *Evaluation and comparison of Multicem with 150 kg/m^3*

G

Construction phases

This appendix displays the analysis scheme used for the embankment study. The construction phases implemented in Plaxis 2D analysis are displayed in table G.1.

Table G.1: *Construction phases, description of each phase and type of procedure.*

Phase	**Description**	**Type of procedure**
Initial phase	Calculation of initial stresses	K0 procedure
Phase 1	Import and load UDSM (VAT)	Plastic
Phase 2	Column installation - initialise VAT	Plastic
Phase 3	Construction of first layer embankment in 1 day	Plastic
Phase 4	First layer consolidate for 15 days	Consolidation
Phase 5	Construction of second layer embankment in 1 day	Plastic
Phase 6	Second layer consolidate for 15 days	Consolidation
Phase 7	Construction of third layer embankment in 1 day	Plastic
Phase 8	Third layer consolidate for 30 days	Consolidation
Phase 9	Construction of fourth layer embankment in 1 day	Plastic
Phase 10	Fourth layer consolidate for 30 days	Consolidation
Phase 11	Construction of fifth layer embankment in 1 day Displacements are reset to zero	Plastic
Phase 12	Embankment consolidate for 14000 days (40 years)	Consolidation

H

Transformed column parameters from volume ratio

In this appendix, a summary of the input parameters for the life cycle assessment tool is displayed. Graphs representing center to center distance dependent on diameter and volume ratios for square column pattern can be seen in figure H.1. Obtained volume ratios from the optimisation; 22 %, 23 % and 28 % are highlighted. Table H.1 displays the converted center to center distances and number of columns with respect to the diameters of 500, 600 and 800 mm. The sum of columns per meter embankment varied from 16 to 27, equivalent to c-c distances from 1.5 meters to 1.0 meter.

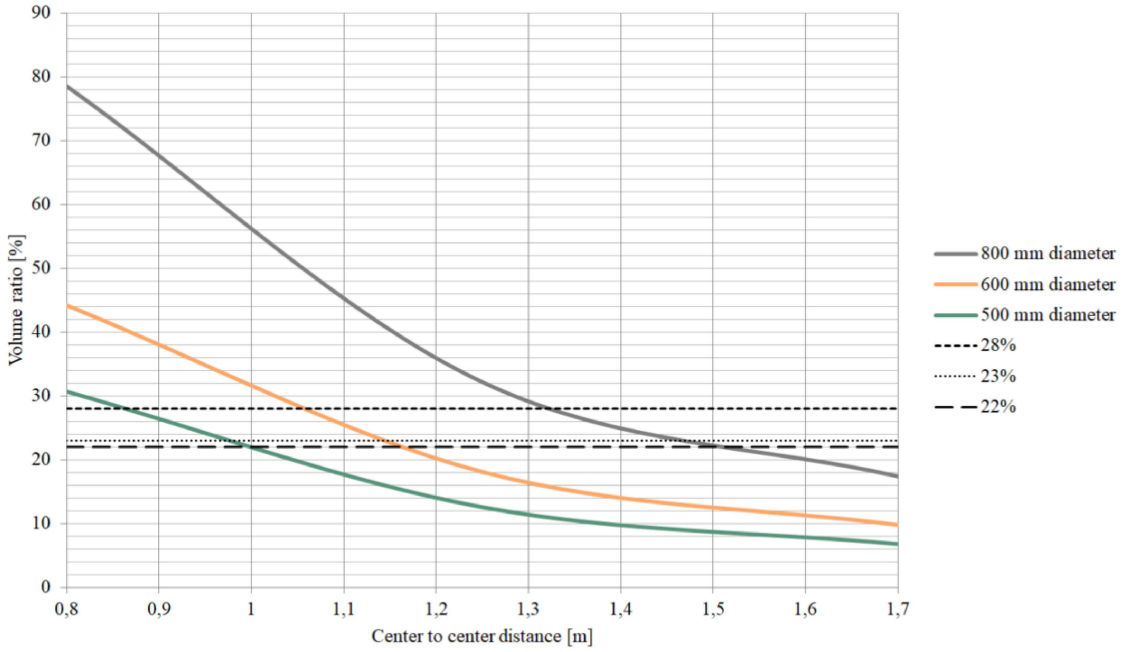

Figure H.1: *Column volume ratio [%] dependent on center to center distance [m] and diameter [mm]. Obtained volume ratios from optimisation; 22 %, 23 % and 28 % are highlighted in the graph.*

Table H.1: *Theoretical input parameters in Carbon Cost for the assessed binders.*

Type of binder	**Concentration** $[kg/m^3]$	**Diameter** $[mm]$	**C-C distance** $[m]$	**Number of columns**
SH cement	100	500	1.0	24
		600	1.2	20
		800	1.5	16
Slag Bremen mixture	100	500	1.0	27
		600	1.0	23
		800	1.3	18
Slag Bremen mixture	150	500	1.0	24
		600	1.1	21
		800	1.5	16
Multicem	100	500	1.0	24
		600	1.1	21
		800	1.5	16
Multicem	150	500	1.0	24
		600	1.2	20
		800	1.5	16

I

Environmental product declaration

In this appendix, the environmental product declaration for each binder type is attached. First SH cement (quick hardening cement) is declared, followed by information regarding the $kg\ CO_2$-eq for Slag Bremen, received from personal contact with Ingemar Löfgren - RD manager at Thomas Concrete Group and Adj. professor at Chalmers University of Technology. Lastly, declarations for Portland Cement and Multicem are attached.

ENVIRONMENTAL PRODUCT DECLARATION

as per /ISO 14025/ and /EN 15804/

Owner of the Declaration	Cementa AB, HeidelbergCement Group
Programme holder	Institut Bauen und Umwelt e.V. (IBU)
Publisher	Institut Bauen und Umwelt e.V. (IBU)
Declaration number	EPD-HCG-20190141-CAA1-EN
Issue date	21/11/2019
Valid to	20/11/2024

Portland Cement CEM I 52.5 R
(Portlandcement SH P Slite)
Cementa AB, HeidelbergCement Group

Institut Bauen und Umwelt e.V.

www.ibu-epd.com / https://epd-online.com

CEMENTA
HEIDELBERGCEMENT Group

General Information

Cementa AB, HeidelbergCement Group

Programme holder
IBU - Institut Bauen und Umwelt e.V.
Panoramastr. 1
10178 Berlin
Germany

Declaration number
EPD-HCG-20190141-CAA1-EN

This declaration is based on the product category rules:
Cement, 07.2014
(PCR checked and approved by the SVR)

Issue date
21/11/2019

Valid to
20/11/2024

Dipl. Ing. Hans Peters
(President of Institut Bauen und Umwelt e.V.)

Dr. Alexander Röder
(Managing Director IBU)

CEM I 52.5 R

Owner of the declaration
Cementa AB
Marieviksgatan 25, Box 47210
SE-100 74 Stockholm

Declared product / declared unit
1 metric t of CEM I 52.5 R

Scope:
This Environmental Product Declaration (EPD) covers the product life cycle stages A1-A3. It is valid for CEM I 52.5 R bulk Portland cement, manufactured by Cementa AB in the plant Slite, Sweden, in 2018. This analysis relies on transparent, plausible and documented basis data. All the model assumptions, which influence the results, are declared. The life cycle assessment is representative of the products introduced in the declaration for the given system boundaries.

The owner of the declaration shall be liable for the underlying information and evidence; the IBU shall not be liable with respect to manufacturer information, life cycle assessment data and evidences.

Verification

The standard /EN 15804/ serves as the core PCR
Independent verification of the declaration and data according to /ISO 14025:2010/
☐ internally ☒ externally

Dr. Eva Schmincke
(Independent verifier appointed by SVR)

Product

Product description / Product definition
Cement is a hydraulic binder. It consists of finely ground, non-metallic inorganic compounds. Cement is produced by grinding cement clinker and other main or minor constituents. When water is added to cement, a cement paste is formed, which sets and hardens by means of hydration reactions. After hardening, it retains its strength and stability even under water. The declared product is a cement conforming with the composition of Portland cement CEM I 52.5 R manufactured by Cementa in the plant Slite in 2018. The calculation is based on plant-specific data. The considered cement belongs to the main cement type CEM I in accordance with /EN 197-1/.

For the placing on the market of the product in the European Union/European Free Trade Association (EU/EFTA) (with the exception of Switzerland) Regulation /(EU) No. 305/2011 Construction Product Regulation (CPR)/ applies. The product needs a Declaration of Performance taking into consideration /EN 197-1/ and the CE-marking. For the application and use the respective national provisions apply.

Application
The application of cement has a large variety. It is mainly used as a binder for concrete and mortar. The application in concrete is regulated in /EN 206/. According to this standard, general suitability is established for cement conforming to /EN 197-1/.

Technical Data
The declared cement corresponds to the 52.5 standard compressive strength class with rapid early strength development (R) in accordance with /EN 197-1/.

Constructional data

Name	Value	Unit
Strength class acc. to /EN 197-1/	52.5	N/mm²

Performance data of the product in accordance with the Declaration of Performance with respect to its Essential Characteristics according to /EN 197-1/.

CEMENTA
HEIDELBERGCEMENT Group

LCA: Results

DESCRIPTION OF THE SYSTEM BOUNDARY (X = INCLUDED IN LCA; MND = MODULE NOT DECLARED)

PRODUCT STAGE			CONSTRUCTION PROCESS STAGE		USE STAGE							END OF LIFE STAGE				BENEFITS AND LOADS BEYOND THE SYSTEM BOUNDARIES
Raw material supply	Transport	Manufacturing	Transport from the gate to the site	Assembly	Use	Maintenance	Repair	Replacement	Refurbishment	Operational energy use	Operational water use	De-construction demolition	Transport	Waste processing	Disposal	Reuse-Recovery-Recycling-potential
A1	A2	A3	A4	A5	B1	B2	B3	B4	B5	B6	B7	C1	C2	C3	C4	D
X	X	X	MND	MND	MND	MND	MNR	MNR	MNR	MND	MND	MND	MND	MND	MND	MND

RESULTS OF THE LCA - ENVIRONMENTAL IMPACT: 1 metric t CEM I 52.5 R

Parameter	Unit	A1-A3
Global warming potential	[kg CO_2-Eq.]	7.75E+2
Depletion potential of the stratospheric ozone layer	[kg CFC11-Eq.]	1.16E-5
Acidification potential of land and water	[kg SO_2-Eq.]	7.20E-1
Eutrophication potential	[kg $(PO_4)^3$-Eq.]	3.02E-1
Formation potential of tropospheric ozone photochemical oxidants	[kg ethene-Eq.]	9.14E-2
Abiotic depletion potential for non-fossil resources	[kg Sb-Eq.]	1.95E-4
Abiotic depletion potential for fossil resources	[MJ]	1.53E+3

RESULTS OF THE LCA - RESOURCE USE: 1 metric t CEM I 52.5 R

Parameter	Unit	A1-A3
Renewable primary energy as energy carrier	[MJ]	5.15E+2
Renewable primary energy resources as material utilization	[MJ]	0.00E+0
Total use of renewable primary energy resources	[MJ]	5.15E+2
Non-renewable primary energy as energy carrier	[MJ]	2.39E+3
Non-renewable primary energy as material utilization	[MJ]	0.00E+0
Total use of non-renewable primary energy resources	[MJ]	2.39E+3
Use of secondary material	[kg]	3.52E+1
Use of renewable secondary fuels	[MJ]	9.86E+2
Use of non-renewable secondary fuels	[MJ]	1.19E+3
Use of net fresh water	[m³]	6.39E+0

RESULTS OF THE LCA – OUTPUT FLOWS AND WASTE CATEGORIES: 1 metric t CEM I 52.5 R

Parameter	Unit	A1-A3
Hazardous waste disposed	[kg]	0.00E+0
Non-hazardous waste disposed	[kg]	4.81E+2
Radioactive waste disposed	[kg]	0.00E+0
Components for re-use	[kg]	0.00E+0
Materials for recycling	[kg]	3.05E-1
Materials for energy recovery	[kg]	0.00E+0
Exported electrical energy	[MJ]	0.00E+0
Exported thermal energy	[MJ]	0.00E+0

Remark to Global warming potential:
This includes 91.5 kg CO_2-eq. from the incineration of wastes in clinker production. According to the "polluter-pays-principle" /EN 15804/ that would be assigned to the production system, which has caused the waste. In this EPD the CO_2 contribution is not subtracted. This is to ensure comparability across countries of calculated global warming potentials for cements even if the used secondary fuels in other countries do not have waste status.

Remark to Waste categories:
The waste indicators account for wastes from clinker and cement manufacturing only.

References

/IBU 2016/
IBU (2016): General Programme Instructions for the Preparation of EPDs at the Institut Bauen und Umwelt e.V., Version 1.1 Institut Bauen und Umwelt e.V., Berlin.
www.ibu-epd.de

/ISO 14025/
DIN EN /ISO 14025:2011-10/, Environmental labels and declarations — Type III environmental declarations — Principles and procedures

/EN 15804/
/EN 15804:2012-04+A1 2013/, Sustainability of construction works — Environmental Product

XXX

Ingemar Löfgren <ingemar.lofgren@c-lab.se>
Ons 2021-03-03 16:00
Till: Viktoria Prahl Blackby
Kopia: Karin Gäbel <karin.gabel@thomasconcretegroup.com>; Leo Wahlgren

Hej,

Vid tillverkning av mald granulerad masugnsslagg så går det åt energi till att torka granulaten och för att mala dessa. Enligt leverantören (LafargeHolcim) så medför detta följande:

- 74,3 kg CO2-ekv/ton slagg efter malning i Bremen

Slaggen transporteras i båt från Bremen till Sverige och för sjötransporten blir det 16,7 kg CO2-ekv/ton.

Data är baserad på LafargeHolcims energiförbrukning och de energislag som används samt rederiets siffror för transporten.

Med vänlig hälsning

PhD/ Tekn.dr. Ingemar Löfgren

R&D Manager / FoU-Chef
Adj. Professor Chalmers University of Technology

C-lab®
Thomas Concrete Group

Thomas Concrete Group AB – C-lab
Visiting Address / Besökadress: Ringögatan 14
SE-417 07 Göteborg, Sweden

Phone: +46 104 50 51 05
ingemar.lofgren@c-lab.se / ingemar.lofgren@thomasconcretegroup.com
www.c-lab.se / www.thomasconcretegroup.com

ENVIRONMENTAL PRODUCT DECLARATION

as per /ISO 14025/ and /EN 15804/

Owner of the Declaration	**Cementa AB, HeidelbergCement Group**
Programme holder	Institut Bauen und Umwelt e.V. (IBU)
Publisher	Institut Bauen und Umwelt e.V. (IBU)
Declaration number	EPD-HCG-20190045-CAA1-EN
Issue date	06/05/2019
Valid to	05/05/2024

Portland Limestone Cement CEM II/A-LL 42.5 R

Cementa AB, HeidelbergCement Group

Institut Bauen und Umwelt e.V.

www.ibu-epd.com / https://epd-online.com

CEMENTA
HEIDELBERGCEMENT Group

General Information

Cementa AB, HeidelbergCement Group

Programme holder
IBU - Institut Bauen und Umwelt e.V.
Panoramastr. 1
10178 Berlin
Germany

Declaration number
EPD-HCG-20190045-CAA1-EN

This declaration is based on the product category rules:
Cement, 07.2014
(PCR checked and approved by the SVR)

Issue date
06/05/2019

Valid to
05/05/2024

Prof. Dr.-Ing. Horst J. Bossenmayer
(President of Institut Bauen und Umwelt e.V.)

Dr. Alexander Röder
(Head of Board IBU)

CEM II/A-LL 42.5 R

Owner of the declaration
Cementa AB
Årstaängsvägen 25, Box 47210
SE-100 74 Stockholm

Declared product / declared unit
1 metric t of CEM II/A-LL 42.5 R

Scope:
This Environmental Product Declaration (EPD) covers the product life cycle stages A1-A3. It is valid for CEM II/A-LL 42.5 R bulk Portland limestone cement, manufactured by Cementa AB in the plant Skövde, Sweden, in 2017. This analysis relies on transparent, plausible and documented basis data. All the model assumptions, which influence the results, are declared. The life cycle assessment is representative for the products introduced in the declaration for the given system boundaries.

The owner of the declaration shall be liable for the underlying information and evidence; the IBU shall not be liable with respect to manufacturer information, life cycle assessment data and evidences.

Verification

The standard /EN 15804/ serves as the core PCR
Independent verification of the declaration and data according to /ISO 14025:2010/
☐ internally ☒ externally

Dr. Eva Schmincke
(Independent verifier appointed by SVR)

Product

Product description / Product definition
Cement is a hydraulic binder. It consists of finely ground, non-metallic inorganic compounds. Cement is produced by grinding cement clinker and other main or minor constituents. When water is added to cement, a cement paste is formed, which sets and hardens by means of hydration reactions. After hardening, it retains its strength and stability even under water. The declared product is a cement conforming with the composition of Portland limestone cement CEM II/A-LL 42.5 R manufactured by Cementa in the plant Skövde in 2017. The calculation is based on plant-specific data. The considered cement belongs to the main cement type CEM II/A-LL in accordance with /EN 197-1/.

For the placing on the market of the product in the European Union/European Free Trade Association EU/EFTA (with the exception of Switzerland) Regulation /(EU) No. 305/2011 (CPR)/[BS1] applies. The product needs a Declaration of Performance taking into consideration /EN 197-1/ and the CE-marking. For the application and use the respective national provisions apply.

Application
The application of cement has a large variety. It is mainly used as binder for concrete and mortar. The application in concrete is regulated in /EN 206/. According to this standard, general suitability is established for cement conforming to /EN 197-1/.

Technical Data
The declared cement corresponds to the 42.5 standard compressive strength class with high early strength development (R) in accordance with /EN 197-1/.

Constructional data

Name	Value	Unit
Strength class acc. to /EN 197-1/	42.5	N/mm²

Performance data of the product in accordance with the Declaration of Performance with respect to its Essential Characteristics according to /EN 197-1/.

CEMENTA
HEIDELBERGCEMENT Group

LCA: Results

DESCRIPTION OF THE SYSTEM BOUNDARY (X = INCLUDED IN LCA; MND = MODULE NOT DECLARED)

PRODUCT STAGE			CONSTRUCTION PROCESS STAGE		USE STAGE							END OF LIFE STAGE				BENEFITS AND LOADS BEYOND THE SYSTEM BOUNDARIES
Raw material supply	Transport	Manufacturing	Transport from the gate to the site	Assembly	Use	Maintenance	Repair	Replacement	Refurbishment	Operational energy use	Operational water use	De-construction demolition	Transport	Waste processing	Disposal	Reuse-Recovery-Recycling-potential
A1	A2	A3	A4	A5	B1	B2	B3	B4	B5	B6	B7	C1	C2	C3	C4	D
X	X	X	MND	MND	MND	MND	MNR	MNR	MNR	MND	MND	MND	MND	MND	MND	MND

RESULTS OF THE LCA - ENVIRONMENTAL IMPACT: 1 metric t CEM II/A-LL 42.5 R

Parameter	Unit	A1-A3
Global warming potential	[kg CO_2-Eq.]	7.59E+2
Depletion potential of the stratospheric ozone layer	[kg CFC11-Eq.]	1.38E-5
Acidification potential of land and water	[kg SO_2-Eq.]	6.23E-1
Eutrophication potential	[kg $(PO_4)^3$-Eq.]	2.33E-1
Formation potential of tropospheric ozone photochemical oxidants	[kg ethene-Eq.]	8.22E-2
Abiotic depletion potential for non-fossil resources	[kg Sb-Eq.]	1.07E-4
Abiotic depletion potential for fossil resources	[MJ]	1.54E+3

RESULTS OF THE LCA - RESOURCE USE: 1 metric t CEM II/A-LL 42.5 R

Parameter	Unit	A1-A3
Renewable primary energy as energy carrier	[MJ]	3.76E+2
Renewable primary energy resources as material utilization	[MJ]	0.00E+0
Total use of renewable primary energy resources	[MJ]	3.76E+2
Non-renewable primary energy as energy carrier	[MJ]	2.13E+3
Non-renewable primary energy as material utilization	[MJ]	0.00E+0
Total use of non-renewable primary energy resources	[MJ]	2.13E+3
Use of secondary material	[kg]	1.48E+1
Use of renewable secondary fuels	[MJ]	5.05E+2
Use of non-renewable secondary fuels	[MJ]	7.31E+2
Use of net fresh water	[m³]	4.95E+0

RESULTS OF THE LCA – OUTPUT FLOWS AND WASTE CATEGORIES: 1 metric t CEM II/A-LL 42.5 R

Parameter	Unit	A1-A3
Hazardous waste disposed	[kg]	2.22E-2
Non-hazardous waste disposed	[kg]	1.31E-1
Radioactive waste disposed	[kg]	0.00E+0
Components for re-use	[kg]	0.00E+0
Materials for recycling	[kg]	8.21E-4
Materials for energy recovery	[kg]	0.00E+0
Exported electrical energy	[MJ]	0.00E+0
Exported thermal energy	[MJ]	0.00E+0

Remark to Global warming potential:
This includes 55.3 kg CO2-eq. from the incineration of wastes in clinker production. According to the polluter-pays-principle /EN 15804/ that would be assigned to the production system, which has caused the waste. In this EPD the CO_2 contribution is not subtracted. This is to ensure comparability across countries of calculated global warming potentials for cements even if the used secondary fuels in other countries do not have waste status.

Remark to Waste categories:
The waste indicators account for wastes from clinker and cement manufacturing only.

References

/IBU 2016/
IBU (2016): General Programme Instructions for the Preparation of EPDs at the Institut Bauen und Umwelt e.V., Version 1.1 Institut Bauen und Umwelt e.V., Berlin.
www.ibu-epd.de

/ISO 14025/
DIN EN /ISO 14025:2011-10/, Environmental labels and declarations — Type III environmental declarations — Principles and procedures

/EN 15804/
/EN 15804:2012-04+A1 2013/, Sustainability of construction works — Environmental Product

ENVIRONMENTAL PRODUCT DECLARATION

as per ISO 14025 and EN 15804

Owner of the Declaration	**Cementa AB, HeidelbergCement Group**
Programme holder	Institut Bauen und Umwelt e.V. (IBU)
Publisher	Institut Bauen und Umwelt e.V. (IBU)
Declaration number	EPD-HCG-20160236-CAD1-EN
Issue date	2016-12-16
Valid to	2021-12-15

Multicem

Cementa AB, HeidelbergCement Group

Institut Bauen und Umwelt e.V.

www.ibu-epd.com / https://epd-online.com

CEMENTA
HEIDELBERGCEMENT Group

General Information

Cementa AB, HeidelbergCement Group

Programme holder
IBU - Institut Bauen und Umwelt e.V.
Panoramastr. 1
10178 Berlin
Germany

Declaration number
EPD-HCG-20160236-CAD1-EN

This Declaration is based on the Product Category Rules:
Cement, 07.2014
(PCR tested and approved by the SVR)

Issue date
2016-12-16

Valid to
2021-12-15

Prof. Dr.-Ing. Horst J. Bossenmayer
(President of Institut Bauen und Umwelt e.V.)

Dr. Burkhart Lehmann
(Managing Director IBU)

Multicem

Owner of the Declaration
Cementa AB
Årstaängsvägen 25, Box 47210
SE-100 74 Stockholm

Declared product / Declared unit
1 metric t of **Multicem**

Scope:
This Environmental Product Declaration (EPD) covers the product life cycle stages A1-A3. It is valid for Multicem, manufactured by Cementa AB at the plant Slite, Sweden, in 2015. This analysis relies on transparent, plausible and documented basis data. All the model assumptions, which influence the results, are declared. The life cycle assessment is representative for the products introduced in the declaration for the given system boundaries.
The owner of the declaration shall be liable for the underlying information and evidence; the IBU shall not be liable with respect to manufacturer information, life cycle assessment data and evidences.

Verification

The CEN Norm /EN 15804/ serves as the core PCR
Independent verification of the declaration according to /ISO 14025/
☐ internally ☒ externally

Dr. Eva Schmincke
(Independent verifier appointed by SVR)

Product

Product description / Product definition
Cement is a hydraulic binder. It consists of finely-ground, non-metallic inorganic compounds. Cement is produced by grinding cement clinker and other main or minor constituents. When water is added to cement, a cement paste is formed, which sets and hardens by means of hydration reactions. After hardening, it retains its strength and stability even under water.

The declared product Multicem is a blend of cement CEM I in accordance with /EN 197-1/ and cement kiln dust, manufactured by Cementa at the plant Slite. It does not comply with /EN 197-1/. The calculation is based on plant-specific data of 2015.

Multicem was designed within the scope of the continued product development towards better products with higher environmental profile, based on Cementa's zero vision for carbon emissions.

For the use and application of the product the respective national provisions at the place of use apply.

Application
In general, the application of cement has a large variety. Multicem is a special product, which is used for soil stabilization and solidification.

Technical Data
Multicem has, in comparison with products such as Cementa's Kalkcement (a lime-cement product), better stabilization properties.

Multicem is delivered in bulk from the cement plant and comes ready to use. The characteristics of the product are similar as those of lime-cement stabilization products (e.g. Cementa's Kalkcement).

When producing Multicem, the use of raw material such as limestone is replaced with cement kiln dust which also adds to the environmental profile of the product.

Performance data of the product with respect to its characteristics in accordance with the relevant technical provision ((No CE-marking)).

CEMENTA
HEIDELBERGCEMENT Group

LCA: Results

DESCRIPTION OF THE SYSTEM BOUNDARY (X = INCLUDED IN LCA; MND = MODULE NOT DECLARED)

PRODUCT STAGE			CONSTRUCTION PROCESS STAGE		USE STAGE							END OF LIFE STAGE				BENEFITS AND LOADS BEYOND THE SYSTEM BOUNDARIES
Raw material supply	Transport	Manufacturing	Transport from the gate to the site	Assembly	Use	Maintenance	Repair	Replacement	Refurbishment	Operational energy use	Operational water use	De-construction demolition	Transport	Waste processing	Disposal	Reuse-Recovery-Recycling-potential
A1	A2	A3	A4	A5	B1	B2	B3	B4	B5	B6	B7	C1	C2	C3	C4	D
X	X	X	MND	MND	MND	MND	MND	MND	MND	MND	MND	MND	MND	MND	MND	MND

RESULTS OF THE LCA - ENVIRONMENTAL IMPACT: 1 metric t Multicem

Parameter	Unit	A1-A3
Global warming potential	[kg CO_2-Eq.]	3.96E+2
Depletion potential of the stratospheric ozone layer	[kg CFC11-Eq.]	3.28E-6
Acidification potential of land and water	[kg SO_2-Eq.]	3.84E-1
Eutrophication potential	[kg $(PO_4)^3$-Eq.]	1.63E-1
Formation potential of tropospheric ozone photochemical oxidants	[kg ethene-Eq.]	6.12E-2
Abiotic depletion potential for non-fossil resources	[kg Sb-Eq.]	2.07E-5
Abiotic depletion potential for fossil resources	[MJ]	1.47E+3

RESULTS OF THE LCA - RESOURCE USE: 1 metric t Multicem

Parameter	Unit	A1-A3
Renewable primary energy as energy carrier	[MJ]	1.39E+2
Renewable primary energy resources as material utilization	[MJ]	0.00E+0
Total use of renewable primary energy resources	[MJ]	1.39E+2
Non-renewable primary energy as energy carrier	[MJ]	1.43E+3
Non-renewable primary energy as material utilization	[MJ]	0.00E+0
Total use of non-renewable primary energy resources	[MJ]	1.43E+3
Use of secondary material	[kg]	5.19E+2
Use of renewable secondary fuels	[MJ]	3.46E+2
Use of non-renewable secondary fuels	[MJ]	4.98E+2
Use of net fresh water	[m³]	5.09E-1

RESULTS OF THE LCA – OUTPUT FLOWS AND WASTE CATEGORIES: 1 metric t Multicem

Parameter	Unit	A1-A3
Hazardous waste disposed	[kg]	0.00E+0
Non-hazardous waste disposed	[kg]	0.00E+0
Radioactive waste disposed	[kg]	0.00E+0
Components for re-use	[kg]	0.00E+0
Materials for recycling	[kg]	0.00E+0
Materials for energy recovery	[kg]	0.00E+0
Exported electrical energy	[MJ]	0.00E+0
Exported thermal energy	[MJ]	0.00E+0

Remark to Global warming potential:
This includes 61.1 kg CO_2-eq. from the incineration of wastes in clinker production. According to the polluter-pays-principle /EN 15804/ that would be assigned to the production system, which has caused the waste. In this EPD the CO_2 contribution is not subtracted. This is to ensure comparability across countries of calculated global warming potentials for cements even if the used secondary fuels in other countries do not have waste status.

Remark to Waste categories:
The waste indicators account for wastes from clinker and cement manufacturing only.

J

Deformed mesh

In this appendix, a deformed mesh of Slag Bremen mixture with 150 kg/m^3 after 40 years consolidation is displayed in figure J.1.

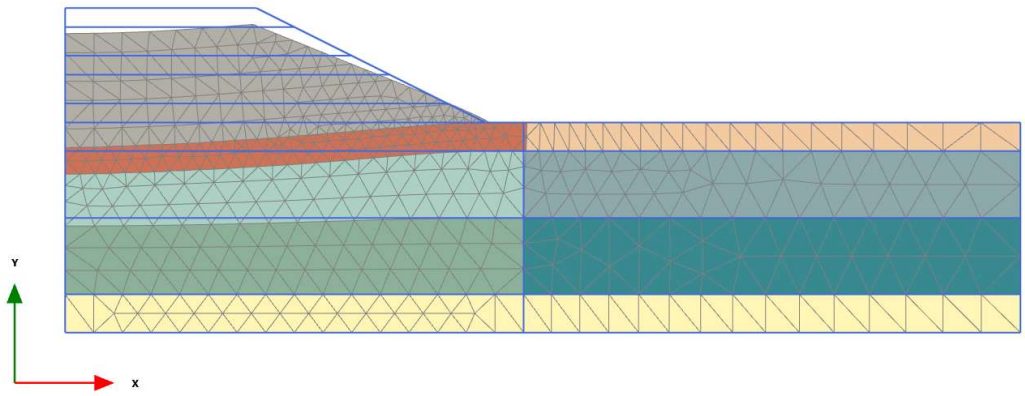

Figure J.1: *Deformed mesh after 40 years consolidation of binder Slag Bremen mixture with a concentration of 150 kg/m^3. Deformed mesh scaled up 5 times.*

CHALMERS
UNIVERSITY OF TECHNOLOGY